OPTOFLUIDIC REACTORS FOR PHOTOCATALYTIC WATER PURIFICATION

WANG Ning

Ph.D

The Hong Kong Polytechnic University

2015

THE HONG KONG POLYTECHNIC UNIVERSITY

DEPARTMENT OF APPLIED PHYSICS

OPTOFLUIDIC REACTORS FOR PHOTOCATALYTIC WATER PURIFICATION

WANG Ning

A thesis submitted in partial fulfilment of the

requirements for the degree of Doctor of Philosophy

November 2014

THE HONG KONG POLYTECHNIC UNIVERSITY

Certificate of Originality

I hereby declare that this thesis is my own work and that, to the best of my knowledge and belief, it reproduces no material previously published or written, nor material that has been accepted for the award of any other degree or diploma, except where due acknowledgement has been made in the text.

_____ (Signed)

Wang Ning (Name of student)

Abstract

Optofluidics is a new technology that enables simultaneous delivery of light and fluids with microscopic precision. This study aims to explore the opportunities of applying the optofluidics technology to the photocatalytic systems for water purification.

In this study, three types of optofluidic reactors for photocatalysis water purification are designed, fabricated and characterized to overcome the fundamental limitations of current bulk reactors. The first design is a planar reactor that attempts to overcome the mass transfer limit and the photon transfer limit in the bulk reactors. It has exhibited promising features such as small sample volume, short reaction time and easy flow control. The degradation percentage reaches 94% at the effective residence time of 36 s and the degradation rate gets up to 8%/s at the effective residence time of 6 s. Its success has encouraged the proposal of the second design, which uses $BiVO_4$ as the visible photocatalyst and mounts a blue-light LED panel as the integrated light source. The mounted LED provides uniform irradiation of light and enables to utilize the heat of light source to assist the photodegradation. The degradation efficiency was increased by 4 times and the heat contribution to degradation was about 4~6%. The third design is a novel photoelectrocatalytic microreactor, which aims to eliminate a fundamental limit of photocatalysis – the recombination of photo-excited electrons and holes by applying

an external electric field. In the experiment, positive and negative bias potentials are applied across the reaction chamber to suppress the e^-/h^+ recombination and to select either the hole-driven or electron-driven oxidation pathway. Another important feature is that the degradation percentage increases linearly with the residence time. It is 5.2% s^{-1} for the negative bias state and 4.7% s^{-1} for the positive bias state.

In summary, the optofluidic microreactors have been developed to help overcome different problems in the bulk reactors such as photon transfer limitation, mass transfer limitation, oxygen deficiency, and lack of reaction pathway control. These reactors may find niche applications in rapid screening and standardized tests of photocatalysts and may also be scaled up for large-throughput industrial applications of water process.

List of Publications

Journal Publications

1. **Ning Wang,** Furui Tan, Li Wan, Chunmeng Wu and Xuming Zhang, Microfluidic reactors for visible-light photocatalytic water purification assisted with thermolysis, ***Biomicrofluidics,*** 8(5), 054122, 2014.
2. **Ning Wang**, Xuming Zhang, Yu Wang, Weixing Yu and Helen L. W. Chan, Microfluidic reactors for photocatalytic water purification, ***Lab on a Chip***, vol. 14, no. 6, pp. 1074 – 1082, 2013.
3. Ngai Yui Chan, Meng Zhao, **Ning Wang**, Kit Au, Juan Wang, Lai Wa Helen Chan and Jiyan Dai, Palladium Nanoparticle Enhanced Giant Photoresponse at $LaAlO_3/SrTiO_3$ Two-Dimensional Electron Gas Heterostructures, ***ACS Nano***, vol. 7 , no. 10, pp 8673–8679, 2013.
4. **N. Wang**, X. M. Zhang, B. L. Chen, W. Z. Song, N. Y. Chan, and Helen L. W. Chan, Microfluidic photoelectrocatalytic reactors for water purification with integrated visible-light source, ***Lab on a Chip***, vol. 12, no. 20, pp. 3983–3990, 2012.(***Highlighted by Nature Photonics***)
5. **N. Wang**, M. Feng, Z. Q. Feng, M. Y. Lam, L. Gao, B. Chen, A. Q. Liu, Y. H. Tsang and X. M. Zhang, Narrow-linewidth tunable lasers with retro-reflective external cavity, ***IEEE Photonics Technology Letters***, vol. 24, no. 18, pp. 1591 – 1593, 2012.
6. Feng Zhiqing, Bai Lan, **Wang Ning**, Gao Lei, Chen Bo, Zhang Xuming, Narrow linewidth Tunable Semiconductor Lasers Based on Dual lens External cavity Structure, Chinese Journal of Luminescence, vol. 33, no. 10, pp. 138-1142, 2012, in

Chinese.

7. Yeung Yu Hui, Guo'an Tai, Zhenhua Sun, Zihan Xu, **Ning Wang**, Feng Yan and Shu Ping Lau, n- and p-Type modulation of ZnO nanomesh coated graphene field effect transistors, ***Nanoscale*** 4, 3118-3122 (2012).
8. **Ning Wang**, Yupeng Zhang, Lei Lei, Helen L.W. Chan and X.M. Zhang, Photocatalytic microreactor using monochromatic visible light, ***Advanced Material Research***, vol. 254(2011), pp. 219-222.
9. **N. Wang**, L. Lei, X. M. Zhang, Y. H. Tsang, Y. Chen, and Helen L.W. Chan, A comparative study of preparation methods of nanoporous TiO_2 films for microfluidic photocatalysis, ***Microelectronic Engineering***, vol. 88, no. 6, pp. 2797–2799, 2011.
10. L. Lei, **N. Wang**, X. M. Zhang, Q. D. Tai, D. P. Tsai and Helen L.W. Chan, Optofluidic planar reactors for photocatalytic water treatment using solar energy, ***Biomicrofluidics***, vol. 4, no. 4, paper no. 043004, 2010.

Conference papers

1. **Ning Wang**, Ngai Yui Chan, Chi Man Luk and Xuming Zhang, Optofluidic microreactors for photocatalysis water purification, The 4th International Conference on Optofluidics (***Optofluidics 2014***), 28-30 August 2013, Guangzhou, P. R. China, ***Best poster award***.
2. Furui Tan, **Ning Wang** and Xuming Zhang, Visible-light photocatalysis using plasmonic coupling for optofluidic microreactors, The 4th International Conference on Optofluidics (***Optofluidics 2014***), 28-30 August 2013, Guangzhou, P. R. China.
3. **Ning Wang**, Ngai Yui Chan, Chi Man Luk and Xuming Zhang, Optofluidic microreactors using surface plasmon enhancement for photocatalysis water

purification, The 3rd International Conference on Optofluidics (***Optofluidics 2013***), 15-17 August 2013, Hong Kong, P. R. China.

4. Furui Tan, **Ning Wang** and Xuming Zhang, Bubble microreactors for photocatalytic water treatment, The 3rd International Conference on Optofluidics (***Optofluidics 2013***), 15-17 August 2013, Hong Kong, P. R. China.
5. Li Wan, Mengchun Wu, **Ning Wang** and Xuming Zhang, Photocatalytic water prification: Photon transfer and mass transfer limitation solved by planar microractors, The 3rd International Conference on Optofluidics (***Optofluidics 2013***), 15-17 August 2013, Hong Kong, P. R. China.
6. Mengchun Wu, Li Wan, **Ning Wang** and Xuming Zhang, Photocatalytic water prification: Photocatalysis performance of planar microractors enhanced by composite thin films, The 3rd International Conference on Optofluidics (***Optofluidics 2013***), 15-17 August 2013, Hong Kong, P. R. China.
7. **Ning Wang**, Ngai Yui Chan, Chap Hang To, Furui Tan and Xuming Zhang, Photocatalytic microreactors for water purification: Selective control of oxidation pathways, The 8th Annual IEEE International Conference on Nano/Micro Engineered and Molecular Systems (***IEEE-NEMS 2013***), 7- 10 April 2013, Suzhou, China.
8. **N. Wang**, Furui Tan and Xuming Zhang, Photocatalytic water purification using planar microreactor, Photonics Global Conference 2012 (***PGC 2012***)**,** 13-16 Dec 2012, Singapore.
9. **N. Wang**, Z. K. Liu and X. M. Zhang, Microfluidic solar reactor for photocatalytic water treatment, The 16th International Conference on Miniaturized Systems for Chemistry and Life Sciences **(*MicroTAS 2012***), 28 Oct - 1 Nov 2012, Okinawa,

Japan.

10. **N. Wang**, Z.K. Liu, and X.M. Zhang, Microfluidic platform for photocatalytic reactions using sunlight, The 6th Asia-Pacific Conference on Transducers and Micro/Nano Technologies (***IEEE APCOT 2012***), 8 – 11 July 2012, Nanjing, China, paper no. ac12000219, pp. 51.
11. **N. Wang**, Z.K. Liu, Helen L.W. Chan and X.M. Zhang, Microfluidic reactor for solar photocatalysis using $BiVO_4/TiO_2$ film, International Symposium on Integrated Functionalities (***ISIF2012***), 18 – 21 June 2012, Hong Kong, China, paper no. O504.
12. A. Q. Jian, **N. Wang**, K. Zhang, Y. Wang, Y.H. Tsang and X. M. Zhang, Optofluidic manipulation using continuous-wave laser, The 1st International Conference on Optofluidics (***Optofluidics 2011***), 11 – 13 Dec 2011, Xi'an, China (Best Paper Award).
13. **N. Wang** and X. M. Zhang, Optofluidic reactors for visible-light photocatalysis, The 1st International Conference on Optofluidics (**Optofluidics 2011**), 11 – 13 Dec 2011, Xi'an, China.
14. X. M. Zhang, **N. Wang**, L. Gao, M. Feng, B. Chen, Y.H. Tsang and A.Q. Liu, Narrowlinewidth external-cavity tunable lasers, The 10th International Conference on Optical Communications and Networks (***ICOCN 2011***), 05 – 07 Dec 2012, Guanzhou, China.
15. **N. Wang**, Y. P. Zhang, L. Lei, Helen L. W. Chan and X. M. Zhang, Photocatalytic Microreactor Using Monochromatic Visible Light, International Conference on Materials for Advanced Technologies (***ICMAT 2011***), 26 June – 1 July 2011, Singapore.
16. A. Q. Jian, **N. Wang** and X. M. Zhang, Micro-bubble generation using

continuous-wave laser, International Conference on Materials for Advanced Technologies (***ICMAT 2011***), 26 June – 1 July 2011, Singapore.

17. **N. Wang**, L. Lei , X. M. Zhang, D. P. Tsai and H. L.W. Chan, Solar-powered microfluidic photocatalysis, The 6th Annual IEEE International Conference on Nano/Micro Engineered and Molecular Systems (***IEEE-NEMS 2011***), 20-23 February 2011, Kaohsiung, Taiwan, R.O. China

Academic award

1. **Best poster award,** The 4th International Conference on Optofluidics (Optofluidics 2014), August 2014, Guangzhou, China, paper title: Optofluidics microreactors for photocatalytic water purification, authors: **Ning Wang**, Furui Tan and Xuming Zhang.

Acknowledgements

I would like to express my sincerest appreciation to my chief supervisor **Dr. Xuming Zhang** and co-supervisor **Dr. Yu Wang** in Department of Applied Physics in The Hong Kong Polytechnic University. Without their excellent guidance, constant encouragement and support during the past three years, it would be impossible for me to complete my PhD study. Their high requirement, profound academic insight and inspired discussions greatly contribute to the quality of my doctorial research.

I specially appreciate Dr. Lei Lei in School of electrical and electronics engineering in Nanyang Technological University, Singapore for his helpful encouragement and constructive suggestions on my research project.

I would also like to thank Prof. H. L. W. Chan, Prof. S. P. Lau, Dr. Haitao Huang and Dr. Dangyuan Lei in Department of Applied Physics in The Hong Kong Polytechnic University for their guidance on my doctorial research.

I also want to thank Prof. Xudong Fan in Department of Biomedical Engineering in University of Michigan for having hosted me for half a year for the oversea attachment program.

Besides, I would like to thank all the past and present group members for their great help and friendship, including Dr. Ming Feng, Dr. Zhiqing Feng, Ms. Tan Furui, Mr. Qingming Chen, Dr. Aoqun Jian and Ms. Yuki Lam. Special thanks go to my friends and colleagues Mr. Vincent Chan, Dr. Bolei Chen, Dr. Qidong Tai, Mr. Edwin Hui, Dr. Lili Tao, Dr. Jing Ye, Mr. Zhike Liu and Dr. Libin Tang for their great helps in my experiments.

Finally, I would like to thank my parents for their support on my study and life.

THE HONG KONG POLYTECHNIC UNIVERSITY

Table of Contents

List of Figures

List of Tables

CHAPTER 1

INTRODUCTION

1.1 Overview

In recent years, water resources around the world have been seriously polluted along with the rapid economic development. Water pollution is mainly caused by human activity, including industrial pollution, agricultural pollution and living pollution. Increasingly exacerbated problems caused by water pollution have been a significant security threat to human survival and become a major obstacle to human health, economic and social sustainable development. According to the survey from World authority, 80% of diseases spread due to unsafe drinking water each year in developing countries, resulting in the death of at least 20 million people worldwide. Therefore, water pollution is called "the world's number one killer", which also seriously affects industrial production, equipment corrosion and product quality. What is more, it affects people's lives, ecology and human health [1].

For a long time, it is believed that the tap water is safe and healthy. However, due to a variety of pollution, it cannot be regarded as healthy any more. A survey shows that tap water in the world contains as many as 2,221 kinds of chemical pollutants, some of which are recognized as carcinogens or tumor promoters. The composition of urban

wastewater is very complex, in addition to heavy metals, it still contains pesticides, fertilizers, detergents and other harmful residues, even after it is boiled, these residues are still flooding and even increasing the concentration of harmful substances. Boiling the water decreases the amount of dissolved oxygen which is beneficial to human health, but increases the content of carcinogens like nitrite and chloroform. Therefore, the safety index of drinking water is also not high [2].

Over the last decades, the water quality in some countries especially the developing countries continues to decline and the water environment persistently suffers from deterioration. As a result, water shortages and accidents caused by pollution continue to occur, which directly influences the development of industry and agriculture. All in all, water pollution leads to serious threat to the sustainable development of society and the survival of humanity [3].

Therefore, in view of the increasing demand of clean water and the deteriorating water supply in modern society, we must develop advanced and cost-effective water treatment technology to reclaim and reuse wastewater to increase the available water resources while suppressing the deterioration of water pollution. Reusing and recycling Wastewater is definitely a promising way to constitute the largest source of clean water. As a cycle of economic behavior, it has also been adopted by most of countries,

including the recycling of industrial wastewater and urban sewage. In the meantime, a large number of urban sewage is mostly flowed back to agricultural irrigation, industrial water, municipal use, groundwater recharge and so on. But the recovery is still impossible to accord with the health standards for drinking water.

Recycling wastewater is usually accompanied by health-threat coliforms, suspended solids and dissoluble organic compounds. It is often troublesome and expensive to dispose these contaminants. Water treatment technologies currently in industrial uses, such as adsorption and condensation focus on transferring them into other stages of contaminants, but still cannot be completely eliminated or destroyed [4]. Other conventional water treatment methods, such as precipitation, filtration, chemical and membrane technology, involve high operating costs and may flow into the ecosystem to cause secondary pollutants. Due to the increasing environmental awareness and regulations, these redundant and toxic pollutants have already raised serious concerns over the world. Without doubt, chlorination can effectively kill germs, but it can also produce more halogenated compounds which are the greatest pathogens of gastrointestinal cancer. Moreover, many dissolved toxic chemicals (such as dyes, pesticides, detergents) in the wastewater cannot be treated efficiently by the prevailing physical, chemical and biological water treatment methods [5], [6]. As a result, the

already-treated wastewater still contains some residual of contaminants and is usually discharged into rivers and seas for natural decomposition, causing a huge waste of water resources and also posing threat to environment.

In 1972, Fujishima found that irradiated titanium dioxide (TiO_2) particles could activate sustained redox reaction of water to produce hydrogen and oxygen, which inspired many researchers' interest in heterogeneous photocatalysis. Since then, photocatalytic oxidation technology has been widely appreciated and rapidly developed. As an excellent photocatalyst, with the merits of stable chemical characteristics, non-toxicity and low cost, titanium dioxide has attracted many scientists to explore its industrial applications [7], [8].

Since 1976, Carey etc [9] have successively reported some research work such as detoxifying PCBs to complete dechlorination by using turbid aqueous TiO_2 under near UV irradiation, photolysis process of diphenol, I^-, Br^-, Cl^-, Fe^{2+}, Ce^{3+} and CN^- by TiO_2 under the irradiation of a polymorphs pole xenon lamp and bactericidal action of TiO_2 under UV irradiation. Therewith, a large amount of in-depth research works indicated that the use of photocatalytic technology is not only capable of decomposing a variety of refractory organic pollutants, but also has good sterilization and suppression of viral activity and no harmful intermediates.

During last decades, photocatalysis has been merged into many application fields due to its ability of photoexcited oxidative, reductive and hydrophilic properties. The block schematic diagram in Fig. 1.1 presents the applications of TiO_2 by using its photocatalytic properties. For example, its decomposing capacity is currently popular with the industrial photocatalytic reactors serving for wastewater and air treatment. Its hydrophilic properties show strong application prospects in self cleaning of external coated tile or tent and anti-fogging of coated mirror and glass. Also, it shows good potential for regeneration and recycling of the energy, such as some of biochemical cofactors and methanol and so on [10].

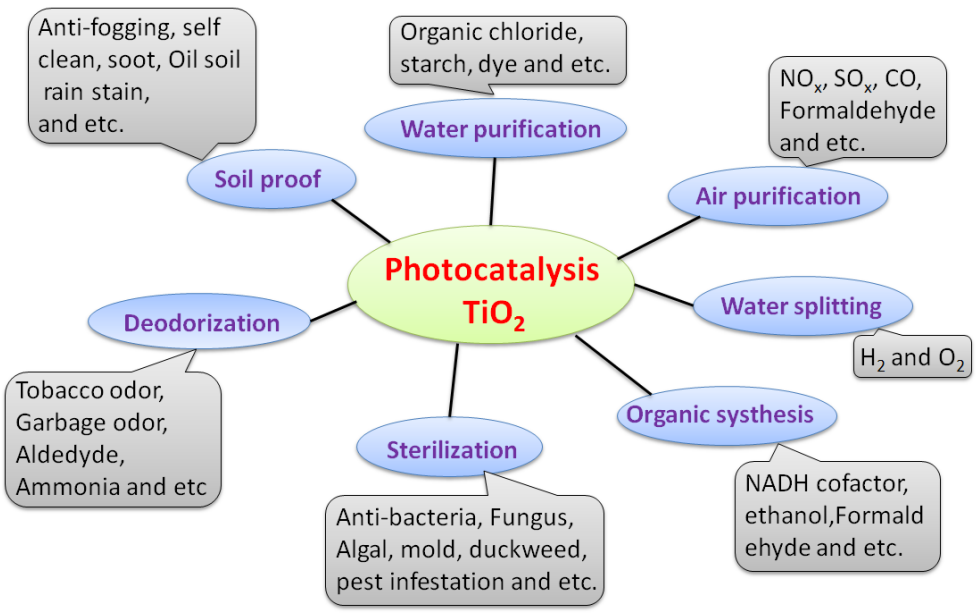

Figure 1.1 The applications of TiO_2 by using its photocatalytic properties.

Due to their excellent behavior, more and more photocatalytic products spring up to the market and our human's life. According to the report of BCC research (a leading market research company) in 2010, it showed that the global market of photocatalyst products in 2009 accounted for $ 848 million, and the compound increasing rate in 2014 was expected to reach 14.3% to nearly 1.7 billion in total revenue. Based on the statistics data, photocatalyst products for the construction sector in recent years always accounted for the largest market share. It is estimated that the revenue of $ 740.3 million in 2009 accounted for 87.4% in the total revenue, the amount of this sector is expected to grow by 14.5% to reach 1.5 billion in 2014. The market segment of consumer products in 2009 was 85 million and was expected to grow by 13.2% to reach $ 158 million in 2014 [11].

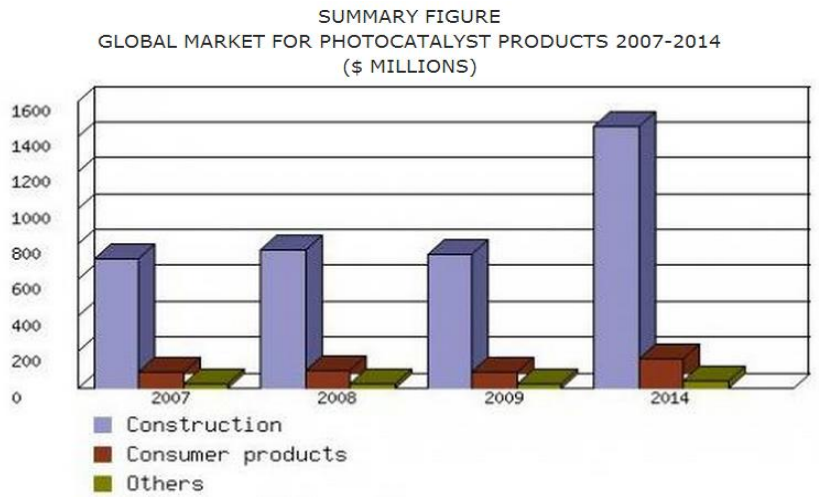

Figure 1.2 The summary of photocatalysis products from 2007 to 2014 (data source: BCC research 2010) [11].

All these data well show the marketing potential of photocatalyst products. This market diagram shows the distribution of overall industry but does not highlight the details about the nanoscale photocatalysts. Actually, during recent years the nanotechnology of photocatalysts has developed more rapidly than expected. Such trend will not change in the near future.

Gradually, the photocatalytic technologies stands out as a promising remedial solution for water purification since it can decompose/mineralize a wide range of organic pollutants into innocuous products (e.g., CO_2, H_2O) under the irradiation of UV or sunlight [12]–[15]. In recent years, a variety of photocatalytic reactors have been reported for water treatment [12], [16]–[20]. But the efficiency is still limited due to many technical challenges such as mass transfer limitation, photon transfer limitation, recombination of photo-excited electrons and holes, and low selectivity of photocatalysts to visible light.

Microfluidics, especially its subarea – optofluidics, may provide a quick solution to these problems. Optofluidics is an emerging field that aims to synergize optics/photonics and microfluidics to leverage the specific advantages of both disciplines [21], [22]. It has inspired the creation of many new devices for biological sensing and chemical analysis [23], [24], imaging [25]–[27], optical manipulation of

particles [28], energy conversion [2], [29], and photonic systems [30], [31]. Recently, some studies start to explore the optofluidic devices to capture and control the solar energy based on a fluidic process [32]–[40]. Among the foci of studies is the photocatalytic water purification [41], [42]. In fact, photocatalytic water purification is naturally an optofluidic system since it shares the same features of optofluidics: light, fluid and their interaction. In this thesis, "optofluidics" and "microfluidics" are used exchangeably as a microfluidic photocatalytic reactor is naturally an optofluidic reactor and the details will be introduced in chapter 3.

At the first glance, microfluidics and water purification seem in contradiction since the former is designed to deal with small volume of solutions while the latter requires large throughput. This mismatch can be bridged over by scaling up the microreactors. Or alternatively, using the microreactors for the application scenarios that do not need high throughput but require repetitive tests, for example, quick test of the photocatalysts, optimization of the operational conditions and rapid screening of various photocatalysts. Compared with the conventional bulk reactors that involve large reaction plates and complicated fluidic tubing, the use of microfluidics introduces immediate benefits such as small consumptions of photocatalyst materials and water samples, precision control of flow states and short test time. Moreover, the microfluidics has more profound

influence on the photocatalytic reactions in the various aspects such as mass transport, photon delivery, reaction site cleaning, new functionalities, and many others.

1.2 Objectives and organizations of thesis

Photocatalytic water purification utilizes light to degrade the contaminants in water and may enjoy many merits of the microfluidics technology such as fine flow control, large surface-area-to-volume ratio and self-refreshing of reaction surface. Although a number of optofluidic reactors have been reported for photocatalysis, there are still many limitations and problems which should be faced and solved for promoting its industrial development. It is the objective of this thesis to design and study the novel microfluidic planar reactors for photocatalytic water treatment.

In chapter 1, an overview of the applications of photocatalysis is presented and its developing potential is analyzed and forecasted. The objectives and organizations of the thesis are also discribed in this chapter.

Chapter 2 illustrates the mechanism and kinetics of photocatalysis and presents a literature review on the current reactors used for photocatalysis water treatement. Through the survey, the physical mechanisms that underpin the synergy of microfluidics and photocatalysis will be identified. The introduction of microfluidics

help overcome different problems in the bulk reactors such as photon transfer limitation, mass transfer limitation, oxygen deficiency, and lack of reaction pathway control.

Chapter 3 presents the first design, a novel planar microfluidic reactor used for decomposing methylene blue, which can overcome the limitations of mass transfer and photon transfer in the previous photocatalytic reactors (especially for bulk reactors) and can improve the photoreaction efficiency by more than 100 times. The microreactor has a footprint of $7 \times 2.5 \times 0.2$ cm^3 and a planar rectangluar recaction chamber (5 cm × 1.8 cm × 100 μm). TiO_2 nanoporous film is immobilized in the reaction as the photocatalyst. The fabrication will also be illustrated in details in this chapter. Then, the performance evaluation test is conducted by using methylene blue solutions as the degradation models. Through the experimental results, it can be demonstrated that optofluidic reactors inherit the merits of microfluidics such as large surface/volume ratio, easy flow control and rapid fabrication and offer a promising prospect for large-volume photocatalytic water treatment.

Chapter 4 presents the second design – an integrated microfluidic planar reactor for visible-light photocatalysis with the merits of fine flow control, short reaction time, small sample volume and long photocatalyst durability. One additional feature is that it enables to use both the light and the heat energy of the light source simultaneously. The

reactor consists of a $BiVO_4$-coated glass as the substrate, a blank glass slide as the cover and a UV-curable adhesive layer as the spacer and sealant. It has a planar reaction chamber ($10 \times 10 \times 0.1$ mm^3). A blue-light LED panel (footprint 10 mm × 10 mm) is mounted on the microreactor to provide uniform irradiation over the whole reactor chamber, ensuring optimal utilization of the photons and easy adjustments of the light intensity and the reaction temperature. This microreactor may provide a versatile platform for studying the photocatalysis under combined conditions such as different temperatures, different light intensities and different flow rates.

Based on the previous microreactors, chapter 5 reports the third and more advanced design – a photoelectrocatalytic reactor. It utilizes the photoelectrocatalytic effect to eliminate another fundamental limit of photocatalysis – the recombination of photo-excited electrons and holes, which can also be demonstrated to control the reaction pathway. All the setup, materials and light source are same with the microreactor presented in chapter 4. But for the glass slide top and bottom covers are replaced by ITO glass for generating a uniform electrical field across the reaction chamber. Both the positive and negative bias potentials are applied and investigated by decomposing methylene blue to evaluate the performance of photoelectrocatalytic microreactor. The negative bias exhibits always higher performance. The optimal

condition is found under -1.8 V and the degradation rate is independent of the residence time, and the limit of oxygen deficiency also might be solved accompanying with electrolysis. Synergetic effect of photocatalysis and electrocatalysis is also proved in this kind of microreactor.

In chapter 6, a general conclusion is drawn to describe the limitations of photocatalytic water treatment solved by the planar microreactors. And the future work is proposed in this chapter.

CHAPTER 2

BACKGROUND OF PHOTOCATALYTIC REACTORS

2.1 Mechanisms and kinetics of photocatalysis

2.1.1 Pricinple of photocatalysis

Photocatalysis is the combination of photochemical and photocatalyst, thus light and photocatalyst are the necessary conditions to promote the photocatalytic oxidation and reduction reactions. Photocatalysis can be divided into two types, depending on the catalysts absorpting photons: sensitized photocatalysis and direct photocatalysis. Sensitized photocatalysis utilizes sensitizer to absorb photons so as to transfer activated electron to the semiconductor catalyst. Direct photocatalysis directly utilizes semiconductor photocatalyst molecules to absorb photons, and for further oxidation and reduction processes. Currently n-type semiconductor oxides are mostly chosen as photocatalysts, which really depend on their own optical characteristics. The energy band structure of the semiconductor particles are generally composed by the valence band with low energy and the conduction band with high energy, between which are the forbidden band. Some popular photocatalysts have been extensively studied such as TiO_2, ZnO, WO_3, CdS, SnO_2, Fe_2O_3, In_2O_3 and so on. TiO_2 is the most popular

photocatalyst for industrial application because it is not only non-toxic and extremely stable but also very effective in the water phase, gas phase, and is even a non-aqueous solvent. Although there are various photocatalysts with different catalytic activities, the photocatalytic principles of the compound semiconductors are similarly consistent, especially for two popular semiconductor oxides ZnO and TiO_2, which are both n-type oxide semiconductor with roughly the same band gap. This section will mainly discuss the basic principles of direct photocatalysis [43]–[45].

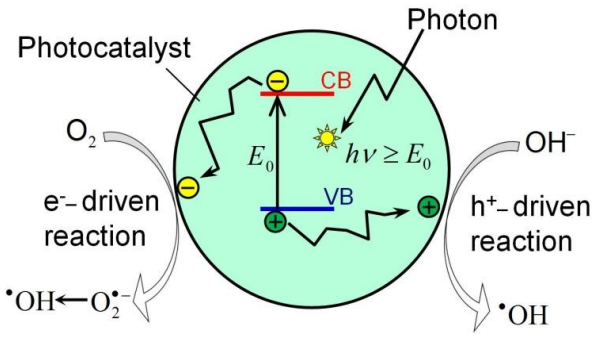

Figure 2.1 Basic principle of photocatalysis. The semiconductor photocatalytic nanoparticle absorbs a photon and excites an electron/hole pair. The electron and hole then migrate to the surface and initiate the reduction and/or oxidation to decompose the water contaminants.

Photocatalysis can be regarded as a series of oxidation and reduction reactions induced by photo-excited electrons and holes [13], [46], [47]. The basic principle of photocatalysis is shown in Fig. 2.1.

Generally, the incoming photon with the energy $h\nu \geq E_0$ is absorbed by semiconductor photocatalysts (SC, e.g., TiO_2, ZnO) to excite an electron to the conduction band, leaving a hole in the valence band. And the activation equation can be expressed by [43], [48]

$$SC + h\nu \rightarrow SC(e_{cb}^- + h_{vb}^+) \tag{2.1}$$

Here E_0 is the bandgap of the semiconductor photocatalyst, e.g., E_0 = 3.2 eV for anatase TiO_2, corresponding to the wavelength λ = 387 nm.

The excited holes can migrate to the surface of SC and then oxidize the adsorbed reactants via the reactions as expressed below,

$$h_{vb}^+ + OH_{ads}^- \rightarrow OH_{ads}^{\cdot} \tag{2.2}$$

$$OH_{ads}^{\cdot} + \text{reactant} \rightarrow \text{oxidized products} \tag{2.3}$$

This represents the hole-driven oxidation pathway.

Similarly, the excited electrons can migrate to the surface of SC too and thus can initiate a reduction reaction (e.g., $Hg^{2+} + 2e^- \rightarrow Hg^0$). Alternatively, the electrons can be captured by dissolved O_2 molecules and can also contribute to the oxidation through

different pathways,

$$e_{cb}^{-} + O_{2,ads} \rightarrow O_2^{\cdot -} \quad (2.4)$$

$$O_2^{\cdot -} + H^{+} \rightarrow HO_2^{\cdot} \quad (2.5)$$

$$HO_2^{\cdot} + HO_2^{\cdot} \rightarrow H_2O_2 + O_2 \quad (2.6)$$

$$H_2O_2 + e_{cb}^{-} \rightarrow OH^{\cdot} + OH^{-} \quad (2.7)$$

$$\text{reactent} + O_2^{\cdot -} (\text{or } OH^{\cdot}) \rightarrow \text{degradation products} \quad (2.8)$$

These form the electron-driven oxidation pathway. It is noted that the production of hydrogen peroxide (Eq. (2.6)) provides much more hydroxyl radicals (Eq. (2.7)), which have super oxidizability in the aqueous phase. Although both electrons and holes can lead to oxidation, some research studies have found that the electron-driven oxidation is apparently more efficient in degrading some organic contaminants (e.g., methylene blue dye).

2.1.2 Influence factors for photocatalysis reactions

The efficiency of photocatalytic reactors can be affected by many factors, such as nature of photocatalysts, light source, species of additive oxidants or reductants, properties of waste water, environment temperature, fluidic dynamics and thermodynamics, residence time in the reactor and so on, which should be taken into comprehensive consideration for the overall design and the operation of photocatalytic reactors.

a) Photocatalysts

Many materials have been employed as the photocatalysts for both research and industrial applications worldwidely, including titanium dioxide, zinc oxide, tin oxide, zirconium dioxide, cadmium sulfide and many other oxide and sulfide semiconductors, among which TiO_2 is most popular because of its strong oxidizing ability, chemical stability and non-toxicity. Early on, CdS and ZnO have been used more often as the photocatalysts. However, due to the unstable chemical nature, they are gradually dissolved under the irradiation and the eluted metal ions carry certain biotoxicity. Therefore, currently they are rarely used as civilian photocatalytic materials in developed countries except for limited utilization in some industrial catalysis fields. At this stage, research and industrial fields are mostly in enthusiasm on Degussa P25 TiO_2, which has also been wildly used as the reference model for other kinds of photocatalysts [49], [50].

First, as the most important factors of the efficiency of photocatalysts, their surface area, roughness and particle size directly determine the adsorption amount of the reaction substrate. Under the same lattice defects and other factors, the larger the surface area is, the more the adsorption amount is, leading to the faster reaction rate and higher photocatalytic activity. Second, photocatalytic activity of photocatalysts can also

be affected by the absorption of photons, separation of charge carriers and transfer efficiency of surface charges. The stronger the absorption is, the more the separating photo-excited electrons and holes pairs are, resulting in a greater probability for oxidation and reduction reactions. Third, crystal structure of photocatalyst can also affect their catalytic performance. For TiO_2, only the anatase phase and the rutile phase show photocatalytic properties, wherein the anatase has superior catalyticity. For bismuth vanadate ($BiVO_4$), the monoclinic phase is significantly superior to the other polymorphs. Fourth, hydroxy on the surface also affects the activity of catalyst via adjusting the light absorption and the electron-hole recombination. For example, the number of TiOH and of Ti^{3+} on the surface of TiO_2 plays an important role in the photocatalytic process. Finally, the loading configuration for the photocatalyst such as suspension and immobilization also strongly influence the reaction efficiency. This will be discussed in detail in next section.

b) Light sources

UV light, visible light and solar light are currently used for photocatalysis. Different photocatalysts must be matched with the proper light sources because the charged electron and hole pairs can only be excited by photons with the energy larger than the band gap （eg. E_g = 3.2 eV for TiO_2, $\lambda < 387nm$）. Currently, TiO_2 is often

accompanied with the UV light source including UVA, UVB and UVC (most often 365nm). For ecological and economical reasons, more and more research efforts have been made to develop the photocatalysts that absorb the visible light and solar light, such as $BiVO_4$ and doping TiO_2. However, the effect does seem as good as expected and has not been accepted by industrial applications [51]–[54].

It is more complicated for the relationship between irradiation density and photocatalytic reaction efficiency. At low light intensity and correspondingly low carrier concentrations ($<1*10^{-5}$ mol/m^2·s), the rate of oxidation of a particular compound is linearly proportional to light intensity, while at higher light intensity ($>2*10^{-5}$ mol/m^2·s) the rate is dominated by the second-order charge carrier recombination and has a square-root dependence on the light intensity. As one of the evaluation index of photocatalytic reaction, the photon utilization efficiency is dependent on the light density and the photocatalyst material. When the reaction rate is still proportional to the light intensity, it indicates the unsaturated state of photon absorption, which also stands for the optimal photon utilization efficiency.

Obviously, a photoreaction system with a good transparency is a prerequisite for the smooth photocatalytic degradation reactions. In most of the research work, the photocatalytic degradation models used to simulate the industrial wastewater often

possess the characteristics of low concentration, no impurities and good light transmission. However, the actual industrial wastewater often shows high concentration, more impurities, high turbidity and poor light transmission, which cause the difficulties to photocatalytic degradation reactions. Therefore, the photocatalytic degradation in real wastewater treatment system must be pre-treated to filter out the suspended solids in water to obtain a good light transmission. In addition, the light source must be suitably fixed to the reaction system for the best performance. The internal embedded light sources are often fixed at centre of the slurry reaction system. But for the immobilized reaction system such as fixed–bed thin film reactor, the light sources are often fixed outside and right above the reaction chamber to gain the best utilization of photons.

c) pH

Acidity or alkalinity is an important factor for the photocatalytic reactions by influencing the semiconductor photocatalyst including its surface charge, the band edge potential and the size of aggregates [55], [56]. In the process of photocatalytic degradation, organics with different structures can be most effectively decomposed under an optimal pH value. Many research studies have found that the maximum photodegradation rate often occurs near the zero point charge of photocatalyst, which depends on the pH value of the reaction environment, e. g., pH= 6.25 for P25 TiO_2. The

surface of the TiO_2 should be positively charged when the pH is less than 6 and negatively charged when larger than 6.

Generally, the reducing capacity of the conduction band electrons increases with the pH value. According to the Nernst's law, the energies of the band edges can be shifted by adjusting the pH value of reaction system, often 0.059 V per pH unit under ambient temperature. This indicates that higher pH value would make valence band holes of photocatalyst less active and conduction band electrons more potent.

d) Initial concentration of pollutants

Higher concentration of pollutants would result in reduction of active sites on the surface of photocatalyst [13]. Saturated adsorption of organic molecules on the surface of the photocatalyst is harmful to the reaction system. From the reaction kinetics of the Langmuir- Hinshelwood model, the photocatalyst reaction can be reduced to the zeroth order when the initial concentration of pollutants is larger than $5 * 10^{-3}$ M. However, the reaction shows the first order obviously when the initial concentration is controlled less than 10^{-3} M.

e) Temperature

Usually the photocatalytic water treatment is conducted at the ambient temperature without artificial heating because the reaction is mostly by photon activation. But the actual temperature of industrial wastewater is often higher than the room temperature

and the light source can also cause the variation of reaction temperature in a photodegradation system. Therefore, the temperature effect should be taken into account. In fact, some research studies have investigated and proved the effect of temperature on photocatalytic reactions. When the temperature of reaction is varied a little higher than the room temperature, the adsorption nature of photocatalyst surface would be improved and the thermodynamics of chemical reaction may be a beneficial. The photodegradation rate is usually increased over the reaction temperature range of 20 – 80 ℃, and goes down at larger than 80 ℃ due to the reduction of exothermic adsorption of reagents. Moreover, the increase of temperature often reduces the solubility of dissolved oxygen, which is adverse to a photo-oxidative reaction, especially for a closed reaction system [13], [57].

f) Additional oxidants and reductants

Oxidants are effective electron capture agents which can promote the photocatalytic oxidation. Many effective oxidants have been reported such as: O_2, H_2O_2, $S_20_8^{2-}$, IO_4^-, Fe_2O_3 and so on. In the system of catalytic oxidation, O_2 and H_2O_2 are absolutely ideal electron trapping agents because the reaction product is H_2O without any intermediate pollutants. Many research studies reported the dissolved oxygen as an important factor for photocatalytic reactions. It acts as a highly efficient electron acceptor to prevent the

recombination of charge carriers. For commercial uses, air is more economical, simpler and safer than the pure oxygen [58], [59].

Completely on the contrary, the presence of O_2 is adverse to the photocatalytic reduction because the reduction of metal ions is often activated and promoted by the organic electron donors. Therefore, the O_2 should be eliminated by other protecting gas such as N_2 or Ar for a photocatalytic reduction system.

g) Saline or Ion

Impact of water soluble salts on the photocatalytic degradation of organics is often complicated, dependent on the species of salts [60], [61]. The adsorption and the reactions may compete in the process of photodegradation. Some have reported that Cl^- can affect the photodegradation of some organic dyes.

2.1.3 Recombination of electrons and holes

Enhancement of the catalytic activity of the photocatalyst is generally attributed to the increase of specific surface area and the reduction of the recombination centres for the photogenerated electrons and holes. These have been mentioned in thousands of publications but the direct evidence for recombination has rarely been presented [62-65] .

Typically, the process of recombination of photogenerated carriers consists of the

radiative recombination and the non-radiative recombination. The former is characterized by the release of photons, which can be obtained by recording the fluorescence spectra. However, the non-radiative recombination is characterized by its release of heat due to the relaxation processes of electrons and holes. Normally, the non-radiative recombination is much faster than the radiative recombination, and thus the whole recombination can be attributed to the radiative recombination. It will be more helpful for the photochemical application of photocatalyst by studying the radiative recombination process.

TiO_2 has a high optical absorption coefficient and the electron-hole pairs induced emission is mainly located at the surface of TiO_2, therefore the densities of electrons and holes go down rapidly from the surface into the interior. Meantime, its destroyed surface periodic lattice results in an excess of surface energy, which causes the surface to adsorb some ions or polar groups from the environment to form the surface state. Electrons and holes located on the surface can recombine by the surface state (electron injection and capture). Meanwhile, the fabrication process can easily form oxygen vacancies inside the lattice of TiO_2 and may result in the indirect recombination process. It is important to study the complex recombination processes including both the indirect and the direct process.

The kinetics of electron-hole recombination may be affected by their recombination style. It generates one recombination centre when one electron-hole pair is excited by the photon energy. The recombining rate should obey the first-order law. However, if several electron-hole pairs are simultaneously exited on a photocatalyst particle, the recombination rate should obey the second-order law.

Take TiO_2 particles as an example, its absorption at 620 nm by the trapped electrons shows the second-order decay with a baseline component when it is analyzed by the femtosecond pump-probe diffuse reflection spectroscopy, which can be expressed as [66]:

$$\mathrm{Abs} = \alpha \left\{ \frac{e_0}{1+k_r e_0 t} + B \right\} \tag{2.11}$$

where α, e_0, k_r, t, and B, respectively, represent constant, the initial concentration of trapped electrons, the second-order rate constant, the time after the excitation pulse and the baseline component, which might be attributed to the electrons trapped in depth but without participation in the reaction.

2.1.4 Visible-light driven photocatalysis

a) Narrow-bandgap semiconductors

Some semiconductors with narrow bandgap such as CdS (2.15 eV)、Fe_2O_3 (2.12 eV)

and Cu_2O (2.10 eV) have been utilized for photocatalytic water treatment and water splitting due to their visible-light-responsive properties, simple structure and easy preparation [67]–[69]. After that, many researchers have attempted to fully activate the UV-Vis response of these narrow-bandgap semiconductors by modifying them and combining them with TiO_2, which can help investigate the interface effect of both surface and bulk phase compounds.

However, many narrow-bandgap semiconductors become unstable under the irradiation of UV-visible light, causing the light corrosion. For example, there are some reactions under long-time irradiation in the photocatalytic aquous suspension system of CdS, in which CdS can be transformed to Cd^{2+} by the hole of valence band.

Many studies have reported that the monoclinic $BiVO_4$ (M-BVO) has a stable photocatalytic ability under visible light (< 517 nm) because of its small bandgap (< 2.7 eV) and high charge mobility [70]. Mingce Long et al. combined BVO with Co_3O_4 to form a heterojunction for photocatalysis and obtained a significant enhancement of photocatalytic activity in the phenol degradation as compared to the pure BVO.

b) Doping ions

Due to the popularity of TiO_2 in the industrial photocatalysis field, many research efforts have been made to dope the ions into TiO_2 to enhance its photocatalytic

performance under both UV and visible light. Doped ions normally get into the lattice of TiO_2 by substitution or caulking, which would vary not only the optical response range of materials but also their crystalline structures, chemical stability and photocatalytic performance. For example, some cations (V^{5+}, Cr^{3+}, Mn^{3+}, Fe^{3+}) [71] have been injected to replace Ti^{4+} in TiO_2 lattice, leading to the absorption of visible light. However, the current research work shows more interests on anion-based injection [72], including C^{4-}, N^{3-}, F^{-}, P^{3-} and S^{2-}. Although these ions are unable to absorb visible light directly, they can be easily adsorbed onto the surface of metal oxides via weak coordination and can generate new electron donor level above the valence band of metal oxide from the 2p orbital of S or N, leading to weak visible light absorbance. These electron-rich atoms can be easily activated and the activated electrons can be smoothly injected into the conduction band of TiO_2 under visible light irradiation, which are ultimately transferred to O_2 or other electron acceptors. In short, the interaction between TiO_2 and these anions could induce visible light absorbance and consequent activation of the substrates.

c) Dye sensitization

To modify wide bandgap semiconductors, photosensitization is one of the important methods to render them the capability to absorb visible light. Currently, dye

sensitization technology has been widely studied. It combines wide bandgap semiconductor materials with some specific organic dyes, humic acid, polyunsaturated fatty acids and other compounds, which are capable of absorbing visible light to form compound photocatalysts with visible light response. As long as the excited state potential of these substances is more negative than the conduction band of the semiconductor, it is possible to transport the visible-light excited electrons to the conduction band of the semiconductor and ultimately transfers them to an electron acceptor (e.g., O_2) [73], [74]. Meanwhile, the positive charge is left on the dye molecules to produce Dye^+ free radicals, which can indirectly drive the transformation of the substrate to the product via the catalytic cycle of an organocatalyst. During the process, the excitation wavelength of the wide bandgap semiconductor is expanded to the visible range of light.

Commonly used photosensitizers include ruthenium pyridine complex, erythrosine B, fluorescein derivative, thionine (Lloyd purple), eosin, rose red, leaf green acid and so on. But metal-based photosensitizers such as ruthenium pyridine complex are reported and studied more extensively due to their high efficiency and good stability.

Although a lot of work related to the photosensitive photocatalyst has been conducted, it still faces the problem of low photoelectric conversion efficiency, which is

mainly attributed to that the excited electrons injected into the conduction band of semiconductor from the excited state of dye can go reverse recombination. In addition, the method of dye sensitization also shows some other disadvantages: (1) the sensitizer occupies a large surface of the adsorption sites of the semiconductor material and affects adversely the photocatalytic performance, especially when it is applied in organic pollutant treatment, because the competitive adsorption between the organic pollutants molecules and the sensitizer should be taken into consideration. (2) the photosensitizer is easily lost from the catalyst surface, resulting in a decrease of photosensitive capacity. It also generates the secondary contamination when the contaminants are from the polluted water [73].

d) Plasmonic enhancement

Plasmonic photocatalysis has recently come into focus as a very promising technology for high-performance photocatalysis [75]–[80]. It involves dispersal of noble metal nanoparticles (mostly Au and Ag, in the sizes of tens to hundreds of nanometers) into semiconductor photocatalysts and obtains drastic enhancement of photoreactivity under the irradiation of UV and a broad range of visible light.

Under visible light irradiation, electrons below the Fermi level (E_f) of the plasmonic nanoparticles (NPs) will be excited to the surface plasmon (SP) states,

leaving positive charges (h^+) below E_f. Since plasmonic NPs are commonly supported on the surface of metal oxide, the SP state electrons will be injected into the conduction band (CB) of the metal oxide, and ultimately transferred to electron acceptors such as O_2. Meanwhile, the left h^+ would be quenched by the organic substrate to complete the photocatalytic cycle. To comprehensively understand the functionality of a plasmonic photocatalyst, both the properties of plasmonic NPs and metal oxide support should be taken into consideration. In addition to stabilizing plasmonic NPs and shuttling electron transfer, the metal oxides also possess surface acid-base properties, which can facilitate the formation of product for the overall heterogeneous reaction processes. In addition, metal oxide supported Au, Ag, and Cu NPs are excellent heterogeneous catalysts for thermally induced redox conversions, which also benefits the plasmonic photocatalysis.

For example, in the TiO_2 film embedded with Au nanoparticles, the Au nanoparticle is able to absorb visible light, independent of the absorption of the UV light by the TiO_2 nanoparticle itself. Due to the localized surface plasmon resonance (LSPR) created in response to the electromagnetic field of the incident light, the Au nanoparticle drives a collective oscillation of the electrons, which excites more electrons and holes by energy transfer and/or charge carrier transfer. This is the essential and distinctive mechanism of plasmonic photocatalysis and enables the creation of active

electrons and holes in the TiO_2 nanoparticle even in the absence of any light absorption by TiO_2.

2.1.5 Photoelectrocatalysis

Photoelectrocatalysis is a special heterogeneous catalysis, which can accelerate photoelectrochemical reactions by selecting specific semiconductor serving as photoelectrode or changing the surface state of the photoelectrode. Here it can be vulgarly understood that the electron-hole pairs generated by reaction between light irradiation and the interface of electrolyte / photocatalyst are separated by the internal and external electrical field and react with the ions in the reagent [81], [82].

It is well known that the holes and electrons can recombine quickly and release heat. Another simple recombination under irradiation can be expressed as:

$$2H_2O + 4h^+ \rightarrow O_2 + 4H^+ \quad (2.12)$$

$$O_2 + 4H^+ + 4e^- \rightarrow 2H_2O \quad (2.13)$$

Obviously, the separation and recombination of electrons and holes are completed by the same species but without transferring the energy to the organics and the decomposition reactions, forming a meaningless short circuit on the surface of photocatalyst shown in Fig. 2.2

To complete the photocatalytic process, the other half-reaction should be enabled

by the oxidative species and the organics as shown in equations (2.2) and (2.3), the principle can be referred to Fig. 2.1.

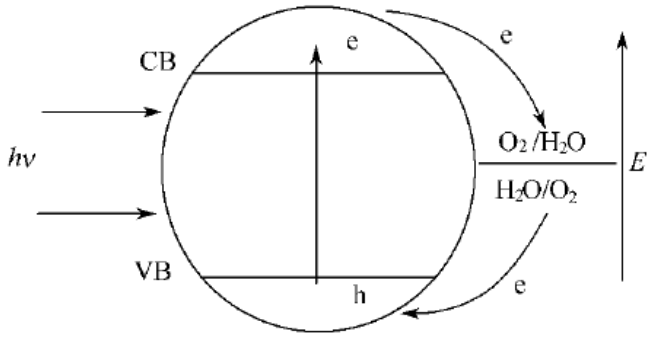

Figure 2.2 Schematic diagram of short-circuit cell with TiO_2 as the photoeletrode [83].

In fact, the probability of forming a short circuit cell on the catalyst surface is much larger than that of the degradation reactions, leading to a relative low photon utilization efficiency. To improve the efficiencies of photocatalytic degradation and photon utilization, some methods should be employed to eliminate the phenomenon of short circuit cell. Since the electrons and the holes accompany with each other with equal quantity, the simple recombination would certainly occur. However, if there is an applied external voltage force them to move toward different directions, the possibility of recombination would be greatly reduced, which ultimately promises an improvement of the photocatalytic efficiency, the principle can be seen in Fig. 2.3.

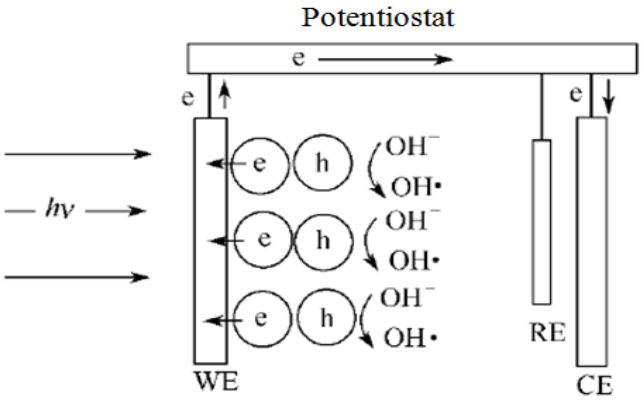

Figure 2.3 Basic principle of photoelectrocatalysis [83].

In summary, the photoelectrocatalytic method aims to achieve the following objectives: (1) the electrode can act as a catalyst carrier and thus avoid after-separation of catalyst, simplifying the reuse and recycling procedures; (2) under the effect of external electrical field, the reduction of recombination will extend the lifetime of the holes, which greatly improves the efficiency of the degradation of organics.

2.1.6 Thermal photolysis

Catalytic reaction and photochemical reaction can be simply described by:

$$A \xrightarrow{K} B \tag{2.14}$$

$$A \xrightarrow{h\nu} B \tag{2.15}$$

$$\Delta F = -RTln\frac{[B]_e}{[A]_e} = -RTlnK_e \tag{2.16}$$

where *A*, *B*, *ΔF*, *R*, *T* and K_e, respectively, represent the reactant and the reaction product, Gibbs energy change, gas constant, reaction temperature and reaction rate constant.

For the thermal catalytic reaction (2.14), the catalyst (*K*) is defined as the media that can increase the rate of reaction but without changing the reaction equilibrium at a certain temperature. From the thermodynamic point of view, the driving force of the reaction is just the thermal energy in the catalytic reaction and may be limited to some reactions based on thermodynamics. For the photochemical reactions, the light energy can be used to achieve a chemical reaction directly. The reaction needs to overcome the potential energy barrier. The photochemical reaction is usually "quantum" or "threshold" reaction and the light energy is absorbed by a single quantum. Quantum energy should exceed the threshold of the reaction barrier. According to two rules in photochemical reactions: (1) only the photons absorbed by substance can induce the photochemical variation; (2) quantization activation rule, the absorbed light activating a molecule at the beginning of the photochemical reaction is referred to as a quantum of light, and therefore the quantum yield of the sum must be equal to 1 [82].

If the absorbed energy are all used for the reaction, ΔF in equation (2.16) will increase with the transfer of oxygen into ozone. Or inversely, if the light energy

absorbed by the reaction system is transferred into heat energy and is then released, ΔF will decrease. Photocatalytic reaction should be the combination of photochemical and thermal catalytic reaction, which means that the reaction should be kept with both light and heat at the same time. Hence, according to the reaction equation (2.15), the reaction of equation (2.17) should include all those reactions that increase ΔF, as expressed by:

$$A \xrightarrow{hv,K} B \qquad (2.17)$$

From this view point, some reactions not allowed under mild conditions can be carried out in the thermodynamical scope. Obviously, this is contradictory to the definition of catalysis. But most researchers still prefer using the reaction equation (2.17) to define the photocatalytic reactions.

2.2 Major designs of current photocatalytic reactors

2.2.1 Principles of designing a photocatalytic reactor

Heterogeneous photocatalysis for pollutant treatment mainly focuses on two distinct areas. On one hand, many research workers concentrate upon semiconductor photocatalysts and try to improve their catalytic performance by material modification. Most researchers preferred to improve the photon utilization efficiency by doping some elements (C, N, etc.) into TiO_2, causing a red shift of light absorption band, to absorb

and utilize visible light. Interface effects in some synthesied compound photocatalysts can also cause the separation of electrons and holes. Some semiconductor photocatalysts that can directly absorb visible light have also been used for visible light photocatalysis. However, due to the unsatisfactory performance and efficiency, these photocatalysts are not ideal for large-scale industrial applications [17].

On the other hand, in order to verify the photocatalytic characteristics of these semiconductor photocatalysts, another critical factor should be taken into consideration. This is the photocatalytic reactor. The design and setup of the photocatalystic reaction system determines the overall photoreaction efficiency directly. Some configurations of photocatalytic reactors in the laboratory bench scale have been demonstrated to work efficiently for pollutants treatment, which also paves the way to industrial scale applications. Actually, the process of scaling up the photocatalysis reactors is extremely complicated and needs to consider not only the production technology but also the economic cost.

Beyond that, many other aspects should be taken into comprehensive consideration for designing a photocatalytic reactor, which include the geometry of reaction chamber, the distribution status of photocatalysts and the setting of light source. For a scaled reactor, some more should be considered such as the concentration of pollutants, the

throughput and the irradiation density. Some detailed aspects have been distinctively highlighted for a photochemical reactor by Cassano et al. when compared with the conventional chemical reactors [84]. First, the reactor geometry must be designed according to the irradiation range and the intensity of light source. Second, the photocatalyst can be suspended or immobilized in the reactor, which should be chosen to be most beneficial for the reaction system. Finally, the light source directly influences the performance of photocatalytic reactors by many elements such as efficiency of output power, utilization of spectrum, geometry, cooling system and other auxiliary equipment for increasing the light utilization efficiency. For a configuration of photoreactor for the polluted water treatment, it is especially important to satisfy all these requirements.

2.2.2 Classification of photocatalytic reactors

A wide range of photocatalytic reactors have been developed and used in both basic research and pilot scale studies. They can be classified by the specifications in different aspects [85].

a) Spectral range of irradiation source: The spectrum of irradiation source is a major effecting factor for photocatalytic reactors. Currently, most photocatalytic reactors can be irradiated with UV lamps (UVA, UVB and UVC), visible light (monochromatic and

UV-excluded) and solar light (concentrating and nonconcentrating). In fact, the light source must match with the absorbing spectrum of photocatalyst. Then the UV light are often used for the semiconductor photocatalysts that absorb the wavelength less than 400 nm, such as TiO_2 and ZnO. Because the proportion of UV in the solar light is only 4~5%, this inspires the exploration of visible light photocatalysis. Some research reports the monochromatic light or UV-excluded light to investigate the different photocatalysis mechanisms such as plasmonic enhanced photocatalysis. As the cleanest and greenest natural energy, the solar light becomes undoubtedly the most popular light source for industrial photocatalysis applications. Concentrating solar light is often used for higher irradiation intensities over one sun.

b) Position of light source: The photoreactors can also be distinguished by the position of the light source. Different reactors with different configurations need adjust the most suitable position for the light source including inserting, external and distributed. Most reactors of suspended system are often fixed with an immersing light source to improve the photon utilization efficiency. For many microsized reactors and fixed–bed reactors, the light sources which are difficult to be fixed in the interior are often located outside the reaction chamber. There are some other reactors fixed with distributed light sources, which can transport the light energy to the reaction area by some media such as light

guides and reflectors.

c) Loading state of photocatalyst: Photocatalytic reactors are most commonly divided according to the loading state of the photocatalyst in the reactor which are suspended (slurry) or immobilized on a support.

In the slurry reactors, the photocatalyst nanoparticles are suspended in the aqueous phase to gain the maximum surface area. But in the immobilized photoreactors, the photocatalyst are often loaded on a fixed support in the reaction chamber such as optical fibers, glass tubes, glass plates and so on. The advantages and disadvantages of these two kinds of photoreactors will be introduced in details in the next section.

2.3 Photocatalytic reactors for water treatment

Undoubtedly, reactor designs play a crucial role in tackling these limiting factors of photocatalysis and have attracted numerous efforts in the last thirty years [43], [86], leading to a number of innovative reactor designs such as optical fiber based photoreactors, fluidized bed reactors [10, 11], thin film bed sloping plate reactors [3], and many others that will be introduced with more details in following section. Most are referred as bulk reactors due to the large dimension of the reactor systems. Generally, the bulk reactors can be classified into two main types, depending on the formations of

photocatalysts: (1) *slurry reactor*, in which the photocatalyst nanoparticles are suspended in water samples to form a slurry (see Fig. 2.4); and (2) *immobilized reactor*, in which the photocatalyst is immobilized on the substrates in the form of film coating (see Fig. 2.4). The former has large surface area to volume ratio (SA:V) and enjoys fast mass transfer, but the absorption and scattering by the suspended photocatalyst nanoparticles cause a non-uniform distribution of light and thus low photon transfer. In addition, the suspended nanoparticles need to be filtered out after the purification, increasing the operation difficulty. In contrast, the latter type has good photon transfer and needs no post-filtration, but the low SA:V causes a slow mass transfer.

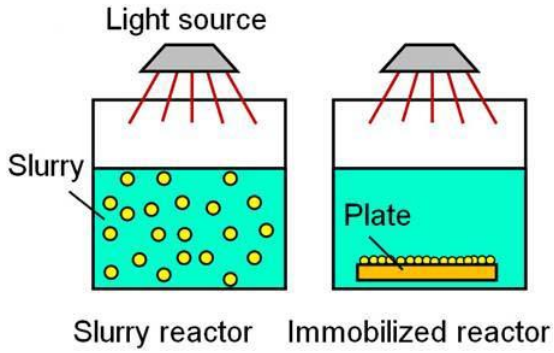

Figure 2.4 Typical bulky reactor designs – slurry reactor and immobilized reactor.

2.3.1 Slurry photocatalytic reactors

a) Annular reactor [87] usually consists of two concentric tubes and the inner tube is usually transparent to an installed light source. If the UV light source is used, usually

quartz glass containers should be employed to avoid the absorption of the light source. And the waste water mixed with the suspended photocatalysts is flowed through the annular reactor from the middle of the two tubes, which can be treated after irradiation. The advantage of this geometry is to provide symmetrical radiation field for the photocatalytic reactions. Such reactors have been widely used in laboratory scale experiments, they have also become attractive in the industrial applications because of the easy operation and simple structure.

b) Fluidized bed reactor [88] generally utilizes the upward flow generated by a fluid (gas or liquid) to keep the stationary phase of photocatalyst under a suspended or "fluidized" state, then the reagent can contact with photocatalyst sufficiently. As shown in Fig. 2.5, this kind of reactors presents the advantages of low pressure drop, high throughput and high surface area, thereby increasing the interaction between the catalyst reactants. The irradiation is often non-uniform for this kind of reactors.

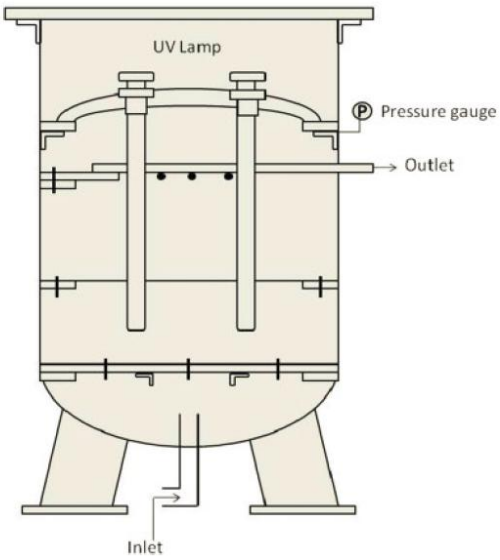

Figure 2.5 Schematic of fluidized bed reactor [88].

c) Membrane reactor [89] involves a well-mixed annular and batch slurry system integrated with hollow-fiber membranes, which possess ultra-filtration capabilities. This kind of reactors allows the separation of photocatalyst from the waste water as well as recycling the photocatalyst to the reactor.

d) Swirl flow reactor [90] is constituted by two circular glass plates. Aqueous suspension of photocatalyst particles is injected into the internal space between the two pieces of glasses along the tangential direction of outer edge of the reactor and flows out from the central hole of the top piece. The vortex generated inside the device can promote the mixing of the photocatalyst suspension. The reaction system provides a good mud mixing function and the non-uniform irradiation leads to a complex model.

e) Taylor vortex reactor [91] is composed of two coaxial cylinders, which have a similar geometry of the annular reactor. The suspension of the photocatalyst can freely flow into the annular channel. Similarly, the light source is mounted in the inner center tube, whose rotation can cause instable vortex in the suspension. Due to the limited irradiating distance of the light source, periodical irradiation on photocatalyst particles is thereby induced, which can be easily understood that a circular locus centered on the vortex nearby the light source is irradiated and the semicircle far from the light source is irradiated less or has no irradiation. Therefore, the photocatalytic reaction may not occur in this area. The advantage of this reactor is not only larger mass transfer caused by the vortex but also higher utilization of the photocatalyst as compared to the conventional slurry reactors. The drawback is the complexity of its moving parts.

f) Falling film slurry reactor [92] also has a central light source. The photocatalyst suspension is pumped into the upper side of the reactor from a storage container below and then falls along the wall parallel to the light source, forming a thin film dropping from top to bottom, and causing a uniform and sufficient light radiation. After that, the aqueous suspension solution flows back to the storage chamber. This process continues until the end of the reaction cycle. The advantages of this kind of reactor is that the photocatalyst is not in direct contact with the light source section to avoid an

intermediate product covering the surface of light source, which can cause unnecessary side reactions and blocking of light.

g) Rotating drum reactor [93] consists of three cylindrical containers, the weir-shaped paddles are distributed along the longitudinal direction of the container and the external lighting source as shown in Fig. 2.6. Rotation of the cylindrical container is driven by three electric motors. And three pairs of fixed UV lamps adjacent to each other are mounted on the reflector mirrors and enclosed in a wooden box to avoid the influence of ambient light. The UV light can be cooled by the free air flow between the gap of reactor and light tube. Suspension photocatalyst solution can flow from the inlet and flow through the three rotating drums and then flow out from the outlet.

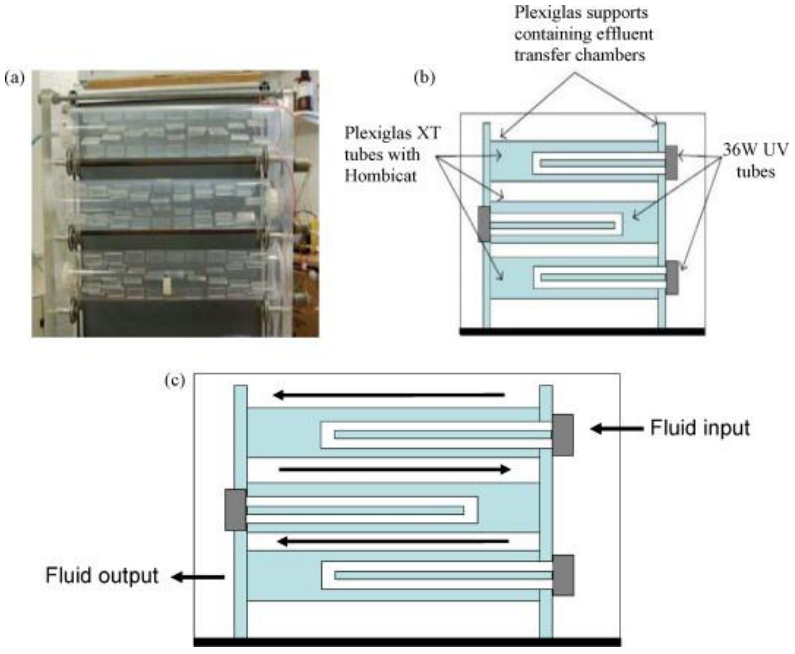

Figure 2.6 Schematic of rotating drum reactor [93].

2.3.2 Immobilized photocatalytic reactors

a) Falling film immobilized reactor [94] is different from the falling film slurry reactor as already discussed in the last section. It is coated with an immobilized photocatalyst film on the internal column wall and the thin descending film of polluted water can flow between the central wall of reactor and photocatalyst film. Like the slurry reactor, the light source is inserted into the central field of the reactor to provide a uniform irradiation on the photocatalyst film. The thin aqueous film can also ensure the penetrating capability of the light source. The immobilized reactor configuration may only activate and utilize the surface of photocatalyst films.

b) Optical fiber based reactor [95] is designed by using optical fiber as both the photocatalyst support and the light carrier. The photocatalysts is loaded and immobilized on the surface of optical fiber. Then a mass of coated optical fibers are gathered to form an optical fiber bundle. The light source can be remotely controlled and the light can be coupled from the end of the optical fiber bundle to transport to the reaction region. This design can promise the photocatalyst with minimum scattering loss and uniform irradiation. However, there are some limitations for this design. If TiO_2 is used as the photocatalyst for this design, the optical fibers should be quartz-based.

c) Hollow tubes reactor [96] is composed of a large cylindrical container and several hollow quartz tubes whose external surfaces are coated with photocatalyst. These hollow tubes are inserted into the cylindrical container and form a tube array. Actually, this design is similar with the optical fiber based reactors. The light source is also fixed at the end of the tube array to transport the light into the reactor. For better utilization of the light source, a lens and an aluminium reflector are employed and fixed at the end of the tube array. The polluted water flowing through the reactor acts also as the cooling reagent for the heat exchanger.

d) Thin film fixed-bed sloping plate reactor [97] has a simple configuration. The most important part in the reactor is the planar substrate coated with photocatalyst thin film, which is obliquely fixed toward to the light sources such as artificial light source or natural solar light. The polluted water is pumped to the top of coated plate and then flow through the thin film with a thin liquid film, which also guarantee a good photon receiving capacity. The treated polluted water is collected at the bottom of coated plate. Fig. 2.7 shows a pilot-scale photocatalytic reactor. Four glass plates are coated with TiO_2 by the spray method and fixed on a large substrate with a slope of 20 degrees under the irradiation of solar light. In term of irradiation area, this configuration is no doubt much larger than the others.

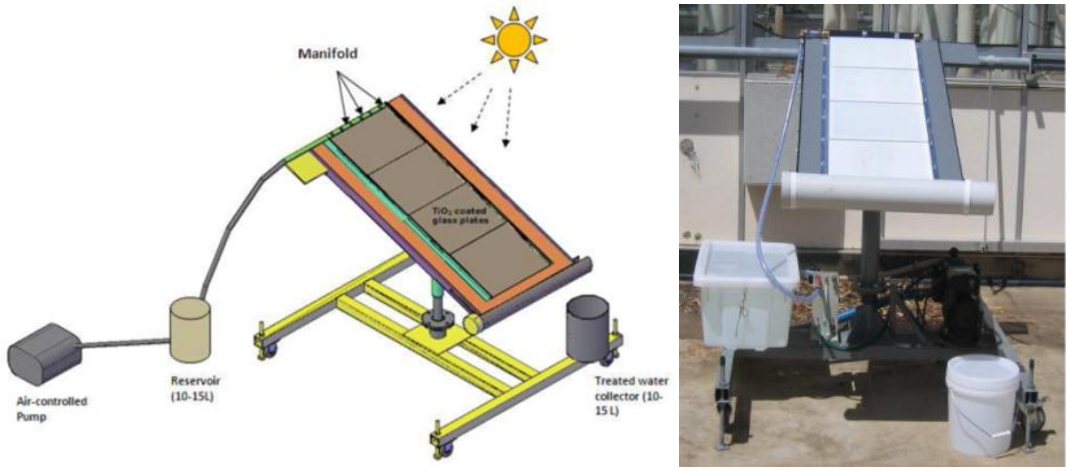

Figure 2.7 Schematic of thin film fixed-bed sloping plate reactor [97].

e) Rotating disk reactor [98] is composed of a high-speed rotating disk coated with photocatalyst film and controlled by a coaxial motor. The light source is fixed right above the disk with high spinning speed. The fluid on the surface can be accelerated by high centrifugal force to form a thin fluid film with high flow rate, which is expected to enhance the mass transfers and photon transfer. As shown in Fig. 2.8, it is a multilayer rotating disk reactor including four aluminium disks coated with TiO_2 and irradiated with UV light. The reagent flows into the reactor from the top inlet and forms liquid film with high rotating velocity and low thickness on each disk. Under the UV irradiation, the liquid film can be quickly treated due to the hydrodynamic.

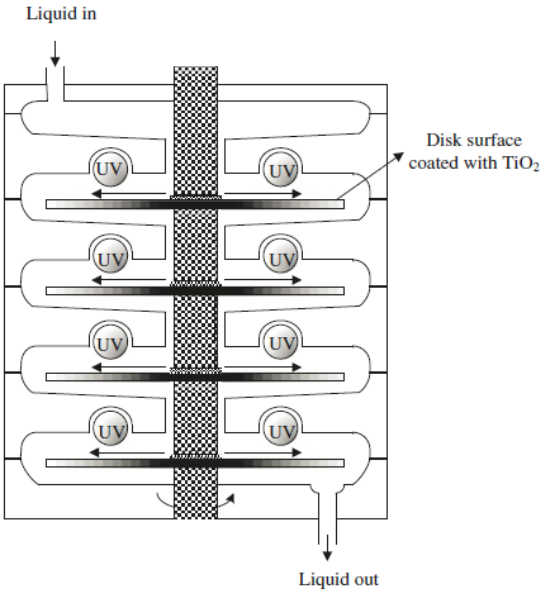

Figure 2.8 Schematic of multi-layer rotating disk reactor [98].

f) Spiral glass tube reactor can be simply understood with a spiral tube coated photocatalyst on its inner wall warping around a light source. The purpose of this design is to prepare irradiation area for the reactor and contact area between fluid and photocatalyst to enhance the mass transfer and photon utilization efficiency as high as possible.

g) Tube light immobilized reactor [99] is different from the others in the aspect of coated substrate. The photocatalyst is coated on the external wall of the light tube and then the coated light tube is inserted into a vessel. Several U-shaped UV light tubes coated with TiO_2 are enclosed into a stainless steel container.

h) Photocatalytic membrane reactor is a kind of device that integrates the merits of photocatalysis and membrane technology. As presented by Sylwia's research work [100], a novel photocatalytic membrane reactor was used to decompose dye by combining the TiO_2 photocatalyst with direct contact membrane distillation. It evaporates volatile organic and lets pass through a porous hydrophobic membrane coated with TiO_2. In the process, the mass transfer through the membrane pores is driven by the vapor pressure difference between across the membrane and the gas phase is maintained inside the pores of the membrane.

j) Corrugated plate reactor [101] is similar with the configuration of plate fixed-bed reactor. However, the difference is that the surface of substrate is not a smooth plane but a corrugated plate. This enlarges the surface area of the photocatalyst to enhance the photocatalytic performance of the reactor.

2.4 Major limitations for current photocatalytic reactors

Based on the above survey, photocatalytic water purification is currently facing several major limitations, such as low mass transfer efficiency, low photon transfer efficiency and deficiency of dissolved oxygen [13]. The mass transfer efficiency affects how easy the contaminant particles are moved to the photocatalyst surface (mostly determined by

the surface area per unit volume, namely, SA:V) and how fast the redox products are removed (affected by the desorption, diffusion and stirring). The photon transfer refers to how to deliver the photons to the photocatalyst reaction sites, a uniform irradiation is often required for better utilization of the photons [13], [102]. For the dissolved oxygen, the electron-driven oxidation consumes oxygen, and thus the limited concentration of naturally dissolved oxygen in water (typically 10 mg/l at room temperature and 1 atmosphere) would affect the photodegradation.

Various reactors have been attempted to break these limitations. For example, spin disc reactors [103] were designed to overcome the mass transfer limitation, optical fiber based reactors [104]–[106] were used to tackle the photon transfer limitation, and some reactors injected H_2O_2 or O_2 to solve the oxygen deficiency [107], [108]. However, most of them aim at either one aspect or two, but none could get rid of all the limitations.

2.5 Benefits of microfluidics to photocatalysis

Microfluidics technology employs microstructures to handle small volume of fluids and exhibits remarkable capabilities in fine flow control, wide tunability and parallel analysis [109]–[111]. Its great success in bioanalysis and drug discovery has triggered a

boom of research to apply microfluidics to other areas, one of which is the photocatalysis.

The microfluidics could bring in many benefits to the photocatalysis. The prominent ones are described below.

(1) Large surface area: Microfluidic structures have inherently large SA:V due to the small volume of fluid [40], [102], [108], typically in the range of 10,000 – 300,000 m^2/m^3, at least two orders of magnitude larger than the bulk reactors (typically < 600 m^2/m^3) [43], [47], [86], [106]. For this reason, significant enhancement of the reaction rate has been observed in the microfluidic reactors (called *microreactors* hereafter) as compared to the bulk reactors. It is noted that SA:V here refers to the nominal surface area of the water sample over the water volume. For a microreactor with a rectangular bottom and a height *h*, it has SA:V = 1/*h*. In an real microreactor, SA:V could be much larger if the photocatalyst film is nanoporous.

(2) Short diffusion length: The microfluidic layer is typically very thin (10 – 100 μm), making it easy for the organic pollutants to diffuse to the reaction surface.

(3) Uniform residence time: The flow in microfluidic structures is typically laminar. This is not ideal for diffusion, but it ensures almost the same residence time (i.e., the time for the water sample to flow through the reactor, equivalent to the photocatalytic

reaction time) and thus an equal level of degradation for different parts of the microflows. As the reaction rate (i.e., the percentage of pollutants converted per unit time) decreases with longer residence time, an even distribution of residence time helps maximize the throughput (the processed water volume per unit time) at a targeted degradation percentage (i.e., how much percent being degraded [48]).

(4) Uniform illustration: The microreactors usually have an immobilized photocatalyst film under the thin layer of fluid, resulting in an almost uniform irradiation over the whole reaction surface and thus a high photon efficiency. This is because the reaction rate constant of semiconducting photocatalysts is usually proportional to the square root of power density [13].

(5) Short reaction time: The combination of above factors drastically improves the reaction speed and thus shortens the reaction time. In the microreactors, it takes only several to tens of seconds to obtain significant degradation (e.g., 90% degraded), whereas the bulk reactors usually needs several hours [112].

(6) Self-refreshing effect: The running fluid naturally refreshes the reaction surface, which helps move away the reaction productions and increases the stability of the photocatalysts. In the bulk reactors, typically the activity of photocatalysts degrades noticeably after 10 runs of photocatalytic reactions [43], [47], [86], [106], whereas in

the microreactors the photocatalysts can easily last for several hundred runs of reactions.

(7) Optimization of operation condition: The fine control of fluids enables to optimize the operation condition of photocatalysis. For instance, by slowing down the flow rate and/or disturbing the laminar flows, the microreactors could clean most of the contaminants in one run, without resorting to the recirculation of flows, which is a common practice in the bulk reactors [43], [47], [86], [106].

(8) More functionalities: The microfluidics has the potential to add more functionalities to the photocatalysis, such as fast heat transfer, parallel process for rapid screening of photocatalysts, micro-mixing [40], on-chip monitoring of photocatalytic reactions, controllable delivery of light using optofluidic waveguides [113]–[120], selection of reaction pathways, and so on.

2.6 Review of microreactors for photocatalytic water purification

Various microreactors have been explored for photocatalytic reactions such as water purification, water splitting [42],[121], photosynthesis [122]–[128], bioparticle deactivation and heavy metal ion mineralization. Here we limit the survey to only the water purification because it is simplest and most representative. A brief survey of the

reported microreactors for photocatalytic studies is listed in Table 2-1. Although their designs vary significantly, they can be simply classified into four configurations as schemed in Fig. 2.9. The major difference can be seen more clearly from the transverse cross section (perpendicular to the flow direction) of the reactors. The *micro-capillary reactor* coats a layer of photocatalyst on the inner wall of a capillary tube and runs the water sample inside the tube. The light can be irradiated from the outside. The *single-microchannel reactor* makes use a single straight microchannel to carry the water sample whereas the *multi-microchannel reactor* exploits an array of the microchannels. The *planar microreactor* enlarges the microchannel in the lateral direction into a planar chamber. The first three configurations are based on microchannels, each of which has comparable dimensions of width and height (or diameter) in the range of 10 – 100 μm, whereas the last one has a much larger width (typically 1 – 100 mm) than the height. For photocatalysis, such a difference significantly affects the throughput, the photon utilization, the fabrication of photocatalysts, and the scalability to macro-scale reactors.

Table 2-1 Typical microfluidic reactors used for photocatalytic water treatment.

Type of microreactor	Catalyst/Light source	Model chemicals
Micro-capillary reactor	TiO_2/SiO_2/UV light	Methylene blue [129]
	TiO_2/UV LED	Rhodamine 6G [130]
	TiO_2/UV lamp	Methylene orange [131]
	TiO_2 /UV LED	Newcoccine, *etc.* [132]
	TiO_2/UV Nd-YAG laser	Salicylic acid [133]
Single straight microchannel	TiO_2/UV led	Chelate（Cu-EDTA）[134]
reactor	P25 TiO_2/UV light	4-chlorophenol [135]
	Pt-TiO_2/UV LED	Methylene blue [127], [136]
Multi-microchannel reactor		
Branched microchannel	TiO_2/UV-A LED	4-chlorophenol [137]
Serpentine microchannel	Nanoporous TiO_2	Methylene blue [108]
	Nanofibrous TiO_2/UV	Methylene blue [47]
	TiO_2/ Tungsten lamp	Methylene blue/phenol [138]
Planar microreactor	TiO_2/Solar light	Methylene blue [139]
	$TiO_2/BiVO_4$/Solar light	Methylene blue [140]
	$BiVO_4$/Blue LED	Methylene blue [141]

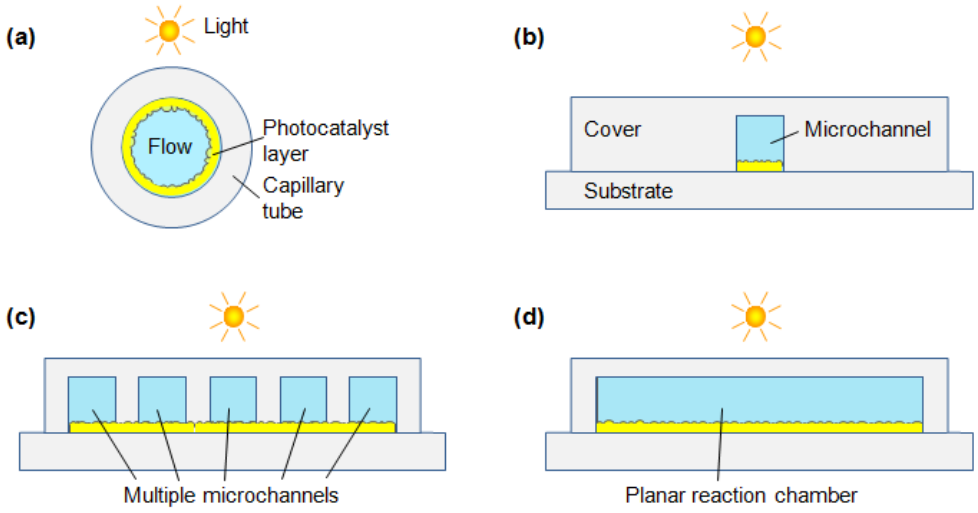

Figure 2.9 Typical designs of microfluidic reactors for photocatalysis water purification. (a) Transverse cross-section of micro-capillary reactor; (b) single-microchannel reactor; (c) multi-microchannel reactor; and (d) planar microreactor.

2.6.1 Micro-capillary reactors

An early work was reported by Li *et al*. [129], who fabricated a microreactor using capillaries with an inner diameter of 200 μm (see Fig. 2.10). The inner wall was coated with TiO_2/SiO_2 film to degrade methylene blue (MB) solution. Micro-capillary based reactors have also been used to decompose various other organic dyes [130]–[132]. It is the simplest design, but the coating on the inner wall is cumbersome. And the external irradiation is not ideal for the utilization of light because the outer part of the photocatalyst layer absorbs light but makes little contribution to the photodegradation.

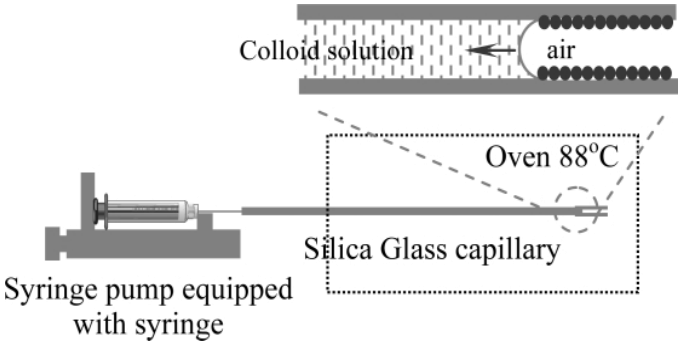

Figure 2.10 Micro-capillary reactor with the inner wall coated with self-assemble SiO_2/TiO_2 for methylene blue degradation, the dimensions of capillary: 5 cm (length) × 530 μm (outer diameter) and 200 μm (inner diameter) [129].

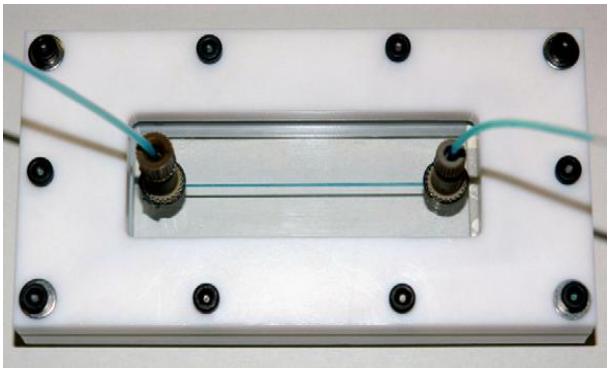

Figure 2.11 Single straight microchannel reactor with immobilized TiO_2-coated silica beads for degradation of 4-chlrophenol [134].

2.6.2 Single-microchannel reactors

With rapid development of various etching techniques such as photolithography, micro/nano imprinting and dry/wet etching, some researchers fabricated microchannels on glass, ceramic and polymer substrates to examine photocatalytic reactions.

Matsushita *et al.* designed a single straight microchannel to degrade some organic models [134] (see Fig. 2.11). The bottom of microchannel was immobilized with a sol-gel prepared TiO_2 thin film loaded with Pt particles. Similar reactors using single straight microchannels can be found in many other studies on the degradation of organic contaminants [133]–[136].

2.6.3 Multi-microchannel reactors

The microreactors based on micro-capillary and single microchannel have small photon receiving areas and waste most of the external irradiation light. And the small cross-sectional area limits the throughput as well. To tackle these problems, multiple microchannels have been introduced. In 2004, Gorges *et al*. [137] designed a microreactor that branched out 19 parallel microchannels. It immobilized a TiO_2 nanoporous film and fixed a UV-LED array above the area of the branched microchannels. The illuminated specific surface of the microreactor surpassed that of conventional bulk reactors by two orders of magnitude. In 2005, Takei *et al.* [142] fabricated a multi-microchannel reactor for photocatalytic redox-combined synthesis of L-pipecolinic acid using an anatase TiO_2 thin film (see Fig. 2.12 (a)). Pt nanoparticles were photodeposited from H_2PtCl_6 as the reduction site. It found that the conversion rate in the microreactor was 70 times larger than that in a cuvette using titania

nanoparticles with almost the same selectivity and enantiomeric excess. In another form of the multi-microchannel reactor, a single microchannel is folded up into a serpentine shape (see Fig. 2.12 (b)) [40], [108], [138]. This increases the photon receiving area and the residence time. However, the cross section remains the same as that of a single microchannel and thus limits the throughput.

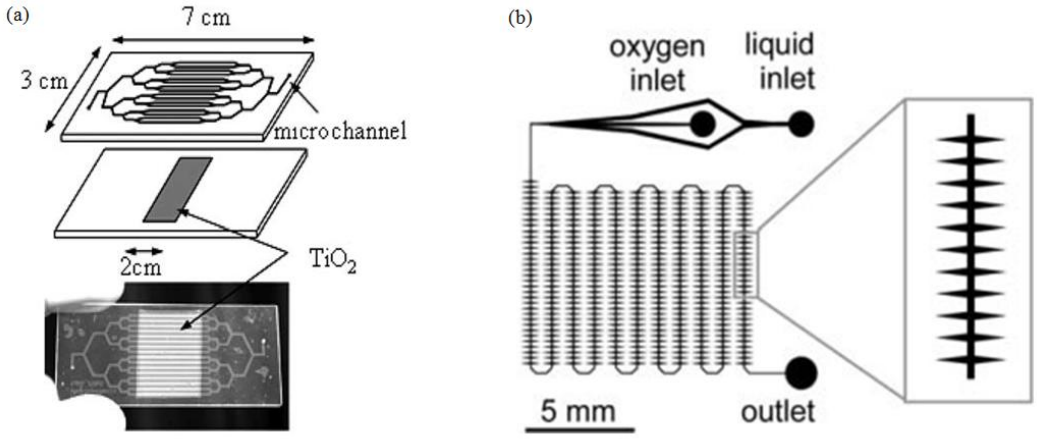

Figure 2.12 (a) branched microchannel reactor for synthesis of L-pipecolinic acid [142]; (b) serpentine microchannel reactor having 11 rows with 32 side lobes per row, coated with porous TiO_2 on the inner wall.

2.7 Summary

In summary, photocatalytic water purification utilizes light to degrade the contaminants in water and may enjoy many merits of the microfluidics technology such as fine flow

control, large surface-area-to-volume ratio and self-refreshing of reaction surface. Although a number of microfluidic reactors have been reported for photocatalysis water treatment, there are still many coexisting limitations such as mass transfer, photon transfer, oxygen deficiency and so on. Therefore, it is necessary to develop microreactors with laboratory bench to solve the current problems which can supply potential support to applications with industrial scale.

CHAPTER 3

OPTOFLUIDIC PLANAR REACTORS FOR PHOTOCATALYTIC WATER TREATMENT USING SOLAR ENERGY

This chapter will present the first design of optofluidic reactor for photocatalysis, covering the device design, material fabrication and experimental study. This design is to demonstrate the great advantages of microfluidic planar structure for the photocatalysis as it helps solve the fundamental problems of current photocatalysis technology such as mass transfer limit and photon transfer limit. This is also the pioneering work of the optofluidic photocatalysis.

3.1 Introduction

Recently, optofluidics technology has made a rapid progress in various applications such as biomedical research, healthcare, pharmaceuticals, environmental protection and homeland security [143]–[145], which has been extensively applied to water pollution treatment [13], air purification [146], disinfection [147], self-cleaning and water splitting [148]. However, industrial applications are now still in the infancy as limited

by the low photocatalytic efficiency and the difficulty to scale up from laboratory proof-of-concept to large-volume production.

The photocatalytic efficiency is mainly determined by the illumination efficiency and the contact between the activated catalyst and the reagents [149]. The former is also called *photon transfer efficiency* and is affected by the illustrated surface per unit liquid volume (related to the illustration area and the surface/volume ratio) and the effective incident power density (related to the power density, the absorption and the wavelength of incidence). The latter is sometimes called *mass transfer efficiency* and reflects how easy the reagents in the liquid are moved to the catalyst surface (related to the catalysis surface area per unit volume) and how fast the reacted products are removed (related to the diffusion, stirring and flow rate).

Microfluidics has a natural synergy with photocatalysis since its inherent large surface/volume ratio could drastically enhance the photon transfer efficiency and the mass transfer efficiency. Indeed, several microfluidic photocatalytic reactors have been demonstrated and showed high reaction efficiency and good controllability as compared to the conventional plate and slurry reactors [108], [137], [150]–[152]. However, the previous microfluidic reactors mostly utilized microchannels-based design and suffered from reduced light absorption area, limited volume of reactants and low throughput.

Besides, they relied on expensive and time-consuming fabrication processes like direct laser -writing [152], dry and wet etching [108], [137], [150]–[152] and thermal bonding [108], [137], [150]–[152] and thus impeded the prospect of industrialization. In addition, most of the demonstrated work made use of UV lamps as the light source, the comparatively high cost associated with the consumption of electricity constitutes one of the major drawbacks for the rapid commercialization of photocatalytic water treatment [153]. Solar-powered photocatalysis presents to be the most viable route to energy conservation and low-cost production. Different types of large-scale solar-powered reactors have been tested in laboratory and field [153]. For instance, the thin-film fixed-bed reactor (TFFBR) design has demonstrated high efficiency of solar energy utilization thanks to its planar structure [154]. Nevertheless, miniaturized version has yet to investigate.

This chapter will demonstrate a planar microfluidic photocatalytic reactor for water treatment using solar energy, which attempts to combine the merits of the microfluidics and planar reactors while circumventing their problems. The device is formed by a UV curable resin NOA81 (Norland Optical Adhesive) and TiO_2 film coated glasses, making the whole fabrication process rapid and low cost. To study the feasibility of solar-powered photocatalytic water treatment, methylene blue will be used as the

organic model and its photodegradation will be examined under solar irradiation. Influences of the reactor parameters (e.g., film preparation methods, thickness of TiO_2 films and flow rate) and characterization of photocatalytic efficiency will be studied.

3.2 Experimental details

3.2.1 Device design

In order to enlarge the light receiving area and to keep the inherent merit of large surface/volume ratio of micro-reactors, a planar microfluidic reactor is designed as illustrated in Fig. 3.1. For simplicity, the planar microfluidic reactor is called *microreactor* hereafter. The microreactor has a rectangular reaction chamber, which is constructed by two porous TiO_2-coated glasses as the top cover and bottom substrate and a 100-μm-thick UV curable adhesive layer (NOA81, Norland) as the spacer and sealant. The dimensions of the reaction chamber are 5 cm × 1.8 cm × 100 μm = 90 μl and the TiO_2 films on the glasses have the same surface area with the reaction chamber. Two syringe needles are used as the inlet and outlet for solution injection and collection. Between the reaction chamber and inlet/outlet, tree-branch shaped microchannels (50 μm high) are adopted to ensure a uniform filling of the solution over the whole reaction chamber and thus a maximum contact of the reagents with the TiO_2 films.

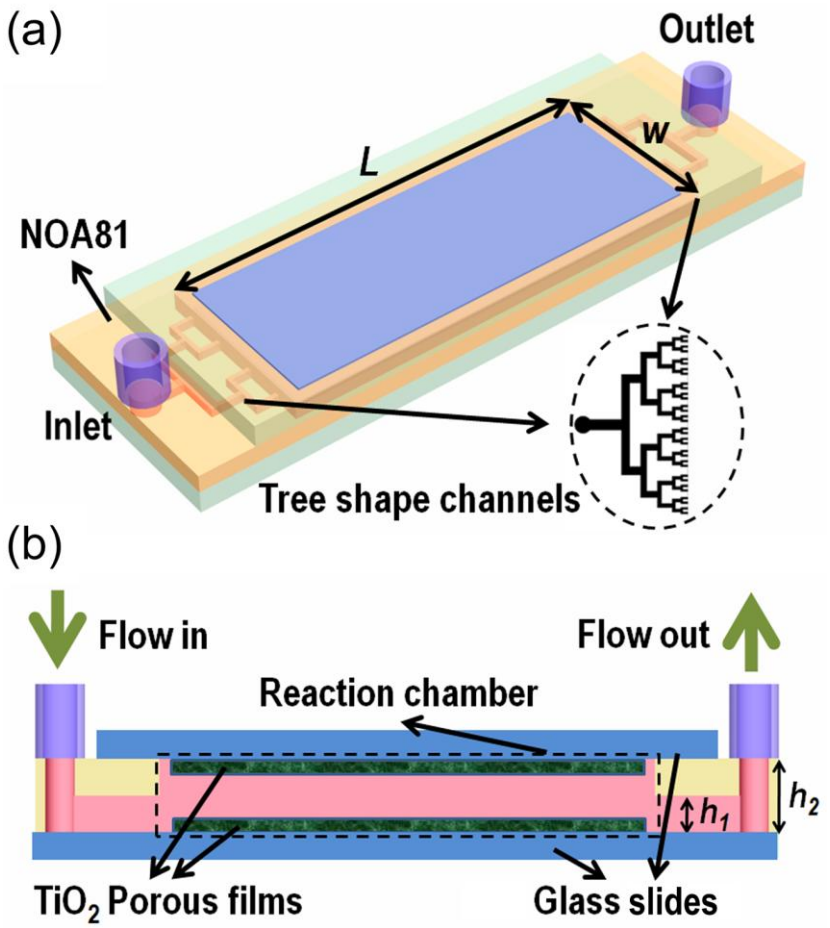

Figure 3.1 Schematic diagram (a) and cross-sectional view (b) of the photocatalytic microfluidic reactor. The device is constructed by two TiO_2-coated glasses separated by a thin layer of microstructured UV-cured NOA81. Tree-branch shaped microchannels are used to ensure that the solution uniformly fills the whole reaction chamber and have maximum contact with the TiO_2 films. The length and width of the reaction chamber are L = 5 cm and W = 1.8 cm, respectively. The TiO_2 films have the same surface area as the reaction chamber. The heights of the microchannels and the reaction chamber are h_1 = 50 μm and h_2 = 100 μm, respectively.

3.2.2 Preparation of TiO_2 films

Since the quality of the TiO_2 film is the key issue to photocatalysis, we have developed the present study to compare the performance of three types of TiO_2 films under microfluidic conditions. The photoreaction efficiencies have been evaluated by considering the influences of porosity, thickness and flow rate.

The porous TiO_2 films were prepared by sol-gel method [155], which included two stages: the preparation of the TiO_2 colloid and the creation of porous TiO_2 film on the glass slide. To find out the TiO_2 films to best match the design of microreactor, three types of colloidal dispersions were employed for the TiO_2 film preparation by sol-gel method using commercially available TiO_2 particles and precursor. The first colloidal dispersion (colloid A) was prepared using TiO_2 powders (Degussa P25, mean particle size ~ 25 nm, anatase: rutile = 70:30) [155]. Firstly, 12 g TiO_2 powders (Degussa P25, a mixture of ca. 30% rutile and 70% anatase, the mean size of primary particles to be about 25 nm, BET surface area 55 m^2/g) was slowly dispersed in 120 ml water, which contained acetylacetone (0.4 ml, Sigma-Aldrich) to prevent aggregation of the particles with the assistance of magnetic stirring. After the powder had been well dispersed, a detergent (0.2 ml Triton X-100, Sigma-Aldrich) was added to facilitate the spreading of the colloid on the substrate. Finally, 2.4 g polyethylene glycol (PEG, Sigma-Aldrich)

was added into the solution under continuous stirring over one whole night. Colloid B was prepared using similar procedures. The main difference is that absolute ethyl alcohol (Aldrich) was used as dissolvent and the PEG was replaced by ethyl cellulose (Aldrich) [156]. This method is named as *alcohol-based P25 method*. Colloid C was prepared by precursor solutions following a hydrolysis reaction [157]. Tetrabutyl titanate (TBT, $Ti(OC_4H_9)_4$) was added into ethanol containing ethanolamine and then hydrolyzed to titanium hydroxide by adding deionized water. After ageing for 24 h, a transparent colloid was formed. This method is named as *TBT synthesis method*.

After preparation, the colloids were applied onto the desired regions of the glass slides by a painting method as follows. A glass slide was covered on four edges with adhesive tapes (about 40 μm thick) to control the thickness of the TiO_2 film and to protect the non-coated areas. As a result, a region of 5 cm × 1.8 cm at the center of the glass was exposed. Then the colloid (10 μl) was applied to one edge of the exposed region of glass and was distributed by sliding a glass rod over the tape-covered edges. With the tapes as the spacer, a uniform layer of colloid was obtained in the exposed region. After air drying at 80 ^oC, the tapes were removed and the glass slide was calcined for 2 h at 500 ^oC in air.

3.2.3 Microfluidic device fabrication

PDMS (polydimethysiloxane) is most popular for microfluidic devices because of its celebrated physical and chemical properties. However, it is not a good candidate for this microreactor because its elastic modulus is too low to support a chamber with high width/height ratio (collapse otherwise) and a thin layer of PDMS can be broken easily. NOA81 is chosen since it has high elastic modulus (typically 1 GPa, 3 orders of magnitude higher than PDMS) and can be easily bonded to the glass by UV exposure [158]. In addition, NOA81 has a better resistance to swelling by solvents than PDMS and allows the replication of submicron features.

Standard UV lithography was used to fabricate the master mold for the microreactor. First, negative photoresist SU-8 50 was spin coated (2500 rpm, 60 s, 50 μm) onto a silicon wafer substrate and baked. Reaction chamber and inlet/outlet were then patterned with a mask. The process was repeated and the microchannels were also patterned with another mask. As a result, the SU-8 master was obtained. After the evaporation of trimethylchlorosilane (TMCS) on the surface of the SU-8 master, a prepolymer solution of PDMS in a 10:1 mixture ratio was poured on and cured at 80 ^{o}C for 1 h. Finally, the cured PMDS slab was then peeled off and ready for making the microreactor.

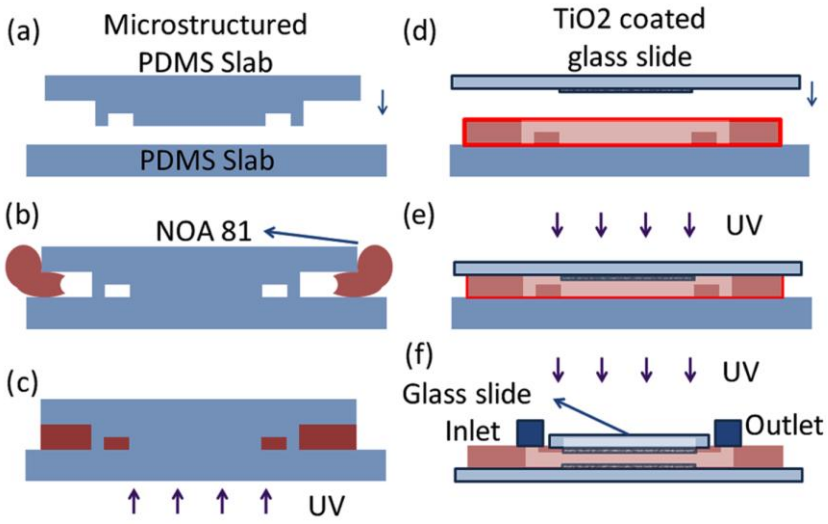

Figure 3.2 Process flow of the device fabrication and integration. Microstructured PDMS slab is replicated from the SU-8 mold in advance. (a) The microstructured slab is attached to a planar PDMS slab. (b) Liquid NOA81 is applied to fill the space between the two PDMS slabs by capillary force. (c) The NOA81 is partially cured by UV light. (d) The microstructured PDMS slab is peeled off and the NOA81 layer is bonded to a TiO_2-coated glass slide. (e) The other glass slide is bonded by UV exposure. (f) Two syringe needles are connected to the inlet and outlet using adhesive.

The process flow for replicating the structures to the NOA81 layer and for eventually forming the microreactor is shown in Fig. 3.2. First, the microstructured PDMS slab was attached to a planar PDMS slab (see Fig. 3.2a). Then, drops of liquid NOA81 was then applied to the edges of the PDMS slab so as to fill the space between the two PDMS slabs by capillary force (see Fig. 3.2b). Next, UV exposure (10 mW/cm^2,

20 s) was applied to cure the NOA81 (see Fig. 3.2c). Since oxygen inhibited the free-radical polymerization of liquid NOA81 [158], the PDMS's permeability to gas ensured that an ultra-thin superficial layer of NOA81 liquid remained uncured in close proximity to each PDMS surface, though the central part of NOA81 had already been hardened. After that, the microstructured PDMS slab was gently peeled and the NOA81 layer was pressed onto a porous TiO_2 film coated glass slide (bottom glass, see Fig. 3.2d). Subsequent UV exposure (10 mW/cm^2, 8 s) cured the remaining liquid NOA81 layer and bonded them firmly. By then there still remained an uncured thin layer of NOA81 on the planar PDMS slab side. By the same method, it was bounded to another porous TiO_2 film coated glass slide (cover glass, see Fig. 3.2e). Finally, two syringe tips were connected to the inlet and outlet using adhesive (see Fig. 3.2f). The process was easy and low cost. It took less than 5 min to run the whole procedures to make a microreactor from the master mold. A photo of the fabricated device is shown in Fig. 3.3. It has a footprint of 7.6 cm × 2.5 cm and encloses a microreactor chamber with the dimensions of 5 cm × 1.8 cm × 100 μm (volume 90 μl).

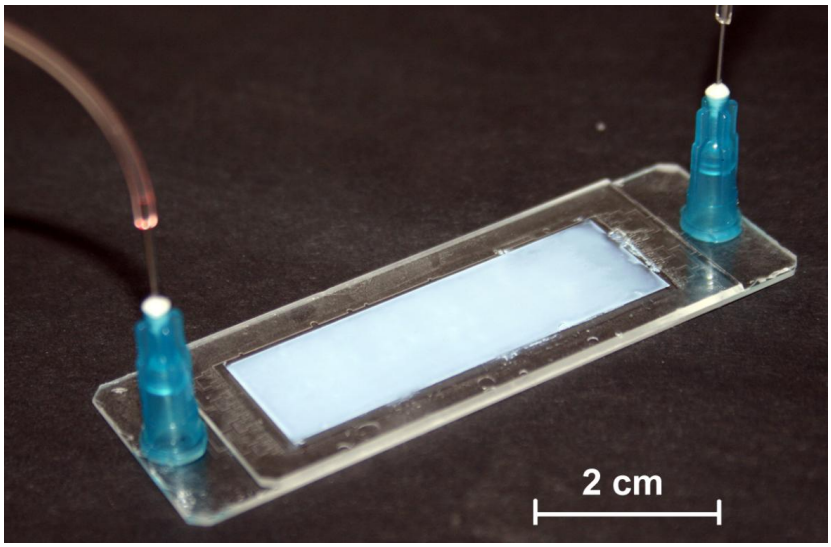

Figure 3.3 Photograph of the fabricated planar microfluidic photocatalytic reactor.

3.2.4 Experimental setup for methylene blue degradation

To characterize the performance of TiO_2 films, the immobilized films was fixed in both bulk reactor and microreactor for measuring the photodegradation capacity under UV irradiation (1.1 mw/cm^2 UV-A irradiation by a portable UV lamp (ZF-7B, 365 nm, 16 W)). In this case, only the bottom glass slide was coated with three different TiO2 films. X-ray diffusion was also employed to characterize their morphology.

After finding out the TiO_2 films with best performance, both the top and bottom glass slides were coated with the TiO_2 films. And the thickness of the TiO_2 film on the top glass slide was investigated for the best photon utilization efficiency. In this section, the photocatalytic reaction was under 100 mW/cm^2 solar irradiation by a solar simulator

equipped with an AM 1.5G filter (Newport 91160, 150w). Methylene blue (MB, Sigma-Aldrich) solution was introduced into the device by a syringe pump (TS2-60, Longer). The degraded MB solutions were collected from the outlet and their absorption spectra were analyzed by a UV-Visible spectrophotometer (UV-2550, Shimadzu).

3.3 Optimization of TiO_2 film

In this section, three methods for preparing TiO_2 films were investigated to find the optimized one for microfluidic photocatalysis.

3.3.1 XRD of different TiO_2 films

Fig. 3.4 (a) – (c) show the film surfaces using scanning electron microscope (SEM). Good homogeneity is present in all three films. Films A and B both exhibit submicron porous structures, but film A has larger pores and thus higher porosity. In contrast, film C shows a compact structure. The film thicknesses are measured by taking the cross-sectional SEM pictures. The films A, B, C have the thicknesses in the range of 0.2 – 2 μm, 1 – 10 μm and 50 – 500 nm, respectively. The different thicknesses mainly come from different colloid absorbability to the substrates. The mineral forms of films A and B are clear as they are from P25. For film C, X-ray diffraction in Fig. 3.4 (d) shows that it is in anatase phase, which has good photoreactivity [13].

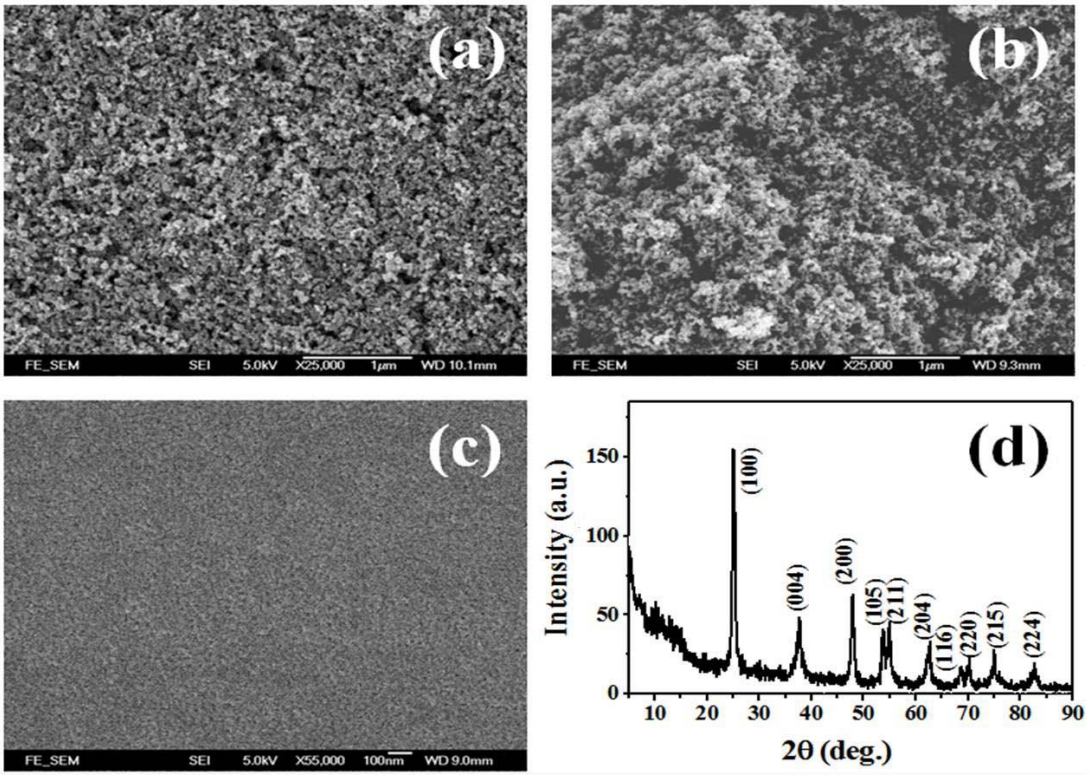

Figure 3.4 Scanning electron micrographs of the surface structures of the fabricated TiO_2 films. (a) – (c) for films A, B and C, respectively. (d) shows the X-ray diffraction spectrum of film C.

3.3.2 Study of photocatalytic performance of TiO_2 films

First, the effect of TiO_2 films thickness was studied using bulk containers, each of which was formed by cutting a 5×1.8 cm^2 square hole at the center of a 7-mm-thick PDMS slab and by then attaching it onto the TiO_2 film coated glass slide. 3 ml MB solution (3×10^{-5} M, PH~7) was then added into each container irradiation of under the UV lamp. The absorption spectra of the degraded MB solutions after different exposure

times were analyzed and the reaction rate constants were deduced. For films A, B and C, the reaction rate constants go up with the increase of thickness but tend to saturate at about 650 nm (film A), 5 μm (film B) and 200 nm (film C).

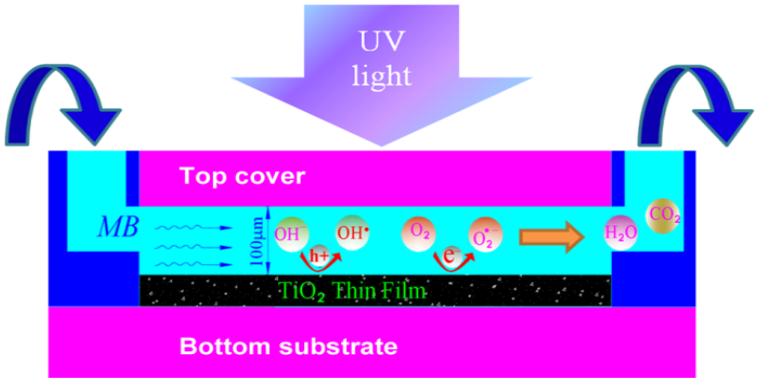

Figure 3.5 Schematic diagram of the photocatalytic microfluidic reactor and the photocatalytic degradation process of MB (methylene blue) in the reactor. The bottom glass slide with immobilized TiO_2 film and the blank top glass slide were separated by the micro-structured NOA81 layer. The reaction chamber has dimensions of 5 cm × 1.8 cm × 100 μm (volume 90 μl).

Next, the photoreaction efficiency of films A, B and C were compared by incorporating them into the bulk container and the microreactor. The schematic of measuring setup was shown Fig. 3.5. Each film has the saturated thickness so as to compare their best performance. Similar to the above test, 3 ml of MB solution was

added into the bulk containers and exposed for 20 min, 40 min and 1 h. The same amount of solution was also introduced into the microreactor and irradiated under the same UV light. The photodegraded solutions under different evacuation times in the microreactor were also examined. Fig. 3.6 (a) and (b) show the degradation data of the microreactor and the bulk container, respectively. It can be observed that in the microreactor film A has a better performance than film B, particularly when the effective residence time is below 40 s. In the bulk container, film B has a better performance than film A and the difference becomes more evident at longer exposure time. In both reactors, film C has a feeble performance. The characteristics are listed in Table 3-1. In the microreactor, the reaction rate of film A is 17% higher than that of film B (1.4% s^{-1} versus 1.2% s^{-1}). In the bulk container, film B is about 13% faster. This can be explained by considering their differences in porosity, intrinsic kinetic reaction rate and intrinsic/external mass transfer rates [159], [160]. Because of the fast flow and the high surface-to-volume ratio, in the microreactor the external mass transfer rate (MTR) is very high and thus the reaction is mainly limited by intrinsic MTR, which results from the diffusion of organic molecules on and within the porous catalyst thin film. The reagent molecules on film A can move to the catalyst surface more easily owing to its better porous surface structure so that it has higher MTR, making it suitable

for the microreactor. However, in the bulk container long effective reaction time contributes to sufficient adsorption of MB onto TiO_2 surface. In this case, the reaction is mainly limited by the intrinsic kinetic reaction rate. The denser structure of film B is beneficial to the intrinsic KRR, which explains its better performance in the bulk container. The feeble performance of film C is attributed to its compact structure. Due to the length limit, further detailed analyses are not given here. A simpler case was discussed in our previous work. Such performance difference also evinces the necessity of this comparative study since the microreactor has an enclosed environment and places different requirements on the film quality and thus the preparation method.

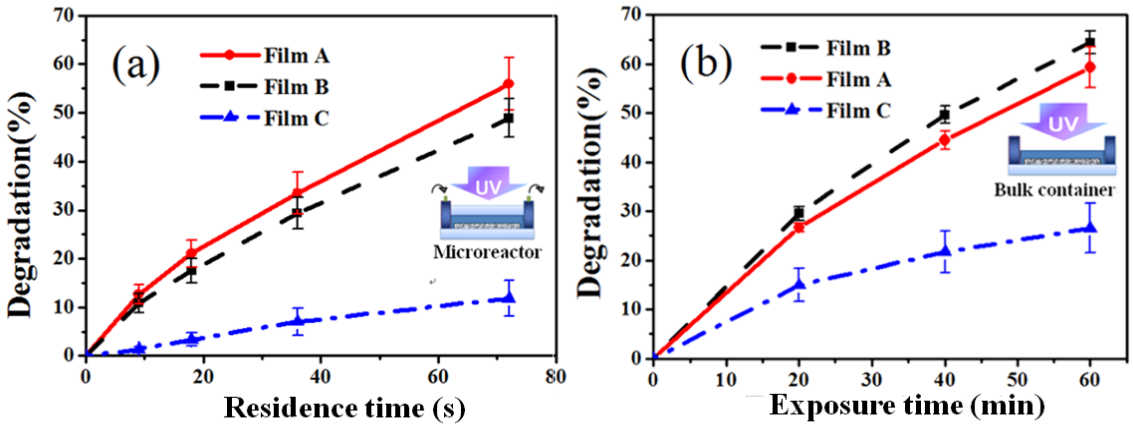

Figure 3.6 Comparison of the photoreactivity of films A, B and C. (a) Degradation percentage as a function of effective residence time of the methylene blue solution in the microreactor; and (b) degradation percentage in the bulk container.

Table 3-1 Comparison of the characteristics of the porous TiO_2 films prepared by the three methods.

Preparation method	Porosity	Saturation thickness	Reaction rate (% s^{-1})	
			Bulk container[#]	Micro- reactor[&]
Water-based P25 method	best porous	630 nm	0.016	1.4
Alcohol-based P25 method	better porous	5 μm	0.018	1.2
TBT synthesis method	compact	200 nm	0.007	0.2

[#]Data for the 60-min exposure time

[&]Data for the 9-second effective residence time

In summary, the first two methods prepared TiO_2 P25 colloids using water and ethanol as the dissolvents, respectively. The third method synthesized the TiO_2 particles using tetrabutyl titanate (TBT). Preliminary experimental results shows that though the alcohol-based P25 method performs better in the bulk container, the water-based P25 method seems to be a better choice for the microfluidic planar reactor. In contrast, the TBT synthesis method produces little photoreaction due to the compact film.

3.4 Results and discussion

After confirming the porous TiO_2 films, the optimized microreactors were employed to investigate the photodegradation using solar energy. The fabricated film was observed using scanning electron microscope (SEM). Fig. 3.7(a) shows the close-up of the film on the bottom glass slide, with an inset showing a much larger region. Fig. 3.7(b) shows the cross-section of the film. It can be observed that the resultant TiO_2 has sub-micron porous structures and good homogeneity. The film thickness is 2 μm and can be varied by changing the colloid concentration.

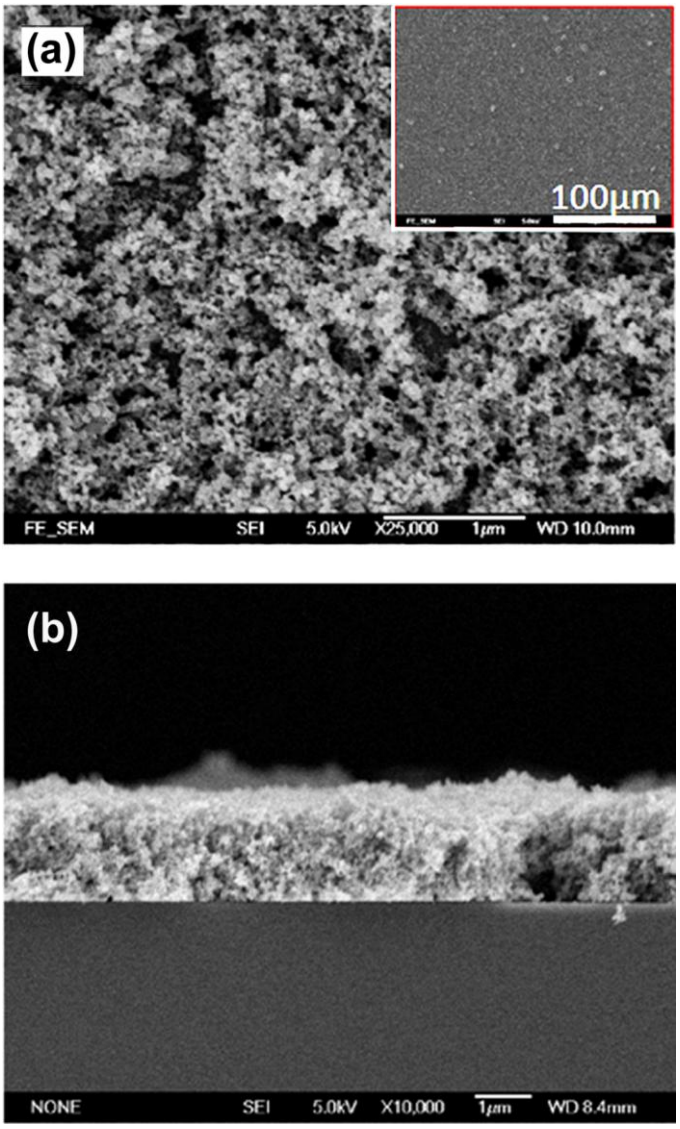

Figure 3.7 Scanning electron micrographs showing the porous structure of the fabricated TiO_2 film. (a) Top view of the film, the submicron porous structures are beneficial as they increase the contact area between the reagents and TiO_2 and thus improve the photocatalytic efficiency. The inset shows the good homogeneity of the film. (b) Cross-sectional view of the film, the film is about 2 μm thick and shows a good homogeneity in the depth direction.

3.4.1 Enhancement of photocatalytic efficiency by microreactor

To quantify the enhancement of photocatalytic efficiency by using the microreactor, a bulk container having the same porous TiO_2 film was used as the reference. The bulk container was formed by cutting a 5×1.8 cm^2 square hole at the center of a 7-mm-thick PDMS slab and by then attaching it onto a TiO_2-film coated glass slide. After the attachment, the TiO_2 film lay on the bottom of the bulk container. The bulk container can hold up to 6.3 ml solution. It is noted that for fair comparison, the microreactor has only one porous TiO_2 film on the bottom glass while the top glass is just a plain glass slide. In this way, the microreactor and the bulk container have the same TiO_2 surface. Microreactor without TiO_2 was also tested to verify the effect of the TiO_2 presence,

To study the photocatalytic degradation, 3 ml MB solution (3×10^{-5} M, PH~7) was added into the bulk container and then irradiated under the solar simulator (100 mW/cm^2). The absorption spectra of the photodegraded solutions after 20 min, 40 min and 1 h of exposure in the container were analyzed. The same amount of solution was also introduced into the microreactor by a syringe pump and irradiated under the same solar light. The photodegraded solutions under different evacuation times such as 5 min, 15 min and 30 min in the reactor with and without TiO_2 were also examined. Here the evacuation time refers to the overall time needed to flow all the solution from the inlet

to the outlet. Therefore, the flow rates corresponding to the evacuation times of 5, 15 and 30 min are 600, 200 and 100 μl/min, respectively. One of the main differences is that in the bulk container the 3-ml solution was constantly exposed to the solar light over the whole exposure time, whereas in the microreactor the residence time (i.e., the effective exposure time) of the solution is much shorter than the evacuation time. For instance, the residence time is only 0.15 min for the evacuation time of 5 min.

From the Beer-Lambert law

$$\text{absorbance} = \varepsilon c l \tag{3.1}$$

where ε is the molar absorptivity, l the optical path and c the concentration. The degradation can be evaluated by monitoring the absorbance change at 664 nm wavelength of MB solutions before and after degraded [108].

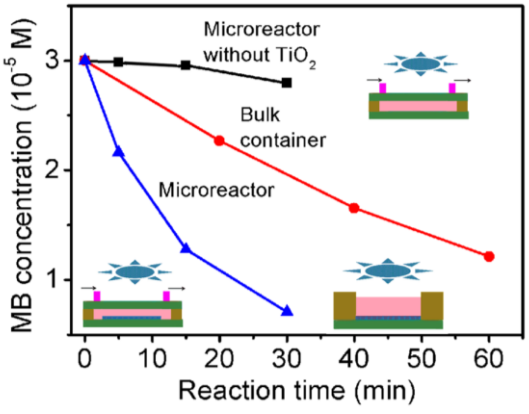

Figure 3.8 Comparison of the photocatalytic reaction efficiencies. The microreactor shows much higher reaction efficiency than the container. For further comparison, the microreactor without TiO_2 is also tested and its reaction is found negligible.

Figure 3.8 plots the MB concentration changes over the reaction time for the bulk container and the microreactor with and without TiO_2. Here the reaction time refers to the exposure time for the bulk container but the evacuation time for the microreactor. It is seen that the microreactor with TiO_2 exhibited faster decrease of MB concentration than the bulk container. For example, a degradation of 30% of MB (from the initial 3×10^{-5} M to the level of 2×10^{-5} M) took 5 min in the microreactor but more than 20 min in the bulk container. However, the photoreaction in the microreactor without TiO_2 is negligible, which validates the significant effect of TiO_2 presence on the reaction efficiency.

Such improvement can be explained by considering the mass transfer efficiency [161]. In the bulk container, the mass transfer presents to be the main limitation. Nevertheless, in the microfluidic reactors, the mass transfer coefficient and the ratio of the TiO_2 surface to the reactor volume are very high because of its inherent microscale and large surface/volume ratio. As a result, the reaction efficiency is only limited by the intrinsic kinetics. This is one of the key merits of using microfluidics for photocatalytic reaction.

3.4.2 Effect of TiO_2 film thickness

In the structure of microreactor, two TiO_2 films are utilized, one is on the bottom glass

while the other on the top glass. For simplicity, they are named as bottom film and top film, respectively. For the bottom film, the effective surface area would increase with the thickness due to the porous morphology of the TiO_2 film, particularly when the film is very thin. As a result, the reaction efficiency is expected to increase with the TiO_2 thickness. However, when the film goes to very thick, the pores in the inner part are not exposed to the solution or the light and thus do not contribute to the photoreactivity. As a result, there exists a thickness at which the reaction efficiency starts to saturate. This conclusion would apply equally to the reactors with only one TiO_2 film (such as the bulk container and the microfluidic reactor having only one glass coated with TiO_2). Nevertheless, it is very different for the top film. On one hand, the top film absorbs some light for photocatalysis. On the other hand, it has to transmit some light to the bottom film for further photocatalysis. Too thin a top film would have low contribution to the overall photoreactivity, but too thick a top film would block the light and render the bottom film useless. There exists an optimal thickness for the top film.

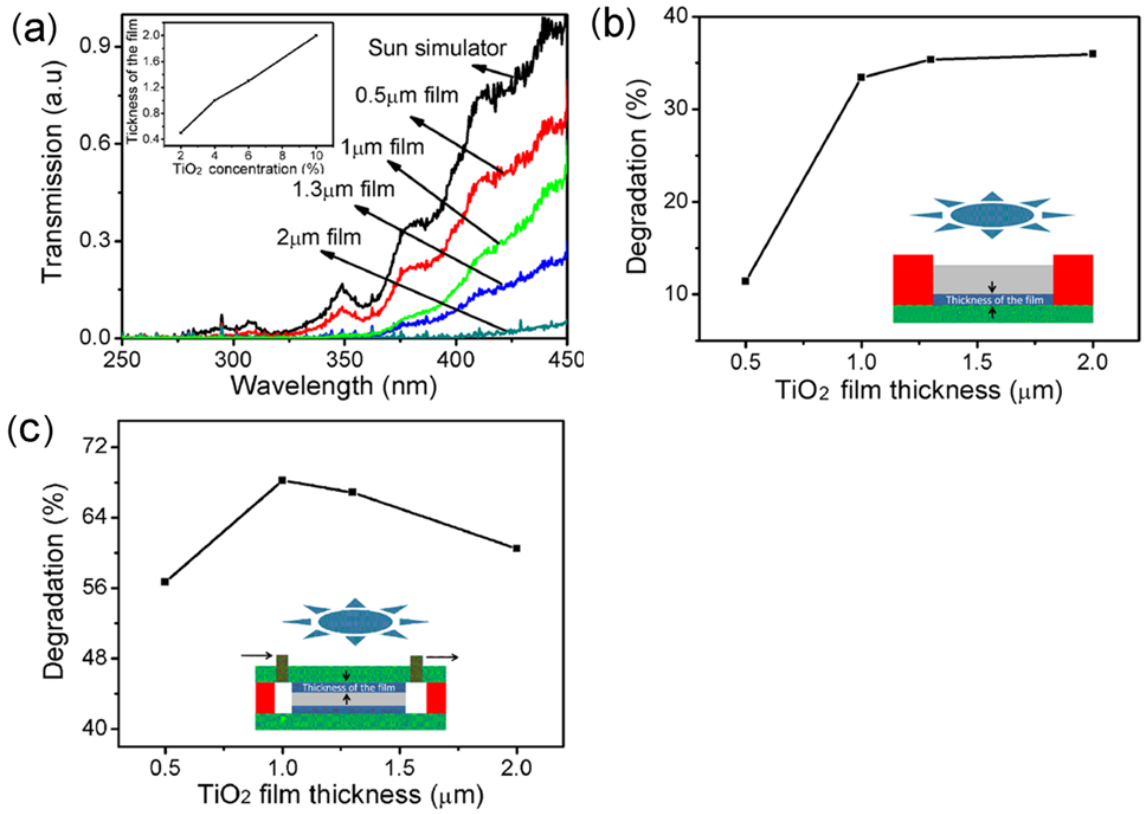

Figure 3.9 (a) Transmission spectra (in UV region) of the TiO_2 porous films with different thicknesses under the irradiation of solar simulator. The inset shows the relationship between the thickness of the obtained TiO_2 porous film and the concentration of the TiO_2 aqueous solution using the sol-gel method. (b) Degradation percentage as a function of the TiO_2 film thicknesses using the bulk container. (c) Degradation percentage as a function of the TiO_2 film thicknesses on the top glass using the microreactor. The TiO_2 film thickness on the bottom glass is kept at 2 μm.

In experiment study, porous TiO_2 films with different thicknesses (0.5 μm, 1 μm, 1.3 μm and 2 μm) were prepared using the TiO_2 P25 aqueous solutions with different concentrations (2%, 4%, 6% and 10%, respectively) following the procedures as discussed in section 3.2.2. The obtained film thickness as a function of the TiO_2 concentration is plotted in the inset of Fig. 3.9a, showing roughly a linear relationship. Fig. 3.9a shows the transmission spectra (over the wavelength 250 – 450 nm) of the films under the solar irradiation. The transmission intensities decrease with the thicknesses of the films and approach to zero when the thickness of the film goes up to 2 μm. In other words, a 2-μm TiO_2 film would absorb almost all the light.

Reaction efficiencies of the TiO_2 films with different thicknesses were compared using the bulk container configuration. The degradation percentages of 3-ml MB solution (concentration 3×10^{-5} M) after 30-min exposure time were measured to indicate the reaction efficiencies. Here the degradation percentage refers to the percentage of the initial MB being degraded during the exposure time. The results are shown in Fig. 3.9b. The degradation percentage increases rapidly when the thickness goes from 0.5 μm to 1 μm, and tends to saturate at larger than 1 μm thickness. This matches well with the above prediction. For this reason, the final microreactor is chosen to use a 2-μm thick TiO_2 film on the bottom glass.

The influence of the top film thickness was determined using four microreactors that had the same bottom film thickness of 2 μm but different top film thicknesses (0.5 μm, 1 μm, 1.3 μm and 2 μm, respectively). The reaction efficiencies were obtained by measuring the degradation of MB solutions at a flow rate of 600 μl/min. The results are plotted in Fig. 3.9c. It is found that the thickness of 1 μm is the best choice for the top film. The following experiments will be done with this optimized device.

3.4.3 Effect of flow rate

The influence of the flow rate on the photocatalytic reaction efficiency was also studied. The flow rate is related to the effective residence time of the MB solution in the reaction chamber by the relationship (effective residence time) = (chamber volume) / (flow rate). Here the chamber volume is 90 μl as already given above. The experimental results are plotted in Fig. 3.10. The degradation percentage increases with the effective residence time and reaches 94% at 36 s (corresponding to the flow rate 150 μl/min). This is easy to understand because the longer the residence time is, the more the photoreaction occurs. However, it is shown in Fig. 3.10 that the reaction rate actually decreases with longer residence time (equivalently, it increases with the flow rate). For instance, it is as high as 8%/s at the effective residence time of 6 s (corresponding to the flow rate 900 μl/min) and drops to only 2.6%/s at the effective residence time of 36 s.

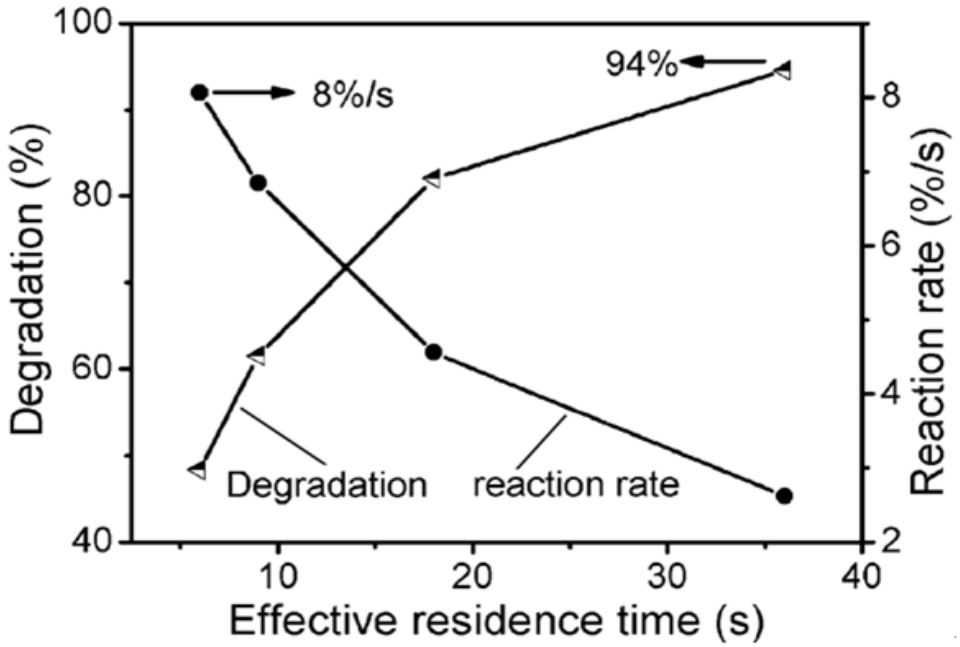

Figure 3.10 Degradation percentage and reaction rate with respect to different effective residence times of the methylene blue solution in the reaction chamber. The degradation percentage increases with the effective residence time, whereas the reaction rate decreases.

In this device, the illuminated specific surface/volume of the photocatalyst in contact with the reactant can be calculated to be $r = 2(LW)/(LWh_2) = 20{,}000\ \mathrm{m}^{-1}$, where L, W and h_2 are the length, width and height of the reaction chamber, respectively (see Fig. 1a). The value of 20,000 m^{-1} is just the lower limit. The actual value should be much larger due to the porous morphology of the TiO_2 film. Such a high surface/volume ratio would significantly improve the mass transfer efficiency. To reach a quantitative

estimation, detailed photoreaction kinetics has to be considered. According to the previous studies [108], [137], the heterogeneous Damköhler number Da_{II}, which represents the ratio of the heterogeneous reaction rate at the catalyst surfaces to the diffusion from the bulk solution toward the catalyst surfaces, can reflect the mass transfer limitation in the microreactors. The Da_{II} number of our device is calculated to be 0.003 using the equations and parameters from Lindstrom *et al.* [108]. When the Da_{II} number is less than 0.1, the reaction rate is dominated by the intrinsic kinetics of the photoreactions, which indicates that there is no mass transfer limitation for the photocatalytic reaction in this microreactor. The calculation also indicates that the height of the reaction chamber should not exceed 570 μm to avoid the adverse effect of the mass transfer limitation.

3.4.4 Effect of dissolved oxygen content

Oxygen availability is crucial to the MB photocatalytic degradation, which can be seen by the reaction equation:

$$C_6H_{18}N_3SCl + 25.5O_2 \xrightarrow{TiO_2 + h\nu \geq 3.2eV} HCl + H_2SO_4 + 3HNO_3 + 16CO_2 + 6H_2O \quad (3.4)$$

According to this equation, the full degradation of 3×10^{-5} M MB solution requires 7.5×10^{-4} M oxygen, which is approximately 3 times of the content of naturally dissolved oxygen (9 ppm, or equivalently 2.8×10^{-4} M), which is 3 times higher than

the dissolved oxygen at room temperature and atmospheric pressure. At low flow rate, the consumption of oxygen would cause a deficiency of oxygen and thus a reduction of the reaction efficiency. In contrast, a high flow rate helps refuel the photoreaction using the dissolved oxygen in newly arrived solution. The deficiency of oxygen is supposed to be the main reason for the decrease of reaction efficiency at lower flow rate. To solve this problem, a recycle design [161] or an addition of small amount of H_2O_2 [162] might be used.

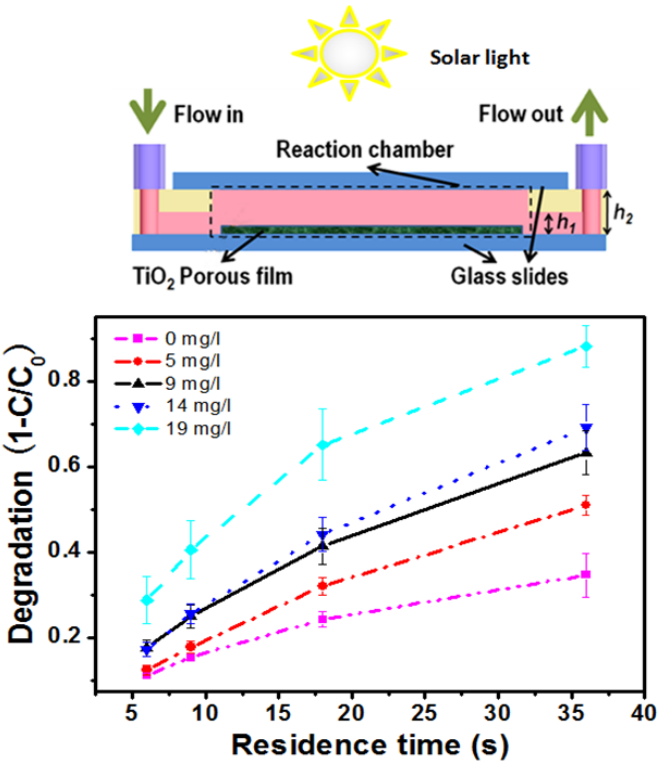

Figure 3.11 Influence of the content of dissolved oxygen on the photodegradation efficiency of microreactors. Microreactor with a single layer of TiO_2 film (2 μm thick) on the bottom glass side.

Here, in order to investigate the effect of dissolved oxygen content, we chose to blow oxygen and nitrogen into original MB solutions to adjust the dissolved oxygen content. Experiments have been conducted and the results are plotted in Fig. 3.11.

The dissolved oxygen in water at room temperature and atmospheric environment is about 9 ppm (or equivalently, 2.8×10^{-4} M). To adjust the oxygen content, oxygen and nitrogen gases were blown into the original MB solution to prepare the samples with 0, 5, 9, 14, 19 ppm oxygen. The oxygen content was tested by using a dissolved oxygen meter (Model: YSI 55, measuring limit: 20 ppm). After that, the newly-prepared MB solutions were used for measuring the degradation efficiency of microreactors. Here, I investigated two microreactors, one had a single layer of TiO_2 film and the other had two layers of TiO_2 films.

Fig. 3.11 plotted the experimental results. It can be seen obviously that higher oxygen content leads to faster degradation, and the relationship between degradation and residence time is always exponential for different oxygen contents, including those > 9 ppm. But the commercial dissolved oxygen meters have often the measuring upper limit of 20 ppm. Therefore, though I have increased the dissolved oxygen to 19 ppm, it is still in the state of oxygen deficiency.

Fig. 3.12 plots the relationship between the dissolved oxygen and the degradation efficiency when the flow rate is set at 300 μl/min (residence time ~ 18 s). The microreactor shows an increase of degradation efficiency when the content of dissolved oxygen goes higher.

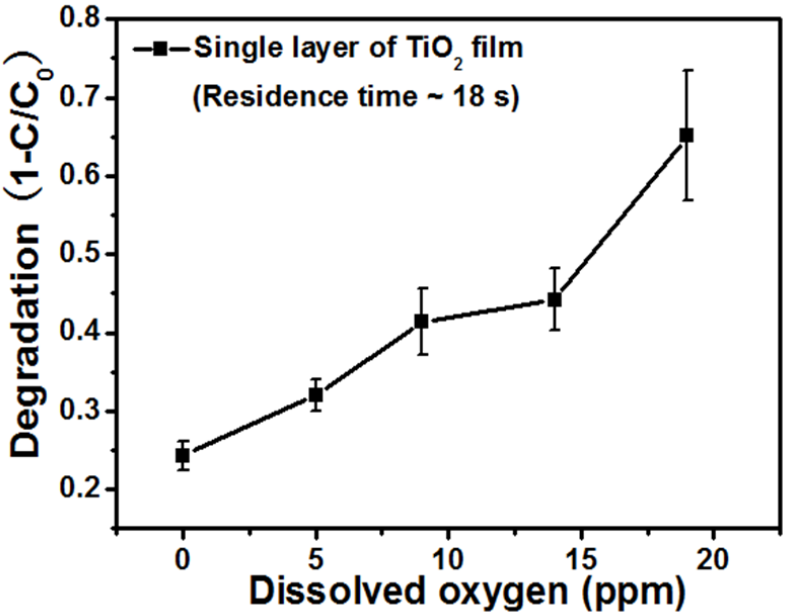

Figure 3.12 Degradation as a function of the oxygen content for the microreactor.

Therefore, I have experimentally shown that the dissolved oxygen indeed affects the degradation efficiency of the microreactors, namely, higher oxygen content results in faster degradation. Nevertheless, the degradation is always exponential with respect to the residence time when the oxygen is insufficient for the full degradation of MB.

3.4.5 Light utilization efficiency

Quantum efficiency can be used to evaluate the efficiency of the photocatalytic reactor. It is defined as number of molecules N_{mol} reacted relative to the number of quanta N_{photon} absorbed by the photocatalyst or reactants

$$\Phi = \frac{N_{mol}}{N_{photon}} \tag{3.5}$$

Normally, the quantum efficiency is characterized using a monochromatic light. However, we will study the average quantum efficiency for the whole activating region (≥ 3.2eV, ~ 387.5 nm) of the solar irradiation. Besides, it should be mentioned that the total energy arrived on the device is not just absorbed by the catalyst and reactants but is also lost by diffraction, scattering and reflection of the device. So the quantum efficiency here is not the actual quantum efficiency but the apparent quantum efficiency.

Calculated from the solar irradiation under AM 1.5 condition [163], the number of the photons arrives at the TiO_2 films is 5.887×10^{16} photons/s. The maximum reaction rate of 8%/s corresponds to the decomposition of 1.45×10^{14} molecules/s of MB. In this case, the average quantum efficiency is 0.25%. However, the total mineralization of one MB molecule needs 102 oxidizing equivalents produced by the photoelectrochemical reactions [108]. If we take this into account, the effective apparent quantum efficiency should be as high as 25%.

It should be pointed out that the energy of activating irradiation for the TiO_2-based photocatalysis is only 3.65% of the whole solar irradiation [163]. The total light utilization efficiency is still very low in this case. Fortunately, several methods are being studied for visible light photocatalysis like doping in TiO_2 [164] and plasmonic

sensitization [165]. Further work will be done to improve the light utilization efficiency using these modified materials.

3.5 Summary

In this chapter, a planar photocatalysis microfluidic reactor was designed and characterized with methylene blue photodegradation under solar irradiation for performance evaluation. A low-cost and simple method was used for the device fabrication. Experiments proved that much higher reaction efficiency could be achieved by this microreactor as compared to the bulk container. Different factors such as the TiO_2 film thickness and the flow rate were investigated to optimize the microreactor performance. 8% s^{-1} reaction rate under solar irradiation was achieved at the flow rate of 900 μl/min. The apparent average quantum efficiency of device under the whole activating solar irradiation (≥ 3.2 eV) was found to be 0.25%. The main limitations of the device are the oxygen deficiency in the reactants and the low solar spectrum sensitivity. The subsequent research work will focus on increasing the oxygen availability in the reaction chamber and improving the visible light sensitivity of the photocatalyst.

CHAPTER 4

LED-MOUNTED OPTOFLUIDIC REACTORS FOR VISIBLE-LIGHT PHOTOCATALYTIC WATER PURIFICATION ASSISTED WITH THERMOLYSIS

This chapter presents the second design of optofluidic reactor, which has similar configuration as the first design in chapter 3 but processes three distinctive features. One is the direct mounting of a blue LED panel onto the reaction chamber. Another is the use of visible responsive photocatalyst $BiVO_4$ instead of UV-responsive TiO_2. And mostly important is the use of the heat of the LED to assist the photocatalytic reaction.

4.1 Introduction

The optofluidic microreactor presented in the precious chapter inherits the merits of flexible flow control, large surface-area-to-volume ratio and compact size from the microfluidics, and benefit the photocatalysis [12], [13], [166]–[168] in various aspects such as fast mass transfer[102], [108], [137], [151], [152], [169]–[177], efficient photon transfer[159], [176]–[178], and short reaction time [102], [108], [137], [151], [152],

[159], [169], [177], [178]. However, the use of TiO_2 limits the utilization of visible light in the sunlight. In addition, the small area of TiO_2 film has an obvious mismatch with the light source. These will be solved using a new optofluidic reactor.

On the other hand, thermodynamics is an important factor for photocatalysis but it is usually ignored or deliberately eliminated by using cooling system [179]. As reported in most work, the adsorption process of organic dye molecules onto the photocatalyst is endothermic, higher reaction temperature can improve the surface adsorbability of photocatalyst and the oxidation activity of OH radicals, resulting in more effective decomposition of the water contaminants [180]. What is more, the photocatalytic degradation is always accompanied by self-thermolysis when the reaction temperature rises up. Therefore, it is more energy efficient if we can utilize the light and the heat from the light source at the same time.

In this chapter, we will present an integrated design of planar microreactor by simultaneously using light energy and its spontaneous heat energy. Compared with our previous studies [159] and the microchannel-based reactors [102], [108], [137], [151], [152], [169]–[174], two new features will be incorporated in the new microreactor – integrated light source and visible photocatalysis. The former is achieved by mounting a blue light emitting diode (LED) panel on top of the reaction chamber. The LED panel

matches the reaction chamber in size and provides relatively uniform irradiation over the photocatalyst reaction surface, ensuring the best utilization of photon energy. Moreover, the direct contact of the LED panel and the reaction chamber makes it feasible to use the heat of LED panel to assist the photocatalytic reactions. The latter is done by using the visible-responsive photocatalyst bismuth vanadate ($BiVO_4$, or in short, BVO). Visible-light driven photocatalysis has long been pursued in the hope to use sunlight directly [181], [182] and this work represents probably the first attempt to develop visible-responsive microreactors.

4.2 Design and Experiment

4.2.1 Setup of microreactor system

The setup of microreactor system is shown in Fig. 4.1 (a), which has a blue-light LED panel mounted directly on a microreactor. In experiment, a fan and a heat sink would also be attached to the LED panel for heat dissipation to avoid overheating. Regarding the microreactor, the fabrication processes were described in the previous chapter [159]. It consists of two glass slides as the cover and the substrate. A 100-μm-thick UV curable adhesive layer (Norland NOA81) acts as the spacer and sealant to form a rectangular reaction chamber with volume of 10 mm × 10 mm × 100 μm = 10 μl. The

glass substrate is coated with the BVO film whereas the cover uses only a blank glass slide. The blue-light LED panel has a light-emitting area (10 mm × 10 mm), which matches the area of reaction chamber. The tree-branch shaped microchannels are used to flow the solution uniformly through the reaction chamber so as to get maximum contact with the BVO film. Fig. 4.1 (b) shows the cross-sectional view of the microreactor. The heights of the tree-branch microchannels and the reaction chamber are 50 μm and 100 μm, respectively. Fig. 4.1 (c) shows the top view photo of the microreactor.

4.2.2 Material and Instruments

$Bi(NO_3)_3\ 5H_2O$ (AR, >99.9%) and NH_4VO_3 (AR, >99.9%) were purchased from Shanghai Chemical Reagent Co. Polydimethysiloxane (PDMS, DC184) was purchased from Dow Corning Co.. The optical adhesive (NOA81) was purchased from Norland Products. Other chemicals including methylene blue (MB) reagent, polyethylene glycol (PEG 20000), detergent (Triton X-100) were purchased from Sigma-Aldrich Co. MB solutions with different concentrations were prepared by dissolving in deionized water. The blue-light LED panel was purchased from Shenzhen Getian Co.

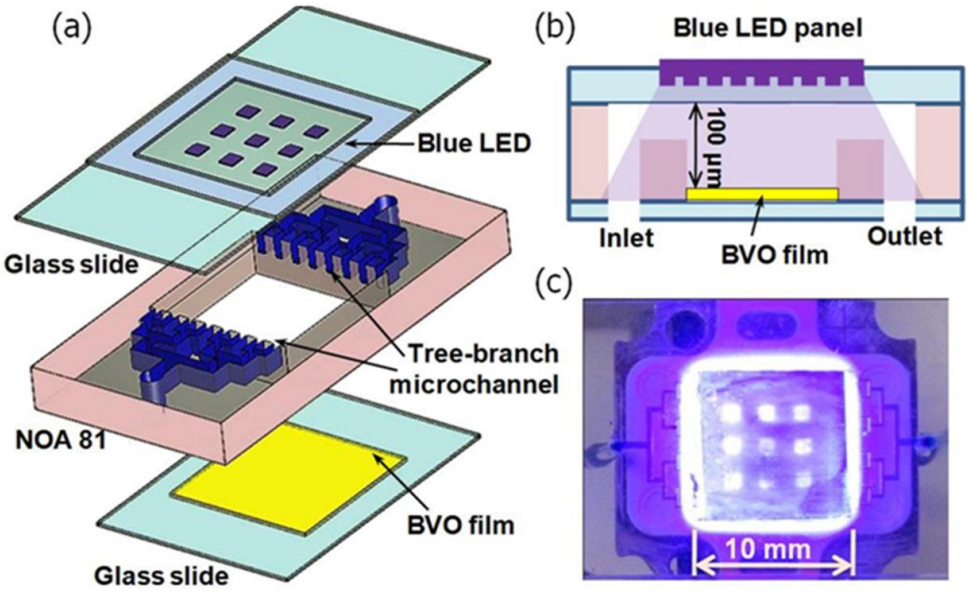

Figure 4.1 Schematic diagram (a) and cross-sectional view (b) of the photocatalytic microreactor system. The microreactor consists of one $BiVO_4$-coated glass slide as the substrate, a blank glass substrate as the cover and a 100-μm-thick UV curable adhesive layer (NOA81) as the spacer and sealant. On top of the reaction chamber (dimensions of $10 \times 10 \times 0.1$ mm^3) is mounted a blue-light LED panel, which has a light-emitting area (10 mm × 10 mm) matching the reaction chamber. The tree-branch shaped microchannels in the NOA81 layer ensure a uniform flow of the solution through the reaction chamber. (c) photo of the integrated microreactor system.

The standard UV lithography was used to fabricate the PDMS mold and the UV lamp to cure the NOA 81 adhesive [159]. Characterization of the synthesized BVO nanoparticles was conducted using a field-emission scanning electron microscope

(FE-SEM) (Bruker, D8 Advanced), a X-ray diffraction (XRD) (JEOL, JSM-633F) and UV-Vis spectrophotometer (UV-2550, Shimadzu). To examine the concentration change between the original and the degraded MB solution, the absorption spectra were analyzed by the same UV-Vis spectrophotometer.

4.2.3 Fabrication of $BiVO_4$ nanoparticles and thin film

Nanosized BVO particles were synthesized by a solid-phase precipitation preparation method assisted with ultrasonic agitation [183]. First, aqueous solutions of $Bi(NO_3)_3$ $5H_2O$ and NH_4VO_3 in 1:1 molar ratio were mixed. The pH value of the final suspension was adjusted to about 7 by adding NH_3 H_2O. Then, the mixture was stirred for 1 h at room temperature. Afterward, the mixture was subject to ultrasonic agitation (100 W) at room temperature in open air for several hours. Next, the yellow precipitates were centrifuged, washed by de-ionized water and absolute ethanol, and then dried at 60 ℃ in air for 10 h. The obtained powders were subsequently calcined at 450 ℃ for 2 h to produce crystalline products.

To enhance the photocatalytic performance of the microreactor, a nano-porous BVO thin film was fabricated to increase its specific surface area. The grinded powders (6 g) were slowly dispersed in deionized water (60 ml) containing acetylacetone (0.2 ml) to prevent reaggregation of the particles. Then, Triton X-100 (0.1 ml) was added to

spread the colloid on the substrate. Finally, PEG 20000 (0.6 g) was added into the aqueous solution under ultrasonic agitation for about 2 h. As a result, the catalyst colloid was formed. Next, a painting method was used to form a BVO thin film on a clean glass slide and dried at 80 ℃. Finally, the BVO thin film was annealed under 500 ℃ for 2 h in air.

4.2.4 Efficiency test of the integrated device

Before the degradation experiment, the LED panel was driven by a DC power supplier and its optical properties were characterized. The light intensity of the LED was measured by a Reference Solar Cell and Meter (91150V, Newport) and the emission wavelength was measured by an integrating sphere (Labsphere). The temperature of microreactor is measured by a thermocouple.

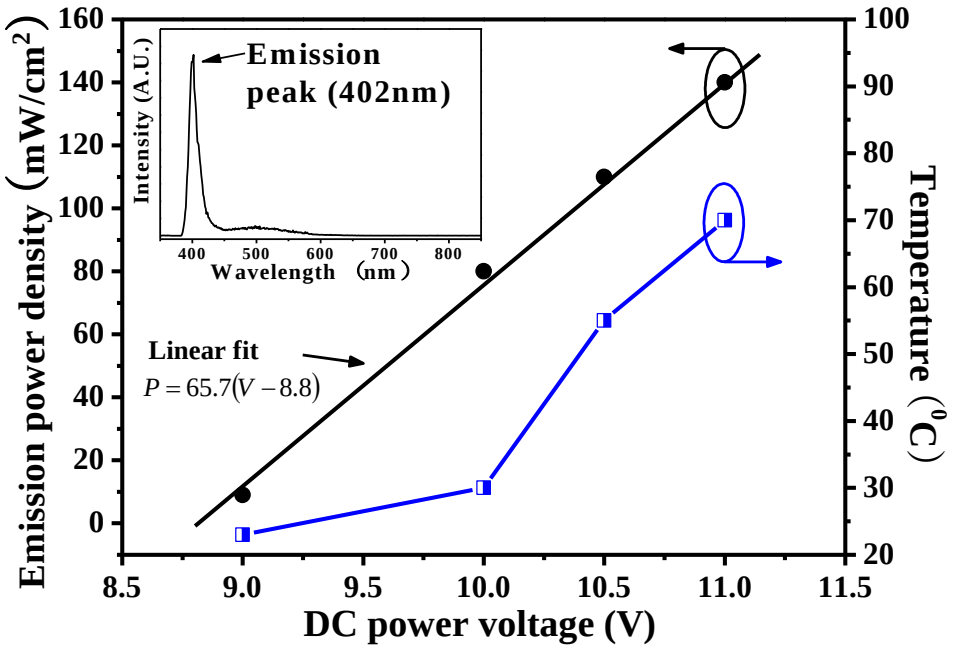

Figure 4.2 Emission power density of the blue-light LED panel and reaction temperature as a function of the driving voltage. The insert shows the LED emission spectrum.

Fig. 4.2 plots the emission power density P of the LED and the reaction temperature T with respect to the driving voltage V. The black round points represents the power density P and follow closely a linear relationship $P = 65.7(V - 8.8)$, here P in the unit of mW/cm^2, V in volt. And the change of reaction temperatures is also plotted as shown by the blue line. The inset of Fig. 4.2 shows the emission spectrum of the LED. A single peak appears at 402 nm with a linewidth of 20 nm. The stability of the LED panel was also tested and the result showed a decrease of the power density by

< 2% in about 2 h. The MB solution as the original reagent was introduced into the microreactor by a syringe pump (TS2-60, Longer). The initial concentration was set to 3 $\times 10^{-5}$ mol/l. The photodegraded MB solution was collected from the outlet.

4.3 Experimental results

4.3.1 Material characterization

The phase and composition of the BVO sample were characterized by XRD, as shown in Fig. 4.3. The diffraction peaks agree well with those of the pure monoclinic BVO according to the JCPDS No. 14-0688. This shows that the synthesized nanosized BVO is in pure monoclinic phase and possesses high photoreactivity.

Since the optical absorption of the photocatalyst is one of the determining factors of photoreactivity [184], UV-Vis diffuse reflectance spectrum (DRS) of the synthesized nanosized BVO samples was also investigated. The result is shown in the inset of Fig. 4.3. It can be seen that the BVO has strong absorption in visible-light region (< 500 nm) and in the UV light region. The absorbance at 402 nm is 86% of the peak absorbance at 284 nm. This implies that the blue-light LED panel can be used as light source.

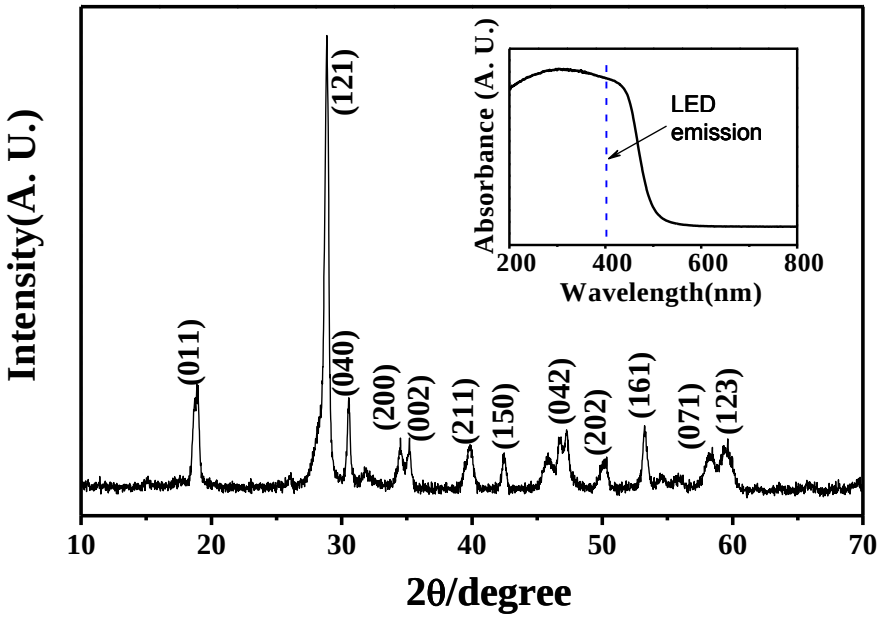

Figure 4.3 X-ray diffraction (XRD) spectrum of the synthetic nanosized $BiVO_4$. The inset shows the UV-Vis diffuse reflectance spectrum.

The morphology and microstructure of the BVO samples were investigated by scanning electron microscopy (SEM). Fig. 4.4 shows the SEM image of the BVO film. It is composed of porous structure and nanosized particles with an average size of about 80 – 100 nm. The inset in Fig. 4.4 shows the cross section of the BVO film. The thickness is about 1.5 μm, which is chosen for high photoreactivity. Through experimental studies, we have found that the photoreactivity increases with the BVO film thickness and tends to saturate when the thickness of the BVO film goes beyond 600 nm. This is reasonable since the photocatalytic reaction only occurred on the

surface of the nanosized photocatalyst. The thickness of 1.5 μm ensures the BVO film works in its highest photoreactivity.

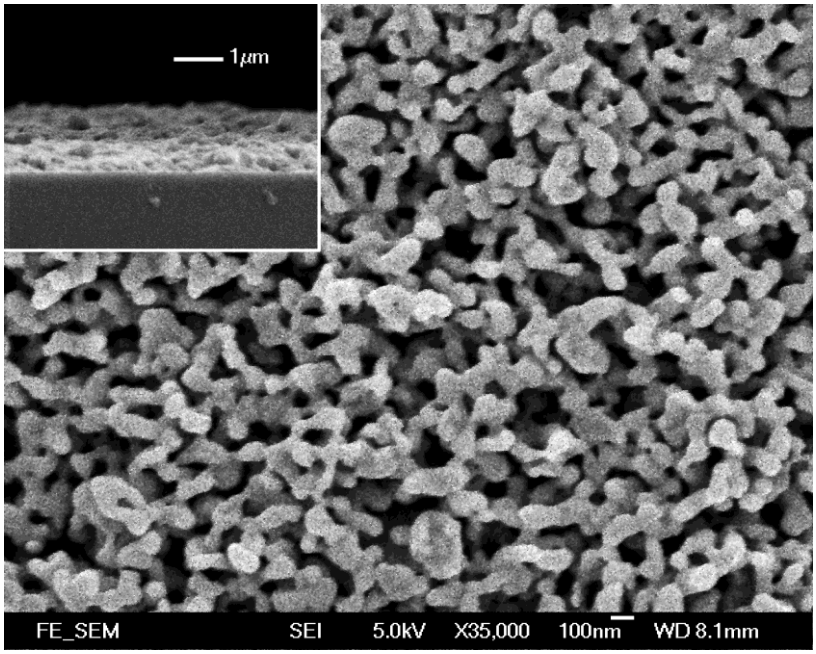

Figure 4.4 Scanning electron micrograph (SEM) of the $BiVO_4$ thin film, which is composed of porous structures formed by the nanosized $BiVO_4$. The inset shows the cross section of the $BiVO_4$ film. The thickness is about 1.5 μm.

4.3.2 Effect of flow rate

In the microreactor system, the flow rate is one of the major factors that affect the photocatalytic reaction efficiency. The flow rate is related to the effective residence time of the MB solution in the reaction chamber by the relationship (*Effective residence*

time) = (*Chamber volume*)/(*Flow rate*).

To investigate the effect of the flow rate, the solutions were pumped at 37.5, 50, 75, 150 μl/min, respectively. The corresponding effective residence time (i.e., the reaction time) is 16, 12, 8 and 4 s, respectively. The blue-light LED is driven at a constant 11V (corresponding to a power density of 140 mW/cm^2). For control experiment, a similar hollow microreactor without the nanoporous BVO film was also tested under the same conditions of flow rates and light intensity. Without the BVO film, the decomposition comes mostly from the thermolysis of MB.

In data analysis, Napierian logarithm of the degradation as a function of the effective residence time was investigated to characterize the performance of the microreactors [181]. The experimental results are plotted in Fig. 4.5. The data points and the error bars represent the averaged values and the standard deviations of three measurements, respectively. A linear fit of the tested data for the control experiment gives a slope of 0.007 s^{-1} owing to the thermolysis. In comparison, the microreactor yields 0.031 s^{-1}, more than 4 times of that of the control. This shows the BVO film works effectively, though not as good as expected.

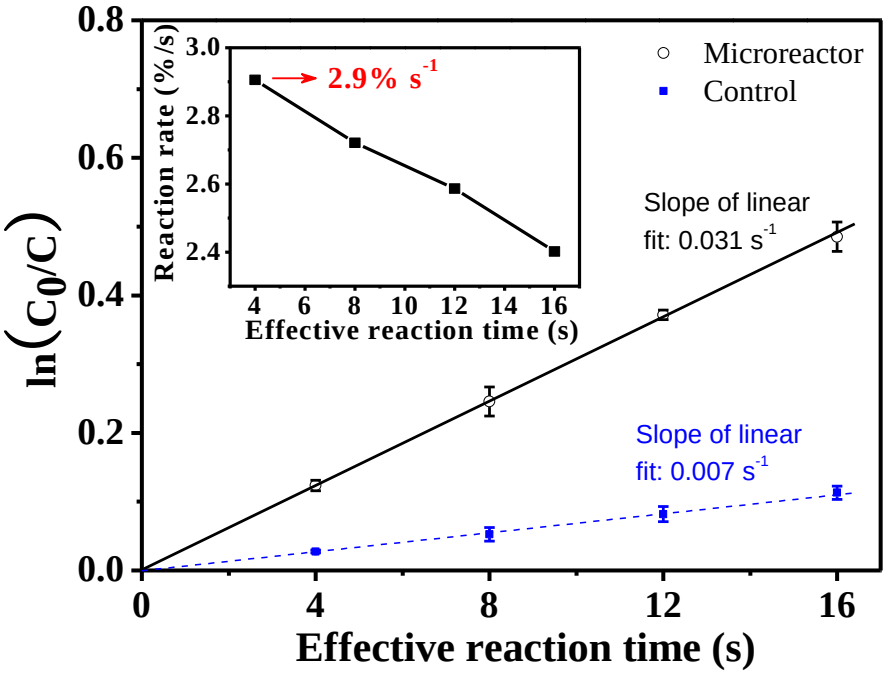

Figure 4.5 Napierian logarithm of the degradation as a function of the effective residence time. The inset shows the reaction rate at different flow rates when the blue light LED panel is driven at 11 V.

The inset in Fig. 4.5 plots the reaction rate with respect to the effective residence time. The data points are the averaged values. Here the reaction rate represents how many percents of the MB are degraded over a unit period of time. It can be observed that the maximum reaction rate 2.9 % s^{-1} corresponds to the shortest residence time 4 s (i.e, the largest flow rate 150 μl/min). The reason for this behavior is not straightforward but can be explained by considering the mass transfer efficiency and the oxygen availability during the reaction [159].

4.3.3 Effects of light source intensity and temperature

The light intensity is obviously a major factor that affects the photocatalytic performance of the microreactor system. The intensity of the LED emission is varied by adjusting the driving voltage from 9 to 11 V. The curves at different flow rates are plotted in Fig. 4.6. It can be seen that the degradation percentage increases with stronger light power density. This is reasonable since more photons would increase the photoreaction. Here the degradation percentage τ is defined as $\tau = (1 - C/C_0) \times 100\%$, it is also called *conversion* in some articles [185]. When comparing the curves of different flow rates, one can see that high flow rate leads to a low degradation percentage. This is because faster flow causes shorter residence time in the reaction chamber (and thus shorter reaction time). These results show clearly that the microreactor system enables easy control of the photocatalysis by adjusting the flow rate and the light intensity of LED. All the error bars shown in Fig. 4.6 was calculated by measuring only one microreactor for 3 to 4 times. The whole measurement took over 40 hours while the BVO film in the reaction chamber degraded by only about 2%. This well demonstrates the long durability of photocatalyst film.

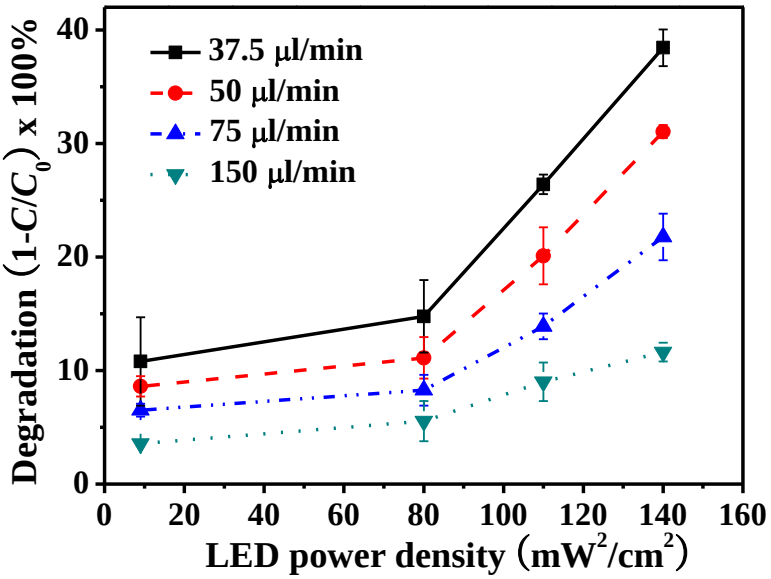

Figure 4.6 Influence of the light intensity on the degradation percentage at different flow rates.

Another important factor, though often ignored, is the reaction temperature. Although a heat sink is fixed on the LED panel, the generated heat still cannot be dissipated fast enough, especially under a high controlled voltage. Therefore, the reaction temperature in the reaction chamber should be higher than room temperature. As mentioned above, this would affect the photocatalysis [180]. Because of the small dimensions of reaction chamber, it is difficult to measure the inner temperature directly. As an approximation, the temperature of the upper surface of reaction chamber is always monitored by a thermocouple during the experiment. The temperature measures to be close to room temperature under 9V, ~30 ^{o}C under 10V, ~55 ^{o}C under 10.5 V, and

~70 ^{o}C under 11V (see Fig. 4.2). As a control experiment to investigate the sole effect of temperature, we used a hot plate to heat the microreactor up to 80 ^{o}C (dark environment, no light). The measured reaction rate constants are plotted in Fig. 4.7 (a) using the blue dashed line. By deducing for degradation rates in Fig. 4.6, the results when the light is on are plotted using the solid red line, which include the combined effect of light and heat generated by visible LED panel. It can be seen from Fig. 4.7 (a) that the thermolysis has an obvious contribution (e.g., degradation percentage > 10% at 60 ^{o}C), though the combined effect of light and heat yields much larger value.

To obtain the direct proof of the contribution of thermolysis, another control experiment was conducted. The reactor was fixed about 1 cm above the LED surface (named as the noncontact setup). With the aid of an air fun, the reaction temperature could be maintained close to the room temperature. The supply voltage was set at 11.5 V so that the irradiation density on the reaction chamber was nearly the same as that of the direct-contact setup under 10V. The experimental results were plotted in Fig. 4.7 (b). It can be seen that the photodegradation rates of the direct-contact setup are 4~6 % larger than that of the noncontact setup. This difference indicates the contribution of heat to the MB degradation.

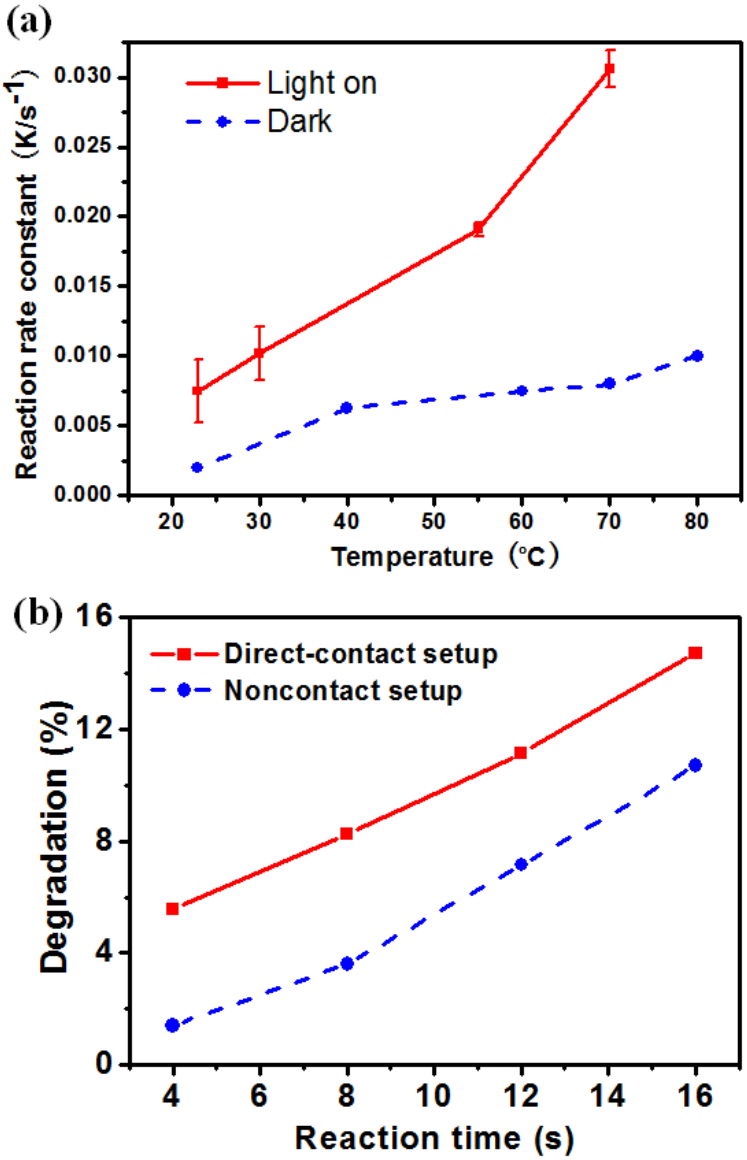

Figure 4.7 (a) Influence of the temperature on the reaction rate constant at the flow rate of 37.5 μl/min; (b) Comparison of the degradation rates with and without the heat. The direct-contact LED setup has similar irradiation densities with the noncontact LED setup, but the former is affected by the heat of LED while the latter is not.

Dissolved oxygen in water is supposed to be an additional key factor that determines the decomposition rate of MB. But when the temperature goes beyond 80 ^{o}C,

air bubbles come out in the reaction chamber, with the repeated growth and collapse of bubbles. This may be attributed to the degassing of dissolved air in the water. Once the bubbles appear, they would also affect the flow in the chamber. This is why the upper limit is set to 70 ^{o}C in the control experiment.

4.3.4 Light utilization efficiency

Apparent quantum efficiency η can be used to evaluate the efficiency of the photocatalytic microreactor. It is defined by $\eta = 102 N_{mol} / N_{photon}$, where N_{mol} is the number of reacted molecules and N_{photon} the number of photons absorbed by the photocatalyst or reactants [159]. The value 102 is because one MB molecule needs 102 electrons for total mineralization [159]. With this relationship, the apparent quantum efficiencies under the LED power densities can be calculated as listed in Table 1. For instance, the number of photons that arrive at the BVO film surface under 140 mW/cm^2 is 2.8 × 10^{17} photons/s [186], and the maximum reaction rate of 2.9 %/s corresponds to the decomposition of 1.3 × 10^{12} molecules/s of MB. In this case, the apparent quantum efficiency is η = 0.048 %. Similarly, the apparent quantum efficiencies for the other conditions can be calculated. It is seen from Table 4-1 that the apparent quantum efficiency reaches its maximum of 0.23 % at the weakest power density of 9 mW/cm^2. This is reasonable since the reaction rate constant k follows approximately $k \propto \sqrt{P}$,

here P is the optical power density. As a result, the apparent quantum efficiency is proportional to $1/\sqrt{P}$ and thus weaker power density enjoys higher apparent quantum efficiency. It is noted that in Table 1 the apparent quantum efficiencies for the other three high-intensity conditions do not follow the $1/\sqrt{P}$ relationship. Oppositely, the apparent quantum efficiency increases with P. This is reasonable if the effect of thermolysis is taken in account. At higher intensity, the temperature goes higher and thus the thermolysis becomes stronger.

Table 4-1 Apparent quantum efficiencies of the microreactor system at different LED power densities and different residence times.

LED driving voltage (V)	Power density (mW/cm^2)	Reaction temp. (^oC)	Apparent quantum efficiency η			
			16s	12s	8s	4s
9.0	9.0	23	0.043%	0.061%	0.10%	0.23%
10.0	80	30	0.007%	0.009%	0.015%	0.04%
10.5	110	55	0.009%	0.012%	0.018%	0.047%
11.0	140	70	0.010%	0.014%	0.022%	0.048%

4.4 Discussions

This microreactor has a very limited throughput (e.g., 9 ml/h for the flow rate of 150 μl/min) and may not be used directly for practical water purification applications (typically threshold throughput > 1,000 l/h). Nevertheless, it may be used a rapid test kit

to quantify the performance of photocatalytic materials [170] and to optimize the operational conditions. In this microreactor, significant degradation can be obtained within about 10 s, this is impressive as compared to the typically a few hours in bulk photocatalytic reactors [102], [152], [167], [181], [187], [188], [189]. In addition, this microreactor requires only a few milli-litres of sample due to the small reaction chamber. This is useful when the photocatalysts and the sample solution are costly. Moreover, the microreactor provides fine control of many conditions of reactions such as flow rate (affecting the mass transfer) and flow condition (laminar or turbulent), making it a useful platform to study the kinetics and detailed mechanisms of photocatalytic reactions [172], [173]. Moreover, many well-developed microfluidic manipulation and detection techniques could be incorporated into the microreactors for in-line monitoring of the intermediate and final products [168], [173], [190].

4.5 Summary

In this chapter, a photocatalytic microreactor system was constructed by directly mounting a blue-light LED panel on a microfluidic planar reactor, which enables to make use of both the heat and the light energy for organic degradation. Experimental studies have shown that the microreactor facilitates the control of photocatalytic process by adjusting the LED light intensity and the flow rate. These correspond to the control

of two important photocatalytic factors: the photon transfer and the mass transfer. The influence of different reaction temperatures to photocatalysis performance of microreactor has also been investigated. Along with other features such as short reaction time and small sample volume, the microreactor system could provide a versatile tool to study the reaction kinetics of photocatalysis and a rapid kit to characterize the performance of photocatalysts. However, this design of optofluidic microreactor still has the problems of oxygen deficiency and electron/hole recombination. New designs of microreactors should be developed.

CHAPTER 5

PHOTOELECTROCATALYTIC MICROREACTORS USING EXTERNAL BIAS VOLTAGE

This chapter presents the third design of optofluidic reator that makes use of the photocatalysis, the electrocatalysis and their synergistic effect. This design is based on the LED-integrated microreactor as described in chapter 4, but introduces an external bias voltage and possesses new features. The first is the new mechanism of photoelectrocatalytic effect. The second is that the electric field helps the separation of photo-excited electrons and holes. The third one is the polarity of external bias enables the selection of oxidation pathways, either electron-driven or hole-driven. The last one is that the bias >1.23 *V* could electrolyze water to generate O_2 to solve the oxygen deficiency problem in the previous microreactor designs. This chapter will elaborate the working principle, the device design and the experimental studies.

5.1 Introduction

Photocatalytic water purification has attracted intensive research but suffers from limited photoreaction efficiency [12], [191], [192]. In the previous studies [159], [193],

[194], we have found that microfluidics (and its new subarea – optofluidics) helps solve two fundamental problems of the photocatalytic water purification – the mass transfer limit and the photon transfer limit [12], [108], [137], [195], [196]. Even in the microreactors, the apparent photonic efficiency (defined as the ratio of the number of photons that participate the photodegradation to the number of total incoming photons) is still quite low, e.g., < 25% for TiO_2 under UV light in [159], ~ 3% for $BiVO_4$ under blue light [194]. One of the fundamental reasons is the recombination of the photo-excited electrons and holes. To solve this problem, a direct approach is to introduce an external bias electric field to force the separation of the electrons and holes, which leads to the photoelectrocatalysis (PEC) [197].

This work will present the working principle of the microfluidic PEC and will study the major physical mechanisms. A microfluidic PEC reactor will be fabricated and characterized in detail so as to verify the physical explanations and to examine the influence of different operational conditions.

5.2 Working principle

The physical principles of the microfluidic PEC can be represented by the illustrations in Fig. 5.1, which show the major processes in the reaction chamber of the

microreactors. Fig. 5.1(a) shows the traditional PC process, which has no external bias. The top layer is transparent (e.g., ITO glass), and the substrate is immobilized with a layer of n-type photocatalyst (e.g., P25 TiO_2, $BiVO_4$). The electrolyte containing the contaminant organic molecules is in the middle. To initiate photoreaction, the excited electrons and holes inside the photocatalyst need to migrate to the same electrolyte/photocatalyst interface by a random-walk diffusion process, causing severe recombination problem and low photonic efficiency. This is the fundamental limit of the traditional PC systems.

The use of a bias electric field could significantly alleviate the recombination problem and thus enhance the photocatalytic efficiency [198], [199]. There are generally two options: positive bias and negative bias. When a positive bias potential is applied to the reactor (here “positive” means the photocatalyst is connected to the positive side of the external bias potential), it generates an electric field inside the photocatalyst layer and forces the photo-excited electrons and holes to separate (see Fig. 5.1(b)).

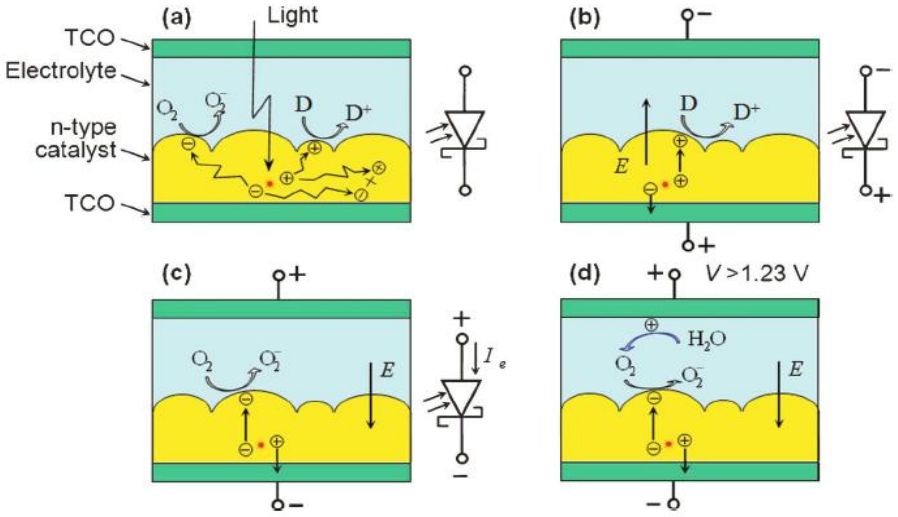

Figure 5.1 Photocatalysis and photoelectrocatalysis in the microfluidic reactors. (a) Photocatalysis in the absence of any external bias potential. The photo-excited electrons and holes need to migrate to the electrolyte/catalyst interface and have plenty of changes to recombine in the course of diffusion and on the interface, causing low photodegradation efficiency. Besides, both of the electrons and the holes can participate the reactions. Here TCO stands for transparent conductive oxide and D for donor. (b) Photoelectrocatalysis in the positive bias state. The induced electric field *E* forces the photo-excited e^-/h^+ to separate. The holes are pushed towards the interface and become the dominant sources of oxidation. For n-type photocatalyst in the positive bias state, its circuit can be represented by a reverse-biased Schottky diode. (c) Photoelectrocatalysis in the negative bias state. The electrons are forced towards the interface and dominate the oxidation. The circuit looks like a forward-biased Schottky diode. (d) When the potential bias potential is > 1.23 V, the electrolysis of O_2 could occur and may provide more O_2 to capture the electrons, eliminating the O_2 deficiency problem.

In fact, the contact of the electrolyte and the n-type photocatalyst layer forms a Schottky-like diode and builds up an internal field pointing from the photocatalyst to the electrolyte [198], [199]. From the circuit point of view, the diode is reversely biased. The external and the internal electric field join force to push the holes toward the interface, at which the contaminants can be degraded by the hole-driven pathway, e.g., $D + h^+ \rightarrow D^+$, here D stands for the electron donor.

When a negative bias potential is applied (see Fig. 5.1(c)), the diode is forward biased and the electrons are driven toward the interface. They can be captured by the dissolved O_2 through $O_2 + e^- \rightarrow O_2^-$, which undergoes further reactions to produce highly oxidative H_2O_2 and OH^* radicals to degrade the contaminants [200]. This shows that selective control of oxidation pathways can be obtained by changing the polarity of the bias potential. For decomposing of organic molecules, the electron-and-O_2 oxidation is generally more efficient than the hole-driven oxidation [201]. Whereas for the degradation of heavy metal ions (e.g., Hg^{2+}, Cr^{3+}), reduction through electrons is more practical [166].

In the PEC process, both the PC and the EC contribute to the degradation of the organic contaminants. However, the degradation efficiency of the PEC is generally larger than the summation of the efficiencies of the PC and the EC. This can be

attributed to the synergetic effect of the PC and the EC [202], [203]. At a low bias potential, the synergetic effect is mainly due to the enhanced electron/hole separation. When the bias potential is larger than 1.23 V, the synergetic effect may have additional contribution from the O_2 evolution (see Fig. 5.1(d)). On the ITO anode, O_2 can be electrolyzed from water by $2H_2O(aq) + 4h^+ \rightarrow O_2 + 4H^+$, here *aq* means the aqueous phase. In the microreactors, these O_2 molecules do not go out as a gas due to the small amount. Instead, they can be diffused to the photocatalyst surface to participate the PC. The diffuse is efficient because the distance between the ITO anode and the photocatalyst surface is only 100 μm. This feature helps to solve the oxygen deficiency problem in the microfluidic PC. Commonly the dissolution of oxygen is low in water and poses a limit to the maximum amount of contaminants that can be degraded. In our previous study, the averaged degradation rate (i.e., degraded percentage of contaminants divided by the whole reaction time) decreased significantly when the reaction time went longer (e.g., from 8% s^{-1} for the 5-s reaction time to 2.5% for the 36-s case) [159]. The common method is by adding H_2O_2, or blowing in O_2 or air. The negatively biased PEC provides an alternative but very efficient method to solve the oxygen deficiency by water electrolysis.

5.3 Device Design

The microfluidics photoelectrocatalytic reactor is shown in Fig. 5.2. The reactor structure consists of mainly three layers: an ITO glass as the cover layer, another ITO glass coated as the substrate and an NOA 81 adhesive layer as the spacer and sealant. A monoclinic $BiVO_4$ (BVO) thin film is deposited on the ITO substrate and acts as the visible-light photocatalyst. To avoid the short circuit, a SiO_2 insulation layer is deposited on the ITO substrate, part of which is exposed to allow a direct contact of the BVO layer with the ITO substrate for electrical connection. The external bias potential can be applied through the two ITO glass layers. The water sample is pumped in from the inlet, through the reaction chamber and to the outlet. Tree-branch shaped microchannel arrays (see Fig. 5.2(a)) are used to lead the flow in and out the reaction chamber. This ensures a uniform flow of the water sample and a maximum contact of the contaminants with the BVO film. Methylene blue (MB) is added into the solution (concentration 3×10^{-5} mol l^{-1}) and is used as the model chemical for characterizing the photoreactivity. The choice of MB is because it is a common residual in the wastewater of textile industry, it is widely used as the model chemical for the PC [159], [193], [194], [204], [205] and it does not absorb the blue LED light used in this experiment. To improve the conductivity of the water sample, NaCl is added to form the electrolyte

(0.001 – 0.3 mol l^{-1}). A blue-light LED panel is mounted on top of the ITO cover. The use of the blue LED panel brings in several merits. For instance, its emission peak is at 402 nm and lies in the high absorption band of the BVO film (absorption edge 500 nm); its flat surface facilitates the direct mount on the microreactor; and its light-emitting area (10 mm × 10 mm) matches the area of reaction chamber. Compared with the other bulky light sources such as Xenon lamps and mercury lamps, the LED panel has higher electrical efficiency and generates less heat; more importantly, it enables direct and uniform illumination of the reaction chamber, ensuring the optimal delivery of photons to the reaction sites. More details of the device fabrication, the test methods and the LED performance are given as below.

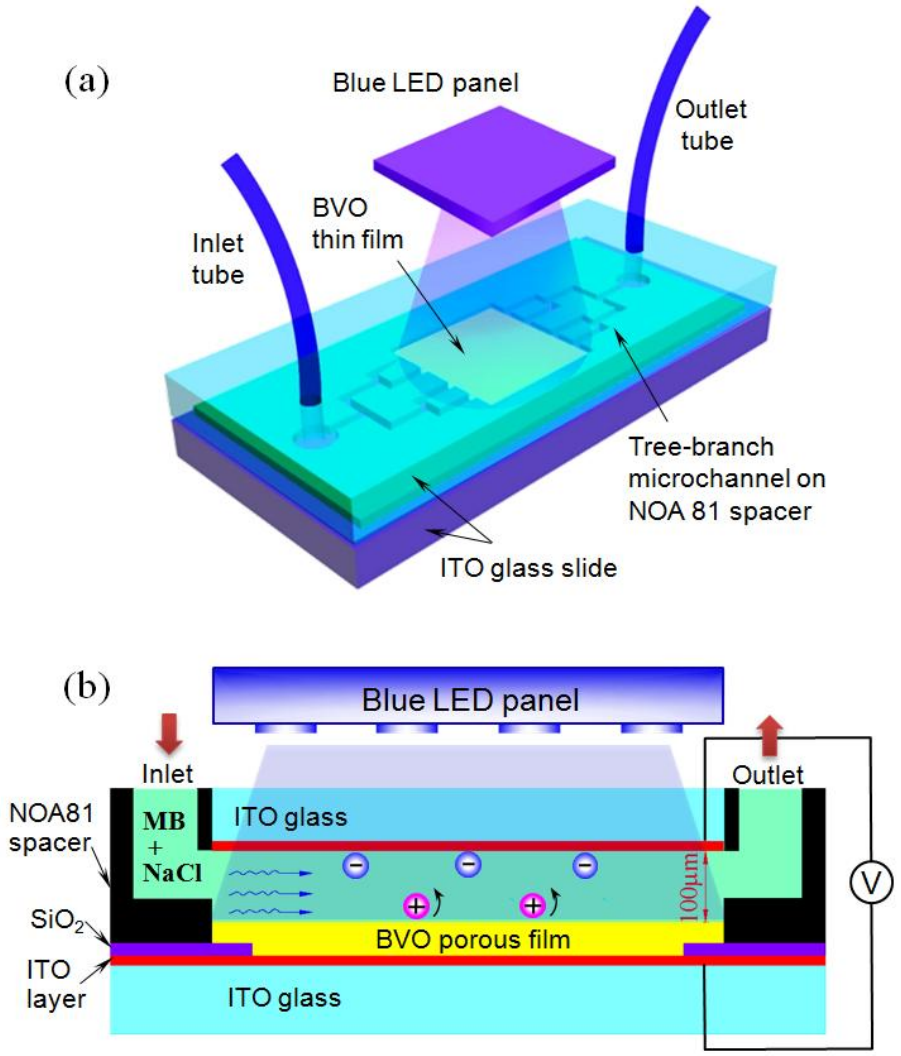

Figure 5.2 Schematics of the microfluidic photoelectrocatalytic reactor. (a) Three-dimensional diagram; and (b) cross-sectional view of the reaction chamber. The reactor consists of a blank ITO glass as the cover, a BVO-coated ITO glass as the substrate and a NOA81 adhesive layer as the spacer. A blue LED panel is mounted on top of the cover for uniform irradiation of the photocatalytic BVO film. A potential is applied across the two ITO layers to force the separation of photo-excited electrons and holes and to help degrade the contaminants by electrocatalytic effect.

5.3.1 Material and Instruments

All the materials used for preparation of $BiVO_4$ nanoparticles and film can be referred to the chapter 4. And all the equipments for characterizing the $BiVO_4$ film, fabrication of microreacor and measuring photocatalytic performance of microreactor are also introduced in chapter 4.

5.3.2 Fabrication of photoelectrocatalytic microreator

First, the synthesized method of $BiVO_4$ nanoparticles and fabrication of $BiVO_4$ film has also been introduced in chapter 4. However, the fabrication and assembly of the microfluidic photocatalytic reactor are more complicated than the previous microreactors because of the necessity to provide proper electrical connection and insulation. Before making BVO thin film, a SiO_2 layer (200 nm) was deposited on an ITO substrate by magnetron sputtering. A window of 9 mm × 9 mm is opened at the center of the SiO_2 film. To fabricate the BVO thin film, the grinded BVO powders (6 g) were slowly dispersed in deionized water (60 ml) containing acetylacetone (0.2 ml) to prevent reaggregation of the particles. Then, Triton X-100 (0.1 ml) was added to spread the colloid on the substrate. Next, PEG 20000 (0.6 g) was added into the aqueous solution under ultrasonic agitation for about 2 h. As a result, the catalyst colloid was formed. Following the manual painting method in [159], the BVO colloid was painted

onto the SiO_2 open window of the ITO glass and then dried at 80 ^oC. Finally, the BVO thin film (10 mm × 10 mm) was annealed under 500 ^oC for 2 h in air. The SiO_2 window ensured the electrical connection of the ITO cover and the ITO substrate in the reaction chamber region and avoided the short circuit of the ITO layers through the electrolyte in the other regions, e.g., the tree-branch microchannels. To obtain a microreactor, the NOA 81 spacer was fabricated and then assembled with the BVO-coated substrate and the ITO cover. The procedures were similar to those reported in our previous work [159], [194].

The photo of the fabricated microreactor before mounting the LED panel is shown in Fig. 5.3. The overall footprint is 4 cm × 2.5 cm (not including the full lengths of the tubes and the wires). The reaction chamber is 10 mm × 10 mm × 100 μm (chamber volume 10 μl). Two syringe needles are used as the inlet and outlet. The yellow region is the BVO_4 film and the light brown regions on the ITO glass slides are Au pad deposited to extract the electrodes conveniently. The tree-branch shaped microchannels can be visualized from Fig. 5.3 as well.

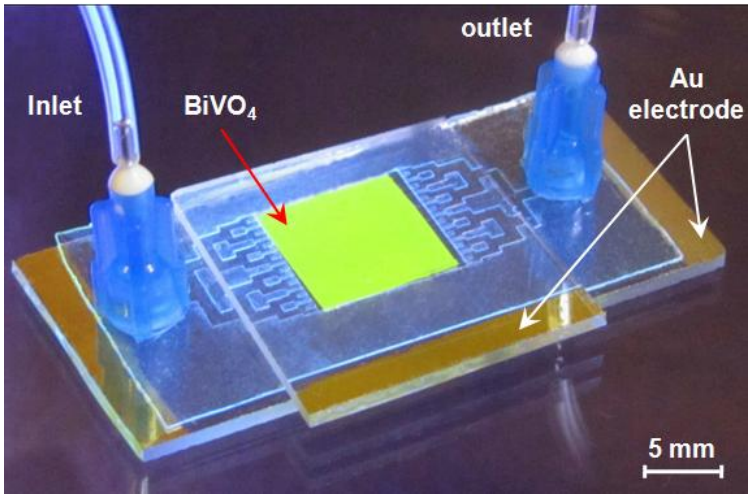

Figure 5.3 Photo of the photoelectrocatalytic microreactor. The $BiVO_4$ film is at the bottom of the reaction chamber, and the tree-branch shaped microchannels connect the inlet and the outlet to the reaction chamber and ensure the solution flows uniformly.

5.4 Results and discussions

5.4.1 Effect of external bias potential

For the degradation of the MB, the oxidizing reactions in the degradation process play the dominant role. Fig. 5.4 plots the MB degradation as a function of the bias potential. To the first order, the MB concentration C can be expressed as $C = C_0 \exp(-kt)$, that is, $\ln(C_0/C) = kt$, here ln is the logarithm of natural base, k is the reaction rate constant, t is the effective reaction time (equivalent to the residence time in the microreactor), and C_0 represents the initial MB concentration. For this reason, the vertical axis of Fig. 5.4 uses the degradation exponent $\ln(C_0/C) = kt$. The upper panel

of Fig. 5.4 shows the photos of the degraded MB samples under different potentials. The insets of Fig. 5.4 show the test configurations.

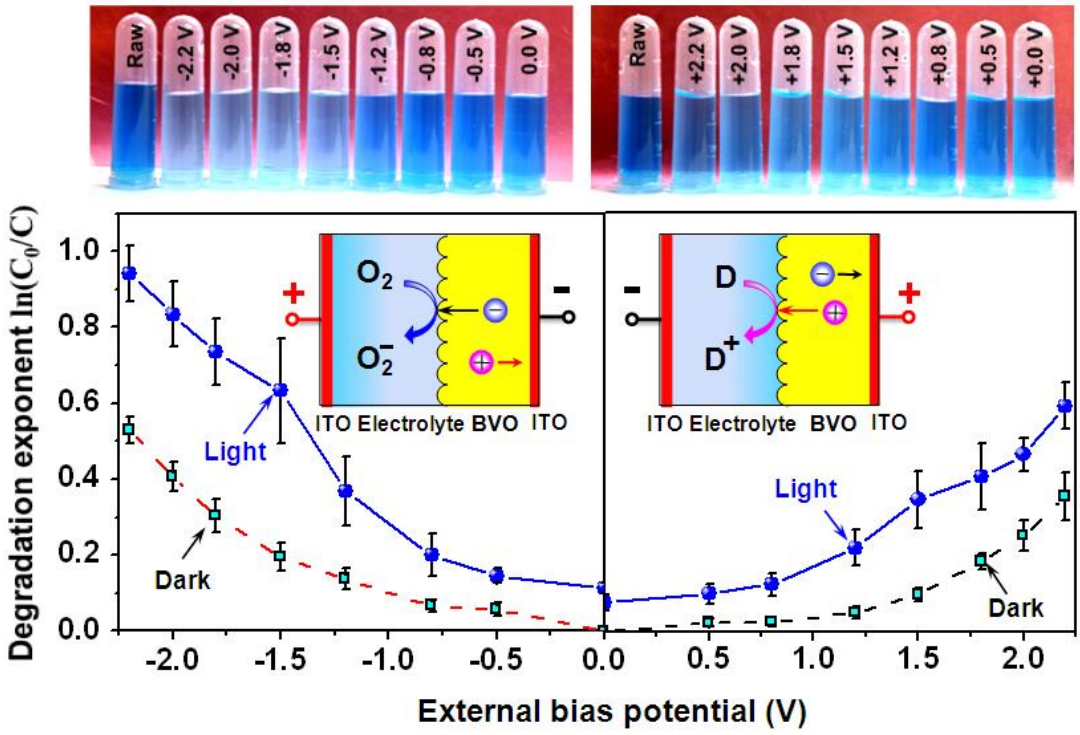

Figure 5.4 Degradation of the methylene blue as a function of the positive and the negative bias potentials. The square dots represent the data points measured in dark environment, the degradation is purely due to the electrocatalytic effect. The round dots represent those with the blue light irradiation, the degradation is due to the combination of photocatalysis and electrocatalysis. The photos on the top panel show the raw samples of methylene blue solutions and the degraded samples under different bias potentials. The insets in the bottom panel illustrate the test configurations.

In the measurement, the bias potential is changed from -2.2 to 0 V (the negative bias state) and then from 0 to 2.2 V (the positive bias state). The power density is maintained at 80 mW cm^{-2} (driven at 10 V). At this level, the LED panel does not heat up significantly (temperature increase < 5 ^{o}C) and avoids the influence of heat on the photocatalytic efficiency. The flow rate is set to 75 μl min^{-1}, corresponding to the flow velocity of 1.25 mm s^{-1} and the residence time of 8 s. For comparison, the MB degradations for both the dark environment and the blue light irradiation are measured. In the dark environment, the MB degradation is purely due to the EC. With the blue light, the degradation at 0 V is purely due to the PC. For the other bias potentials, the degradation is due to the PEC. The data points and the error bars in Fig. 5.4 represent the averaged values and the standard deviations of four measurements, respectively.

To read the curves in Fig. 5.4 properly, one may recall that the degradation exponent $\ln(C_0/C)$ is equivalent to k when t is fixed. In the two curves for the dark environment, the degradation exponent stays at nearly 0 when the magnitude of the bias potential is smaller than 0.8 V and then increases exponentially. This can be understood from the Butler-Volmer formulation [206],

$$k = k_0 \exp\left[A(V - V_{eq})\right] \tag{5.1}$$

where k_0 is the standard rate constant, A is related to the transfer coefficient, and V and V_{eq} represent the electrode potential and the equilibrium potential, respectively. Here V_{eq} = 0.8 V is the electrochemical potential of hydrogen evolution from water by the reaction $2H_2O + 2\ e^- + 0.8\ V(SHE) \rightarrow H_2(g) + 2OH^-$, where g means the gaseous phase and V(SHE) means the potential relative to the standard hydrogen electrode (SHE).

By comparing the two curves of the dark environment, one can see that the negative bias state presents a faster degradation than the positive bias state. This is because the negative bias state corresponds to a forward biasing of the electrolyte/BVO Schottky diode and has a larger current for the EC (see Fig. 5.1(b) and (c)).

For the two curves with the blue light in Fig. 5.4, the degradation exponent increases rapidly when the magnitude of the bias potential is increased from 0 to 2.2 V. However, a kink is observed at 1.5 V, beyond which the increasing of degradation exponent is lowered. Under the blue light, the negative bias state has higher degradation than the positive bias state too. One of the reasons is that the EC in the negative bias state is higher, similar to that in the dark environment. Another reason is that the electron-and-O_2 oxidation in the negative bias state is generally more efficient than the hole-driven oxidation in the positive bias state, as already discussed above. One more

contribution might come from the chloride ions in the electrolyte. It has been found that the chloride ions reduce the photocatalytic efficiency by competing for the surface active sites and by scavenging holes to form weaker oxidative chloride radicals [207], [208]. Under the positive bias, the chloride ions are attracted to the photocatalyst surface and scavenge the holes, deteriorating the photodegradation of MB. In contrast, the negative bias potential pushes the chloride ions away from the photocatalyst surface and circumvents such problem.

It is noted the PEC studies in literature mostly utilized the positive bias (also called "anodic bias" in literature) to go for the hole-driven oxidation and they often chose a low bias voltage so as to avoid the electrochemical oxidation of the targeted organics and the influence of other complicated electrochemical reactions [209]–[212]. A few recent studies on high-voltage PEC systems utilized slurry or slurry-like reactors, which in principle have no performance difference under the positive or negative bias[202], [203]. For these reasons, the negative bias is not very popular. On the other hand, the contribution of electrolyzed O_2 requires a short diffusion length (< 100 μm). This is not effective in the conventional bulky reactors and works only in the planar microreactors. From this point of view, the negative bias is meaningful only in the PEC microreactors and the accompanying O_2 generation is a unique feature of the PEC microreactors.

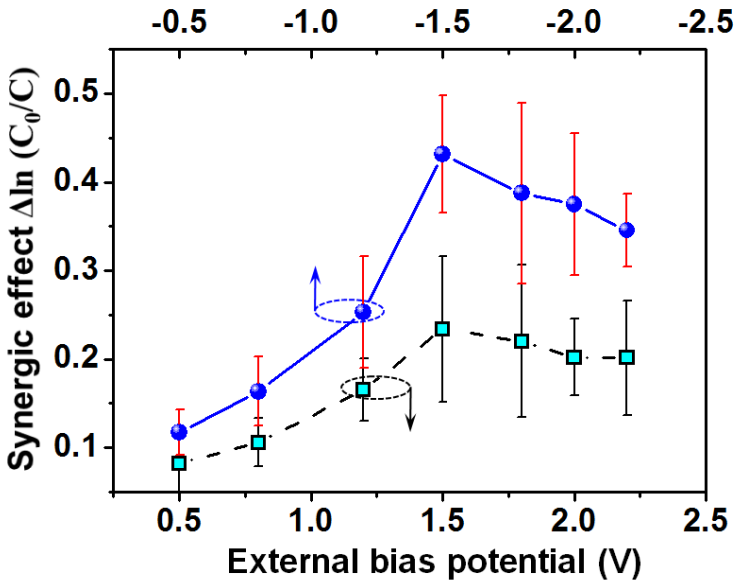

Figure 5.5 Synergetic effect of the photocatalysis and electrocatalysis under the positive and negative bias potentials.

5.4.2 Effect of synergetic effect

The synergetic effect of the EC and the PC is worth further study and is plotted in Fig. 5.5. It can be defined by removing the electrocatalytic and photocatalytic effects from the whole photoelectrocatalytic effect,

$$\Delta \ln\left(\frac{C_0}{C}\right) = \ln\left(\frac{C_0}{C}\right)_{PEC} - \ln\left(\frac{C_0}{C}\right)_{PC} - \ln\left(\frac{C_0}{C}\right)_{EC} \quad (5.2)$$

It can be observed from Fig. 5.5 that both the positive and the negative bias state exhibit maximum synergetic effect when the magnitude of bias potential reaches 1.5 V.

For the synergetic effect, though it has been reported in literature [202], [203], its

physical origin is still not very clear. An and his coworkers studied the PEC degradation of MB using TiO_2 under UV irradiation and attributed the synergetic effect to the conversion of H_2O_2 to the •OH radical[205]. Based on that and our further experimental study, we attempt to explain the synergetic effect in our PEC microreactor. On the anode side, there are $H_2O - 2e^- \rightarrow 2^*OH + 2H^+$ and $MB + {}^*OH \rightarrow product$. These account for the EC oxidation through the •OH radical. On the cathode side, there are $O_2 + e^- \rightarrow O_2^-$ and $O_2^- + e^- + 2H^+ \rightarrow 2H_2O_2$. and then H_2O_2 can oxidize MB. The electrons could come from the photo-excitation or from the external bias with sufficient potential difference (> 0.7 V), and even the photo-excited electrons could be affected by the bias. In this way, the external bias could affect the PC. This might be one of the origins of the synergetic effect. In addition, the external bias could affect the conversion of H_2O_2 to other oxidative species, for instance, $H_2O_2 \rightarrow 2^*OH$ and $H_2O_2 \rightarrow HO_2^* + H^+ + e^-$. This might be another origin of the synergetic effect.

The reasons for the occurrence of maximum synergetic effect at the specific potential of 1.5 V might be attributed to two reasons. One is that at 1.5 V the photo-excited electrons and holes are fully separated and the enhancement effect is saturated. The resistance of the 0.1 mol l^{-1} electrolyte measures a resistance of about 100 Ω and the resistance of the reaction chamber (including both the electrolyte and the

BVO film) is about 1 MΩ. Therefore, most of the potential drop occurs on the BVO film. By estimation, the electric field reaches as high as 10 kV/cm when 1.5 V is applied across the 1.5-μm BVO layer. This is pretty strong for separating the electrons and holes. This effect has been often adopted to explain the saturation of the synergetic effect in slurry reactors [202].

The other reason might be the start of H_2O_2 conversion to HO_2• by the reaction $H_2O_2(aq)$ +1.51 V(SHE) → HO_2• + H^+ + e^-. This is merely our speculation. Little supporting information can be found in literature [202], [203], maybe because of the low bias condition of most of the previous PEC studies and the complication of various electrochemical reactions under the high bias potential. We have conducted cyclic voltammetric measurement of our microreactor in the dark environment and have observed the external current peaks at about ± 1.5 V. This indicates there is some strong electrochemical reaction at 1.5 V. Since H_2O_2 surely exists in the PEC and the value of 1.5 V is very close to the electrochemical potential 1.51 V of the H_2O_2 decomposition, it looks reasonable to attribute the electrochemical reaction at about 1.5 V to the H_2O_2 decomposition.

5.4.3 Effect of flow rate

In the microreactor system, the flow rate is one of the major factors that affect the

degradation efficiency. The flow rate is related to the effective residence time (i.e., the reaction time) of the MB solution in the reaction chamber by the relationship Effective residence time =Chamber volume/Flow rate.

To investigate the effect of the flow rate, the solutions are pumped at 75, 100, 125, 150, 200 μl min^{-1}, respectively. The corresponding effective residence time (i.e., the reaction time) is 8, 6, 4.8, 4 and 3 s, respectively. The blue-light LED maintains a power density of 80 mW/cm^2, the magnitude of the bias potential is fixed at 1.8 V and the NaCl concentration is 0.1 mol l^{-1}.

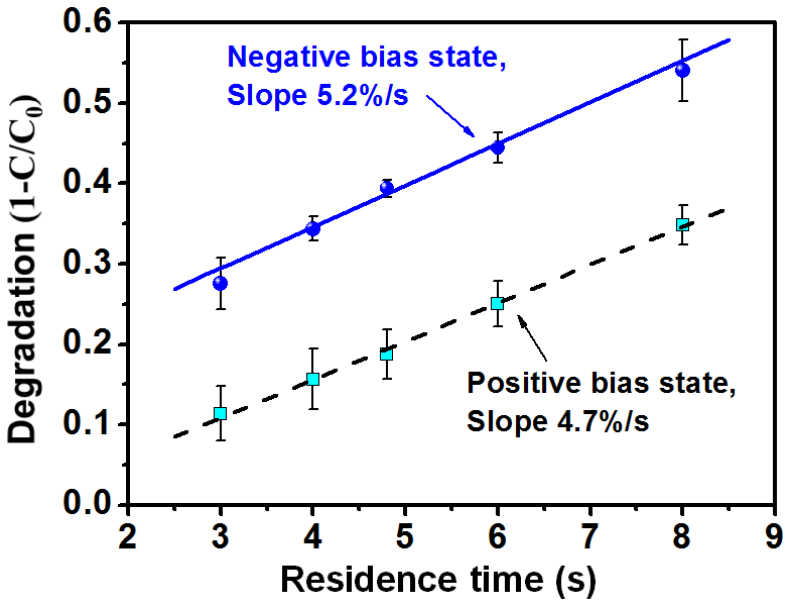

Figure 5.6 Degradation of the methylene blue as a function of the residence time. This shows the influence of the flow rate. The linear dependence of the degradation on the residence time is a distinctive feature of the microfluidic photoelectrocatalysis.

The degradation percentage ($1–C_0/C$) is plotted in Fig. 5.6 as a function of the residence time. It is seen that the negative bias state (the red solid line) has always higher degradation than the positive bias state (the black dash line). Another important feature is that the degradation percentage increases linearly with the residence time. The slope represents the degradation rate (i.e., the change of degraded percentage in 1 s). It is 5.2% s^{-1} for the negative bias state and 4.7% s^{-1} for the positive bias state. One of the preconditions for such linearity in the negative bias state is the sufficiency of O_2. This verifies our prediction that the electrolysis of water can solve the O_2 deficiency problem (here the applied 1.8 V is sufficiently high to electrolyze O_2 from water). Such linear dependence is a signature of the PEC.

It is worth noting that the degradation rate 5.2% s^{-1} is not the upper limit. It is measured at a relative weak power density 80 mW cm^{-2} (the LED driving voltage 10 V). When the LED is driven at 11 V and emits 140 mW cm^{-2}, the degradation rate is increased by more than 2 times. Part of the increase comes from the increased power density. More significant contribution comes from the increased temperature. At 10 V, the temperature of the LED is almost the room temperature; whereas at 11 V, the LED heats up by more than 30 ^oC.

5.4.4 Effect of NaCl concentration

In the above experiments, the concentration of NaCl C_{NaCl} is fixed at 0.1 mol l^{-1}. To investigate the influence of C_{NaCl}, the degradation exponent $\ln(C_0/C)$ is measured for C_{NaCl} = 0.001 to 0.3 mol l^{-1}. The flow rate is maintained at 75 μl/min and the power density at 80 mW cm^{-2}. It is found that the $\ln(C_0/C)$ rises up quickly at low concentration and tends to saturate after 0.02 mol l^{-1}. This trend is reasonable. At low concentration, the charge transport in the electrolyte is the limiting factor of the EC. At high concentration, the charge transport is sufficient to maximize the EC and the overall reaction rate constant goes to saturate.

5.4.5 Effect of electrolytic chlorine

Chlorine might be generated in the PEC microreactor when the external bias is large than 1.37 V, which may cause the decoloring of methylene blue solutions. In this section, several experiments were conducted to investigate the effect of the electrolytic chlorine in the PEC microreactors.

a) Na_2SO_4 used as electrolyte

First, Na_2SO_4 was used as the electrolyte to replace NaCl for the photodegradation experiments of PEC microreactors. The idea behind is that the Na_2SO_4 solution does not generate chlorine in electrolysis. For a fair comparison, both of the Na2SO4 solution

and the NaCl solution have the same concentration of Na^+ in the methylene blue solutions. As the NaCl solution was 0.1 M in our previous study, here the Na_2SO_4 solution was chosen to be 0.05 M in the tests.

The experimental results are plotted in Fig. 5.7, the solid lines represent the results by using NaCl as the electrolyte and the dash lines represent the results by using Na_2SO_4 as the electrolyte. Ideally, the generations of O_2 and Cl_2 need 1.23 V and 1.36 V, respectively. When the bias voltage is below 1.2 V, there is no electrolysis and thus no problem of chlorine generation or decoloring. Therefore, only higher voltages (1.5 V, 1.8 V and 2.2 V) were tested for both the negative and the positive bias by using Na_2SO_4 as the electrolyte. The experimental results are very close to our previous results by using NaCl as the electrolyte. The error bar is the result of four repeated tests. The similar results of the Na_2SO_4 electrolyte with the NaCl electrolyte cannot directly prove whether chlorine is generated, but shows it is not important in term of the methylene blue decomposition (or more actually, decoloring).

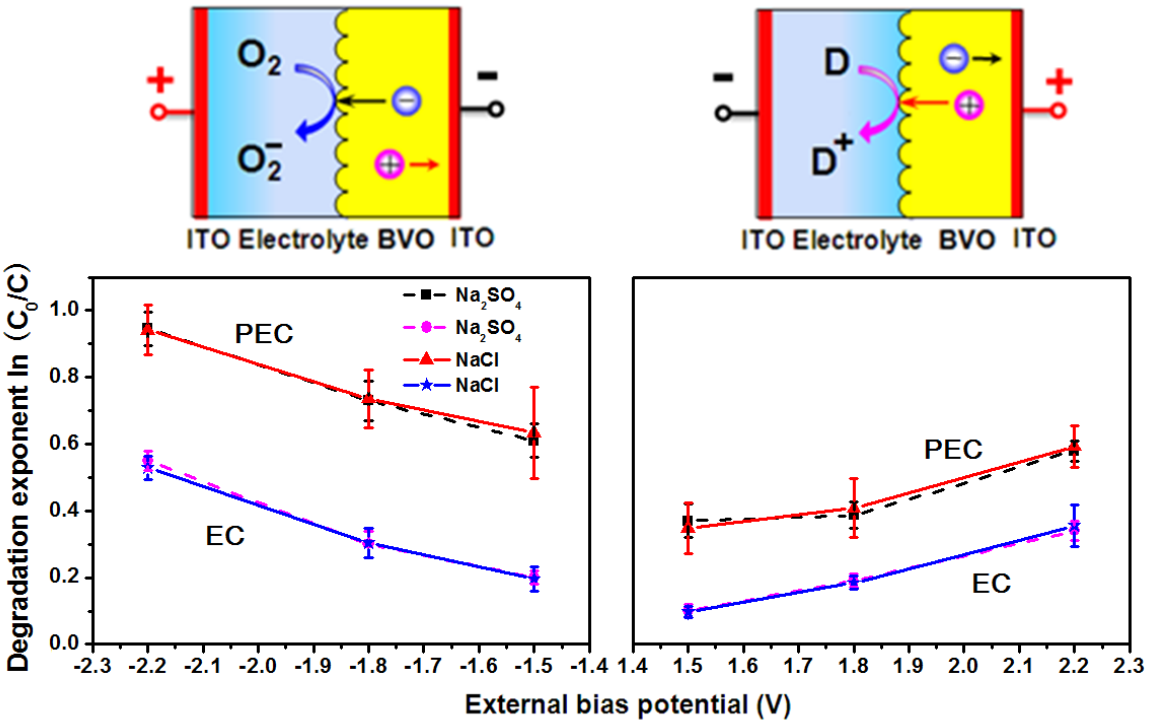

Figure 5.7 Degradation of MB under the positive and the negative bias potential by using NaCl (solid lines) and Na_2SO_4 (dash lines) as the electrolyte. PEC: photoelectrocatalysis; EC: electrocatalysis.

After that, we also investigated the influence of flow rate. The experimental results are plotted in Fig. 5.8, the solid lines represent the results by using NaCl as the electrolyte and the dash lines represent the results by using Na_2SO_4 as the electrolyte. The error bar is the result of four repeated tests. The relationship between the degradation percentage and the reaction time are still shown to have a linear relationship. And the experimental results are nearly the same as our previous results by using NaCl

as electrolyte. For example, for the negative bias state, the slope is 5.3% for Na_2SO_4 and 5.2% for NaCl; and for the positive bias, the slope is 4.4% for Na_2SO_4 and 4.7% for NaCl. Such small differences in the slope can be attributed to the measuring error.

Again, the similarity of Na_2SO_4 with NaCl cannot directly prove the existence of chlorine, but shows the influence of chlorine generation is insignificant.

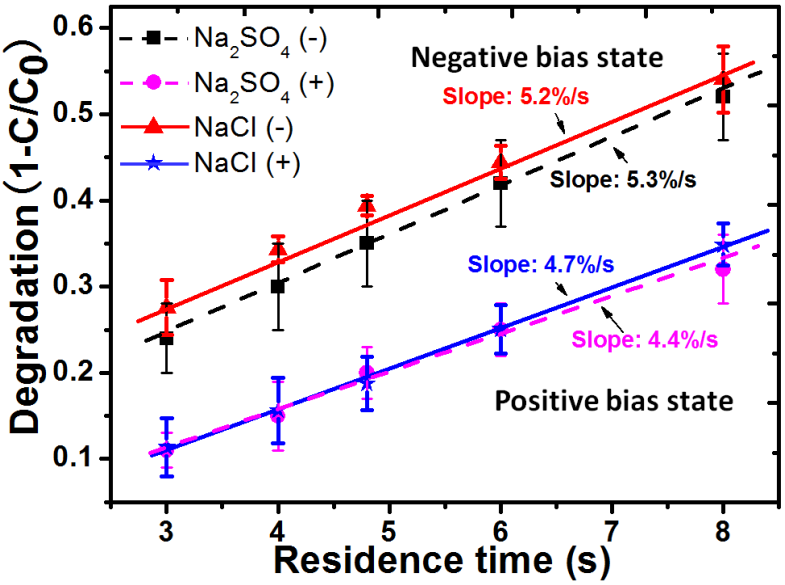

Figure 5.8 Influence of the flow rate on the degradation efficiency of microreactor under ±1.8 V external bias by using NaCl (solid lines) and Na_2SO_4 (dash lines) as the electrolyte.

b) Cyclic Voltammetry

To find some more proofs of chlorine generation in our microreactor, I used a standard three electrode test method (working electrode: ITO, counter electrode: $BiVO_4$ film,

reference electrode: calomel) to measure the IV curve by the cyclic voltammetry. The Na_2SO_4 and NaCl electrolytes are adjusted to the same ion concentration of Na^+. The IV curves of the two electrolytes are shown in Fig. 5.9. They are smooth and present no obvious redox peaks below 1.5 V. As the electric potential of generating chlorine (1.36 V) is larger than oxygen (1.23 V), the rise of current in the Na_2SO_4 curve when > 1.5 V should be resulted mostly from the generated of O_2. Therefore, from the curves, we can see there may be no significant generation of chlorine in this reaction system, though the exact amount of chlorine cannot be quantified using this method. A further experiment was conducted.

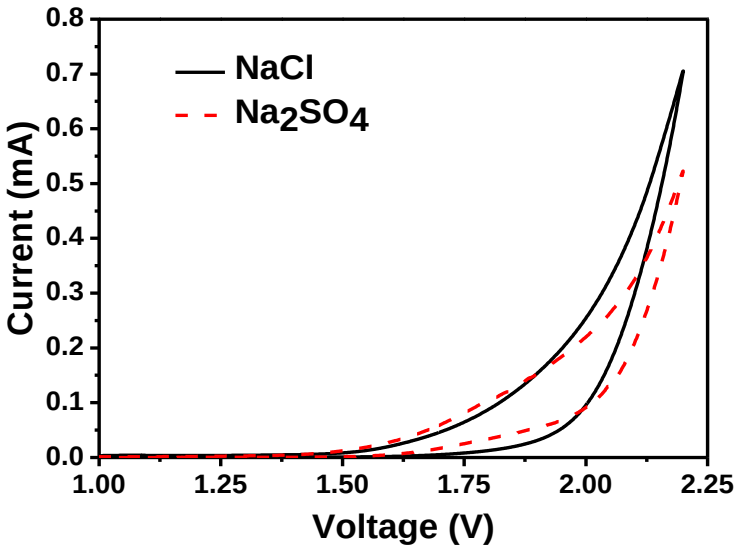

Figure 5.9 IV curves of electrolysis by using Na_2SO_4 and NaCl as the electrolytes. (working electrode: ITO, counter electrode: $BiVO_4$ film, reference electrode: calomel).

c) Electrolytic chlorine content under different electrodes

The above experiments provide no direct proof of the amount of chlorine. I decided to conduct a group of control experiments to electrolyze the NaCl solution and to measure the generated chlorine by using the classical titration method ($2KI+Cl_2 \rightarrow 2KCl + I_2$, $2Na_2S_2O_3 + I_2 \rightarrow 2NaI + Na_2S_4O_5$). Three NaCl solutions (30 ml, 0.03 M) were prepared and electrolyzed using different electrodes as follows for about 1 hour:

(1) Pt-Pt (working electrode: Pt sheet; counter electrode: Pt wire; reference electrode: calomel);

(2) Pt-ITO (working electrode: ITO; counter electrode: Pt wire; reference electrode: calomel);

(3) $BiVO_4$-ITO (working electrode: ITO; counter electrode: $BiVO_4$ film; reference electrode: calomel);

After the electrolysis under 1.8 V for 1 hour, the setup of Pt-Pt electrodes generated chlorine obviously. The consumption of $Na_2S_2O_3$ (wt: 20%) in the titration process was about 0.225 ml. Accordingly, the generated chlorine had a lower limit of 2.65×10^{-2} g/l (some chlorine might be released as the gas into air). But in the other two setups (Pt-ITO, $BiVO_4$-ITO), the consumed volumes of $Na_2S_2O_3$ were both 5 μl, equivalent to the generated Cl_2 of 5.9×10^{-4} g/l, which was at least 2 orders lower than

the Pt-Pt setup. Moreover, it is noted that the time of electrolysis was as long as 1 hour. In our PEC microreactors, the reaction time was only several seconds. Based on the generated chlorine of 5.9×10^{-4} g/l after 1-hour electrolysis, a reaction time of 10 s would correspond to the generation of chlorine of 2.3×10^{-8} M, which is 4 orders smaller than the naturally dissolved oxygen content 2.8×10^{-4} M in the solution. Therefore, the amount of generated chlorine is insignificant to the decomposition of MB.

This may be explained by the large potential drop and/or high overpotentials by the non-perfect conductive ITO and $BiVO_4$ films. Theoretical, the generations of O_2 and Cl_2 need 1.23 V and 1.36 V, respectively. However, the PEC reactor uses the ITO glass as the working electrode and the semiconducting $BiVO_4$ film as the counter electrode, none of ITO and $BiVO_4$ is highly conductive. They would cause some potential drops, especially the semiconducting $BiVO_4$ film. In addition, both may require high overpotentials as compared with the Pt electrode. As a result, even the bias of 2.2 V is still not high enough to electrolyze chlorine from the NaCl solution.

Therefore, we can conclude that the generated chlorine in our microreactor was too low to have an obvious influence.

5.4.6 Stability, test speed and process volume

The microreactor exhibits amazing stability over the repeated testing. For instance, to generate the data points only for Fig. 5.4, the test needs to be repeated for more than 100 times, and the microreactor remains almost similar performance. This is really impressive as compared to many bulky reactors, in which the performance can be maintained only for a few cycles [204]. Such high stability might be attributed to the self-refreshing property of the microreactor. In the experiment, the solution flows quickly over the BVO film, flushes away the reaction products and refreshes the reaction sites. These would significantly reduce the poisoning of the BVO film. Such high stability is another very useful merit of the microreactor.

The testing speed using the microreactor is pretty fast. It can be seen from Fig. 5.6 that significant degradation can be obtained within a few seconds. Assuming the flow rate is 200 μl min^{-1} and the UV-vis spectroscopic measurement requires a sample volume of 1 ml. It takes only 5 min to conduct one run of test. It is very fast as compared to the typical testing time of a few hours using the bulky reactors [197], [213], [214]. From this point of view, the microreactors can be used for rapid characterization of photocatalysts and for study of the reaction kinetics/pathways.

The limited process volume of the microreactors is a big concern for practical

applications. For instance, the PEC reactor has a reaction chamber volume of only 10 μl. If the solution is pumped at 200 μl min^{-1}, the process volume is only 0.12 l h^{-1}. However, the dimensions of the microreactor can be scaled up without affecting the mass transfer. Assuming the reaction chamber has a surface area *S* and a height H, the flow rate is $Q = SH/t$. To maintain the same level of mass transfer, H/t is kept constant. As a result, *Q* scales up with *S*. Assume the PEC microreactor is scaled up by 100 times to have a surface area of 1 m × 1 m, the process volume is scaled up by 10,000 times to 1.2 m^3 h^{-1}. This would be sufficient for many small-scale applications like family uses and field water supply. And, an array of such reactors could further increase the overall process volume.

5.5 Summary

In this chapter, we have demonstrated that the photoelectrocatalytic microreactors could solve a fundamental problem of the photocatalytic water purification – the recombination of photo-excited electrons and holes. Moreover, they enable the selective control of reaction pathways and the synergetic effect of PC and EC. And, the problem of oxygen deficiency can be eliminated by the accompanying water electrolysis under the bias potential. The great advantages of the microfluidics for the photocatalytic water purification may encourage the studies of microfluidics for other photocatalytic

processes such as photoreduction of CO_2 and heavy metal ions, photosynthesis, water splitting and air purification.

CHAPTER 6

CONCLUSIONS AND FUTURE RECOMMENDATIONS

6.1 Conclusions

In this thesis, we have demonstrated that the photocatalytic microreactors could solve several fundamental problems of the photocatalytic water purification – the mass transfer limit, the photon transfer limit, the recombination of photo-excited electrons and holes, the low utilization of visible light in sunlight, the oxygen deficiency and the lack of control of reaction pathways. In addition, we have introduced the photoelectrocatalytic effect and the thermal assistance effect into the photocatalytic microreactors.

In our first design, planar microreactors have been proposed to enhance the utilization of the surface area of microfluidic chips. We fabricated the microreactor of this type to study the photocatalytic degradation of methylene blue under solar irradiation. The design and cross-section of microreactor can be seen in chapter 3. The microreactor had a rectangular reaction chamber, which was constructed by two nanoporous TiO_2-coated glasses [72] as the cover and substrate and a 100-μm-thick epoxy layer as the spacer and sealant. In the planar microreactor, the TiO_2 films on the

glasses had the same surface area with the reaction chamber, making the best use of surface area for light receiving and photocatalytic reaction. In this device, the liquid layer was 100 μm thick, and thus the nominal SA:V of the microreactor was $\mathrm{SA:V} = 2/h_2 = 20{,}000\,\mathrm{m}^{-1}$, where h_2 is the height of reaction chamber. As mentioned above, the actual value should be many times larger due to the nanoporous morphology of TiO_2 film. Such a high SA:V would significantly improve the mass transfer efficiency. According to the experimental results, the photodegradation efficiency of MB could go up to 94% at a reaction time of 36 s, which was really impressive as compared to the reaction time of several hours or even days that are often needed in the bulk reactors [64]. However, the device faced the problems of oxygen deficiency (due to the insufficient dissolved oxygen) and low solar spectrum sensitivity (due to the use of TiO_2). In addition, the recombination of photo-excited electrons and holes was still quite serious because of the use of one type of photocatalyst material (i.e., TiO_2) and thus no internal mechanism to separate electrons and holes.

In our second design, a photocatalytic microreactor using visible irradiation is developed to overcome the limitation of the first generation of microreactor. It has a blue-light LED panel mounted below the reaction chamber of microfluidic planar reactor, which enables to make use of both the heat and the light energy for organic

degradation. $BiVO_4$ is employed to replace TiO_2 as the photocatalyst because it had high photocatalytic reactivity under visible light because of its small bad gap (< 2.7 eV) and good charge migration ability. This ensured a better utilization of the solar spectrum. The methylene blue is also used as the reagent and the degradation experimental studies have shown that the microreactor can utilize the visible light efficiently, which also can be used to control the photocatalytic process by adjusting the LED light intensity and the flow rate, which is respectively related to two important photocatalytic factors: the photon transfer and the mass transfer. The thermolysis existing in the reaction process is also investigated to assist the photocatalysis through set up with different reaction temperatures. Along with the merits such as short reaction time and small sample volume, the microreactor system could provide a versatile tool to study the reaction kinetics of photocatalysis and a rapid kit to characterize the performance of photocatalysts.

In our third design, another new planar microreactor is developed to solve the problems of last two designs of reactors. The photoelectrocatalysis is employed to enhance the separation of electrons and holes by electrical field. The basic structure of the reactor is similar with the second design of microreactor, including the photocatalyst and light source. The unique part is that both the top and bottom of reaction chamber

were enclosed by ITO glass, could be connected with a voltage source to form a planar electrical field. When a bias voltage was applied, the electrons and holes were forced to separate. In fact, the bias voltage introduced other benefits. By changing the polarity of voltage, electrons or holes could be selectively driven to the BVO reaction surface. This enabled the control of electron-driven or hole-driven oxidation for photodecomposition. In addition, when the top ITO layer was driven over 1.23 V, electrolysis of water generated oxygen, which could diffuse to the BVO surface to supply the oxygen for electron-driven oxidation. In this way, it solved the oxygen deficiency problem. According to the experimental results, the negative bias exhibited always higher performance. The device was tested for more than 200 times and showed little degradation of the performance. The photoelectrocatalytic microreactor shows high stability and may be scaled up for high-performance water purification.

6.2 Recommendations for Future Work

The microfluidic reactors have some limitations too. It involves the fabrication of microstructures and the embedment of photocatalysts. Fortunately, fabrication of microfluidic structures using soft materials (but may have hard cover and hard substrate) is already a routine process, and the photocatalyst can be deposited onto the substrate

before being bonded with the microstructure. Another severe problem is the limited throughput, typically in 1 ml/h. This is far from the threshold throughput of about 1,000 l/h for practical applications. To boost up the throughput, several possible approaches could be exploited. A simple way is to use a large array of microreactors to sum up the throughput to a meaningful level (like 1 l/h). A more practical way is to scale up the microreactors to the meter size, while maintaining the performance determining factors such as surface-area-to-volume ratio and the residence time.

New designs could also been introduced, for example, coating the inner surface of capillary tubes with photocatalysts and then piling up the tubes into a large bundle (similar to the structure of a photonic crystal fiber but having much cross section). This design is a combined use of optofluidic waveguide and photonic crystal fiber. The contaminated water could be run through the holes of tubes and the light may be irradiated directly onto the bundle cross section. Each stream of flow inside the tubes acts as an optofluidic waveguide to carry the light, which is absorbed gradually by the photocatalyst layer coated on the tube inner surface for photodegradation. This design ensures a long interaction length of the light with the photocatalyst layer and the water sample, and would lead to a full utilization of the light energy and a total cleaning of the contaminants. Large cross-sectional area and fast flow velocity (using long tubes to

ensure sufficient residence time) join up for large throughput. It is feasible to achieve 1000 l/h. Many other innovative designs could be explored as well. With the techniques and physical understandings accumulated during the development of microfluidic reactors, the prospect for industrial water purification is very promising.

On the other hand, there are many scenarios that do not need large throughput. In fact, the microreactors consume small amounts of liquid sample and photocatalysts. This could be a beneficial factor for some applications, for instance, rapid characterization of expensive photocatalysts, parallel performance comparison of different photocatalysts and optimization of the operation condition. As the photocatalytic reaction is strongly dependent on many factors (e.g., type of photocatalysts, preparation details of photocatalysts, model chemicals, light sources, temperature, pH value, etc.), it has long been a headache to standardize the photocatalytic efficiency tests and to make different tests comparable. The microreactors may provide a standard platform as it enables convenient control of operation conditions (such as flow rate, heat dissipation, etc), rapid characterization and parallel photoreactions (using an array of microchannels or reaction chambers). Similar case in the use of microfluidic chips for drug screening has achieved great success.

Beyond that, the microreactors have potential for other fields. Actually, some

studies have already tried water splitting [37, 38], protein cleavage [65] and photosynthesis [66-75], but most are on the infant stage. There are still a lot more to explore. For example, bulk reaction systems have utilized the photocatalysis for destructing bacteria [85] and viruses [86], inactivation of cancer cells [87], nitrogen fixation [88, 89] and remediation of oil spills [47, 90]. Their corresponding microfluidic designs have yet to come.

References

[1] S. Malato, P. Fernández-Ibáñez, M. I. Maldonado, J. Blanco, and W. Gernjak, "Decontamination and disinfection of water by solar photocatalysis: Recent overview and trends," Catalysis Today, vol. 147. pp. 1–59, 2009.

[2] Y. F. Chen, L. Jiang, M. Mancuso, a Jain, V. Oncescu, and D. Erickson, "Optofluidic opportunities in global health, food, water and energy," Nanoscale, vol. 4, pp. 4839–4857, 2012.

[3] B. Bradley, G. Daigger, R. Rubin, and G. Tchobanoglous, "Evaluation of onsite wastewater treatment technologies using sustainable development criteria," Clean Technologies and Environmental Policy, vol. 4. pp. 87–99, 2002.

[4] W. Viessman and M. J. Hammer, Water Supply and Pollution Control, Sixth edit., Addison-Wesley, 1998, p. 286.

[5] M. A. Shannon, P. W. Bohn, M. Elimelech, J. G. Georgiadis, B. J. Mariñas, and A. M. Mayes, "Science and technology for water purification in the coming decades," Nature, vol. 452, pp. 301–310, 2008.

[6] P. R. Gogate and A. B. Pandit, "A review of imperative technologies for wastewater treatment I: Oxidation technologies at ambient conditions," Advances in Environmental Research, vol. 8. pp. 501–551, 2004.

[7] K. H. Fujishima, "Electrochemical Photolysis of Water at a Semiconductor," Nature, vol. 238, pp. 37–38, 1972.

[8] D. F. O. Ann Lorette. Pruden, "Degradation of chloroform by photoassisted heterogeneous catalysis in dilute aqueous suspensions of titanium dioxide," Environ. Sci. Technol, vol. 17, no. 10, pp. 628–631, 1983.

[9] H. M. T. J. H. Carey, J. Lawrence, "Photodechlorination of PCB's in the Presence of Titanium Dioxide in Aqueous Suspensions," Bull. Environ. Contam. Toxicol., vol. 16, no. 6, pp. 697–701, 1976.

[10] Available: http://www.piaj.gr.jp/roller/en/entry/200706118.

[11] Available:http://www.bccresearch.com/market-research/advanced-materials/photo-catalysts-tech-markets-avm069a.html.

[12] H. A. EKabi and D. F. Ollis, "Photocatalytic Purification and Treatment of Water and Air," Amsterdam, Ed. Elsevier, 1993, pp. 719–725.

[13] J. Herrmann, "Heterogeneous photocatalysis: fundamentals and applications to the removal of various types of aqueous pollutants," Catalysis Today, vol. 53. pp. 115–129, 1999.

[14] P. R. Gogate and A. B. Pandit, "Sonophotocatalytic reactors for wastewater treatment: A critical review," Aiche J., vol. 50, pp. 1051–1079, 2004.

[15] A. Mills and S. K. Lee, "Advanced Oxidation Processes for Water and Wastewater Treatment," in Semiconductor photocatalysis, S. Parsons, Ed. London: IWA Publishing, 2004.

[16] T. Van Gerven, G. Mul, J. Moulijn, and A. Stankiewicz, "A review of intensification of photocatalytic processes," Chem. Eng. Process. Process Intensif., vol. 46, pp. 781–789, 2007.

[17] C. McCullagh, N. Skillen, M. Adams, and P. K. J. Robertson, "Photocatalytic reactors for environmental remediation: A review," J. Chem. Technol. Biotechnol., vol. 86. pp. 1002–1017, 2011.

[18] M. Mehrvar, W. A. Anderson, and M. Moo-Young, "Preliminary analysis of a tellerette packed-bed photocatalytic reactor," Adv. Environ. Res., vol. 6, pp. 411–418, 2002.

[19] H. P. Kuo, C. T. Wu, and R. C. Hsu, "Continuous reduction of toluene vapours from the contaminated gas stream in a fluidised bed photoreactor," Powder Technol., vol. 195, pp. 50–56, 2009.

[20] D. K. Lee, S. C. Kim, I. C. Cho, S. J. Kim, and S. W. Kim, "Photocatalytic oxidation of microcystin-LR in a fluidized bed reactor having TiO_2-coated activated carbon," Sep. Purif. Technol., vol. 34, pp. 59–66, 2004.

[21] D. Psaltis, S. R. Quake, and C. Yang, "Developing optofluidic technology through the fusion of microfluidics and optics.," Nature, vol. 442, pp. 381–386, 2006.

[22] L. L. and C. Y. Y. Fainman, D. Psaltis, Optofluidics: Fundamentals, Devices and Applications. McGraw-Hill, 2009.

[23] F. B. Myers and L. P. Lee, “Innovations in optical microfluidic technologies for point-of-care diagnostics.,” Lab Chip, vol. 8, pp. 2015–2031, 2008.

[24] X. Fan and I. M. White, “Optofluidic microsystems for chemical and biological analysis,” Nat. Photonics, vol. 5. pp. 591–597, 2011.

[25] X. Heng, D. Erickson, L. R. Baugh, Z. Yaqoob, P. W. Sternberg, D. Psaltis, and C. H. Yang, “Optofluidic microscopy - a method for implementing a high resolution optical microscope on a chip,” Lab Chip, vol. 6, pp. 1274–1276, 2006.

[26] X. Cui, L. M. Lee, X. Heng, W. Zhong, P. W. Sternberg, D. Psaltis, and C. Yang, “Lensless high-resolution on-chip optofluidic microscopes for Caenorhabditis elegans and cell imaging.,” Proc. Natl. Acad. Sci. U. S. A., vol. 105, pp. 10670–10675, 2008.

[27] O. Mudanyali, D. Tseng, C. Oh, S. O. Isikman, I. Sencan, W. Bishara, C. Oztoprak, S. Seo, B. Khademhosseini, and A. Ozcan, “Compact, light-weight and cost-effective microscope based on lensless incoherent holography for telemedicine applications.,” Lab Chip, vol. 10, pp. 1417–1428, 2010.

[28] P. Y. Chiou, A. T. Ohta, and M. C. Wu, “Massively parallel manipulation of single cells and microparticles using optical images.,” Nature, vol. 436, pp. 370–372, 2005.

[29] D. Erickson, D. Sinton, and D. Psaltis, “Optofluidics for energy applications,” Nat. Photonics, vol. 5. pp. 583–590, 2011.

[30] C. Monat, P. Domachuk, and B. J. Eggleton, “Integrated optofluidics: A new river of light,” Nat. Photonics, vol. 1. pp. 106–114, 2007.

[31] H. Schmidt and A. R. Hawkins, “The photonic integration of non-solid media using optofluidics,” Nat. Photonics, vol. 5. pp. 598–604, 2011.

[32] K. Mori, H. Ohya, K. Matsumoto, H. Furuune, K. Isozaki, and P. Siekmeier, “Design for a bioreactor with sunlight supply and operations systems for use in the space environment.,” Adv. Space Res., vol. 9, pp. 161–168, 1989.

[33] S. A. Angermayr, K. J. Hellingwerf, P. Lindblad, and M. J. Teixeira de, “Energy biotechnology with cyanobacteria,” Curr. Opin. Biotech., vol. 20. pp. 257–263, 2009.

[34] F. Lehr and C. Posten, “Closed photo-bioreactors as tools for biofuel production,” Curr. Opin. Biotech., vol. 20. pp. 280–285, 2009.

[35] T. V. Laurinavichene, A. S. Fedorov, M. L. Ghirardi, M. Seibert, and A. A. Tsygankov, “Demonstration of sustained hydrogen photoproduction by immobilized, sulfur-deprived Chlamydomonas reinhardtii cells,” Int. J. Hydrogen Energy, vol. 31, pp. 659–667, 2006.

[36] D. J. Bayless, G. Kremer, M. Vis, B. Stuart, L. Shi, E. Ono, and J. L. Cuello, "Photosynthetic CO_2 mitigation using a novel membrane-based photobioreactor," J. Environ. Eng. Manag., vol. 16, pp. 209–215, 2006.

[37] S. Atsumi, W. Higashide, and J. C. Liao, "Direct photosynthetic recycling of carbon dioxide to isobutyraldehyde.," Nat. Biotechnol., vol. 27, pp. 1177–1180, 2009.

[38] C. Tan, S.-J. Lo, P. R. LeDuc, and C.-M. Cheng, "Frontiers of optofluidics in synthetic biology," Lab Chip, vol. 12. p. 3654, 2012.

[39] E. E. Coyle and M. Oelgemöller, "Micro-photochemistry: photochemistry in microstructured reactors. The new photochemistry of the future?," Photochem. Photobiol. Sci., vol. 7, pp. 1313–1322, 2008.

[40] Z. Meng, X. Zhang, and J. Qin, "A high efficiency microfluidic-based photocatalytic microreactor using electrospun nanofibrous TiO_2 as a photocatalyst.," Nanoscale, vol. 5, pp. 4687–90, 2013.

[41] S. S. Ahsan, A. Gumus, and D. Erickson, "Redox mediated photocatalytic water-splitting in optofluidic microreactors," Lab Chip, vol. 13, pp. 409–14, 2013.

[42] S. O. Y. Matsushita, H. M. A. Mohamed, "Micro-flow reaction sustems for photocatalytic carbon dioxidee recycling and hydrogen generation," proceeding of conference (Microtas 2012).

[43] C. McCullagh, N. Skillen, M. Adams, and P. K. J. Robertson, “Photocatalytic reactors for environmental remediation: A review,” J. Chem. Technol. Biotechnol., vol. 86. pp. 1002–1017, 2011.

[44] B. H. Diya’Uddeen, W. M. A. W. Daud, and A. R. Abdul Aziz, “Treatment technologies for petroleum refinery effluents: A review,” Process Saf. Environ., vol. 89. pp. 95–105, 2011.

[45] S. M. Rodríguez, C. Richter, J. B. Gálvez, and M. Vincent, “Photocatalytic degradation of industrial residual waters,” Sol. Energy, vol. 56, pp. 401–410, 1996.

[46] X. M. Zhang, Y. L. Chen, R. S. Liu and D. P. Tsai, “Plasmonic photocatalysis.,” Rep. Prog. Phys., vol. 76, p. 046401, 2013.

[47] Y. L. Chen, L. C. Kuo, M. L. Tseng, H. M. Chen, C. K. Chen, H. J. Huang, R.-S. Liu, and D. P. Tsai, “ZnO nanorod optical disk photocatalytic reactor for photodegradation of methyl orange.,” Opt. Express, vol. 21, pp. 7240–9, 2013.

[48] J. M. Herrmann, “Fundamentals and misconceptions in photocatalysis,” J. Photochem. Photobiol. A Chem., vol. 216, pp. 85–93, 2010.

[49] A. L. Linsebigler, J. T. Yates Jr, G. Lu, and J. T. Yates, “Photocatalysis on TiO_2 Surfaces: Principles, Mechanisms, and Selected Results,” Chem. Rev., vol. 95, pp. 735–758, 1995.

[50] S. Mozia, A. W. Morawski, M. Toyoda, and T. Tsumura, “Effect of process parameters on photodegradation of Acid Yellow 36 in a hybrid

photocatalysis-membrane distillation system," Chem. Eng. J., vol. 150, pp. 152–159, 2009.

[51] Y. Okada, "Surface deformation due to shear and tensile faults in a half-space Okada, Y Bull Seismol Soc AmV75, N4, Aug 1985, P1135–1154," Int. J. Rock Mech. Min. Sci. Geomech. Abstr., vol. 75, pp. 1135–1154, 1985.

[52] D. Ollis, E. Pelizzetti, and N. Serpone, "Photocatalyzed destruction of water contaminants," Environ. Sci. Tech., vol. 25, pp. 1523–1529, 1991.

[53] C. Kormann, D. W. Bahnemann, and M. R. Hoffmann, "Photolysis of chloroform and other organic molecules in aqueous TiO_2 suspensions," Environ. Sci. Tech., vol. 25, pp. 494–500, 1991.

[54] D. Bahnemann, D. Bockelmann, and R. Goslich, "Mechanistic studies of water detoxification in illuminated TiO_2 suspensions," Sol. Energy Mater., vol. 24. pp. 564–583, 1991.

[55] W. Chu, W. K. Choy, and T. Y. So, "The effect of solution pH and peroxide in the TiO_2-induced photocatalysis of chlorinated aniline," J. Hazard. Mater., vol. 141, pp. 86–91, 2007.

[56] C. A. P. Arellano and S. S. Martínez, "Effects of pH on the degradation of aqueous ferricyanide by photolysis and photocatalysis under solar radiation," Sol. Energy Mater. Sol. Cells, vol. 94, pp. 327–332, 2010.

[57] R. Andreozzi, V. Caprio, A. Insola, G. Longo, and V. Tufano, "Photocatalytic oxidation of 4-nitrophenol in aqueous TiO_2 slurries: An experimental validation of literature kinetic models," J. Chem. Technol. Biotechnol., vol. 75, pp. 131–136, 2000.

[58] M. F. J. Dijkstra, H. Buwalda, A. W. F. De Jong, A. Michorius, J. G. M. Winkelman, and A. A. C. M. Beenackers, "Experimental comparison of three reactor designs for photocatalytic water purification," Chem. Eng. Sci., vol. 56, pp. 547–555, 2001.

[59] P. R. Gogate and A. B. Pandit, "A review of imperative technologies for wastewater treatment I: Oxidation technologies at ambient conditions," Adv. Environ. Res., vol. 8. pp. 501–551, 2004.

[60] C. Hu, J. C. Yu, Z. Hao, and P. K. Wong, "Effects of acidity and inorganic ions on the photocatalytic degradation of different azo dyes," Appl. Catal. B Environ., vol. 46, pp. 35–47, 2003.

[61] A. G. Rincon, "Effect of pH, inorganic ions, organic matter and H_2O_2 on E. coli K12 photocatalytic inactivation by TiO_2 implications in solar water disinfection," Appl. Catal. B: Environ., vol. 51. pp. 283–302, 2004.

[62] B. Ohtani, "Preparing Articles on Photocatalysis—Beyond the Illusions, Misconceptions, and Speculation," Chemistry Letters, vol. 37. pp. 216–229, 2008.

[63] B. Jenny and P. Pichat, "Determination of the Actual Photocatalytic Rate of H2o2 Decomposition over Suspended TiO_2-Fitting to the Langmuir Hinshelwood Form," Langmuir, vol. 7, pp. 947–954, 1991.

[64] D. Monllor-Satoca, R. Gómez, M. González-Hidalgo, and P. Salvador, "The 'Direct-Indirect' model: An alternative kinetic approach in heterogeneous photocatalysis based on the degree of interaction of dissolved pollutant species with the semiconductor surface," Catal. Today, vol. 129, pp. 247–255, 2007.

[65] A. V. Emeline, V. Ryabchuk, and N. Serpone, "Factors affecting the efficiency of a photocatalyzed process in aqueous metal-oxide dispersions," Journal of Photochem. and Photobiol. A: Chem., vol. 133. pp. 89–97, 2000.

[66] B. Ohtani, R. Bowman, D. P. C. Jr., H. Kominami, H. Noguchi and K. Uosaki, "Femtosecond diffuse reflectance spectroscopy of aqueous Titanium (IV) oxide suspension: Correlation of electron-hole recombination kinetics with photocatalytic activity," Chem. Lett., pp. 2–3, 1998.

[67] A. J. Bard, "Photoelectrochemistry," Science, vol. 207, pp. 139–144, 1980.

[68] A. S. K. Sinha, N. Sahu, M. K. Arora, and S. N. Upadhyay, "Preparation of egg-shell type Al_2O_3-supported CdS photocatalysts for reduction of H_2O to H_2," Catal. Today, vol. 69. pp. 297–305, 2001.

[69] J. Bandara, J. A. Mielczarski, A. Lopez, and J. Kiwi, "Sensitized degradation of chlorophenols on iron oxides induced by visible light comparison with titanium oxide," Appl. Catal. B Environ., vol. 34, pp. 321–333, 2001.

[70] M. Long, W. Cai, and H. Kisch, "Visible light induced photoelectrochemical properties of n-$BiVO_4$ and n-$BiVO_4$/p-Co_3O_4," J. Phys. Chem. C, vol. 112, pp. 548–554, 2008.

[71] H. Yamashita, M. Harada, J. Misaka, M. Takeuchi, K. Ikeue, and M. Anpo, "Degradation of propanol diluted in water under visible light irradiation using metal ion-implanted titanium dioxide photocatalysts," J. Photochem. Photobiol. A Chem., vol. 148, pp. 257–261, 2002.

[72] R. Asahi, T. Morikawa, T. Ohwaki, K. Aoki, and Y. Taga, "Visible-light photocatalysis in nitrogen-doped titanium oxides.," Science, vol. 293, pp. 269–271, 2001.

[73] R. Abe, K. Sayama, and H. Arakawa, "Efficient hydrogen evolution from aqueous mixture of I^- and acetonitrile using a merocyanine dye-sensitized Pt/TiO_2 photocatalyst under visible light irradiation," Chem. Phys. Lett., vol. 362, pp. 441–444, 2002.

[74] H. Osora, W. Li, L. Otero, and M. A. Fox, "Photosensitization of nanocrystalline TiO_2 thin films by a polyimide bearing pendent substituted-Ru(bpy)(3)(+2) groups," in Journal of Photochemistry and Photobiology B: Biology, 1998, vol. 43, pp. 232–238.

[75] X. Zhang, Y. L. Chen, R.-S. Liu, and D. P. Tsai, "Plasmonic photocatalysis.," Rep. Prog. Phys., vol. 76, p. 046401, 2013.

[76] M. J. Kale, T. Avanesian, and P. Christopher, "Direct photocatalysis by plasmonic nanostructures," ACS Catalysis, vol. 4. pp. 116–128, 2014.

[77] Y. Lu, H. Yu, S. Chen, X. Quan, and H. Zhao, "Integrating plasmonic nanoparticles with TiO_2 photonic crystal for enhancement of visible-light-driven photocatalysis," Environ. Sci. Technol., vol. 46, pp. 1724–1730, 2012.

[78] K. Awazu, M. Fujimaki, C. Rockstuhl, J. Tominaga, H. Murakami, Y. Ohki, N. Yoshida, and T. Watanabe, "A plasmonic photocatalyst consisting of silver nanoparticles embedded in titanium dioxide," J. Am. Chem. Soc., vol. 130, pp. 1676–1680, 2008.

[79] C. Wang and D. Astruc, "Nanogold plasmonic photocatalysis for organic synthesis and clean energy conversion.," Chem. Soc. Rev., 2014.

[80] S. K. Cushing, J. Li, F. Meng, T. R. Senty, S. Suri, M. Zhi, M. Li, A. D. Bristow, and N. Wu, "Photocatalytic activity enhanced by plasmonic resonant energy transfer from metal to semiconductor," J. Am. Chem. Soc., vol. 134, pp. 15033–15041, 2012.

[81] R. Pelegrini, P. Peralta-Zamora, A. R. De Andrade, J. Reyes, and N. Durán, "Electrochemically assisted photocatalytic degradation of reactive dyes," Appl. Catal. B Environ., vol. 22, pp. 83–90, 1999.

[82] K. Vinodgopal, S. Hotchandani, and P. V Kamat, "Electrochemically assisted photocatalysis: titania particulate film electrodes for photocatalytic degradation of 4-chlorophenol," J. Phys. Chem., vol. 97, pp. 9040–9044, 1993.

[83] Shouxin Liu and Hong Liu, Fundamentals and application of photocatalysis and photoelectrocatalysis, Ed. Beijing: Chemical Industry Press, 2005.

[84] O. M. Alfano, D. Bahnemann, A. E. Cassano, R. Dillert, and R. Goslich, "Photocatalysis in water environments using artificial and solar light," Catal. Today, vol. 58, pp. 199–230, 2000.

[85] H. De Lasa, B. Serrano, and M. Salaices, Photocatalytic reaction engineering. 2005, pp. 1–187.

[86] T. Van Gerven, G. Mul, J. Moulijn, and A. Stankiewicz, "A review of intensification of photocatalytic processes," Chem. Eng. Process. Process Intensif., vol. 46, pp. 781–789, 2007.

[87] J. Kumar and A. Bansal, "Photocatalytic degradation in annular reactor: Modelization and optimization using computational fluid dynamics (CFD) and response surface methodology (RSM)," J. Environ. Chem. Eng., vol. 1, pp. 398-405, 2013.

[88] D. K. Lee, S. C. Kim, S. J. Kim, I. S. Chung, and S. W. Kim, "Photocatalytic oxidation of microcystin-LR with TiO2-coated activated carbon," Chem. Eng. J., vol. 102, pp. 93–98, 2004.

[89] L. Erdei, N. Arecrachakul, and S. Vigneswaran, "A combined photocatalytic slurry reactor-immersed membrane module system for advanced wastewater treatment," Sep. Purif. Technol., vol. 62, pp. 382–388, 2008.

[90] A. K. Ray and A. a. C. M. Beenackers, "Novel swirl-flow reactor for kinetic studies of semiconductor photocatalysis," AIChE J., vol. 43, pp. 2571–2578, 1997.

[91] J. G. Sczechowski, C. A. Koval, and R. D. Noble, "A Taylor vortex reactor for heterogeneous photocatalysis," Chem. Eng. Sci., vol. 50. pp. 3163–3173, 1995.

[92] G. Li Puma and P. L. Yue, "Enhanced Photocatalysis in a Pilot Laminar Falling Film Slurry Reactor," Ind. Eng. Chem. Res., vol. 38, pp. 3246–3254, 1999.

[93] C. McCullagh, P. K. J. Robertson, M. Adams, P. M. Pollard, and A. Mohammed, "Development of a slurry continuous flow reactor for photocatalytic treatment of industrial waste water," J. Photochem. Photobiol. A Chem., vol. 211, pp. 42–46, 2010.

[94] G. S. Shephard, S. Stockenström, D. De Villiers, W. J. Engelbrecht, and G. F. S. Wessels, "Degradation of microcystin toxins in a falling film photocatalytic reactor with immobilized titanium dioxide catalyst," Water Res., vol. 36, pp. 140–146, 2002.

[95] N. J. Peill, M. R. Hoffmann, and M. M. K. Laboratories, "Development and Optimization of a TiO_2-Coated Fiber-Optic Cable Reactor : Photocatalytic Degradation of 4-Chlorophenol Development and Optimization of a TiO_2-Coated

FiberiOptic Cable Photocatalytic Degradation of 4-Chlorophenol," Environ. Sci. Technol., vol. 29, pp. 2974–2981, 2002.

[96] A. K. Ray, "A new photocatalytic reactor for destruction of toxic water pollutants by advanced oxidation process," Catal. Today, vol. 44. pp. 357–368, 1998.

[97] S. J. Khan, R. H. Reed, and M. G. Rasul, "Thin-film fixed-bed reactor (TFFBR) for solar photocatalytic inactivation of aquaculture pathogen Aeromonas hydrophila," BMC Microbiology, vol. 12. p. 5, 2012.

[98] C. N. Lin, C. Y. Chang, H. J. Huang, D. P. Tsai, and N. L. Wu, "Photocatalytic degradation of methyl orange by a multi-layer rotating disk reactor.," Environ. Sci. Pollut. Res. Int., vol. 19, pp. 3743–50, 2012.

[99] A. K. Ray, "A new photocatalytic reactor for destruction of toxic water pollutants by advanced oxidation process," Catal. Today, vol. 44. pp. 357–368, 1998.

[100] S. Mozia, A. W. Morawski, M. Toyoda, and M. Inagaki, "Effectiveness of photodecomposition of an azo dye on a novel anatase-phase TiO_2 and two commercial photocatalysts in a photocatalytic membrane reactor (PMR)," Sep. Purif. Technol., vol. 63, pp. 386–391, 2008.

[101] Z. Zhang, W. Anderson, and M. Mooyoung, "Experimental analysis of a corrugated plate photocatalytic reactor," Chem. Eng. J., vol. 99. pp. 145–152, 2004.

[102] H. Lu, M. A. Schmidt, and K. F. Jensen, "Photochemical reactions and on-line UV detection in microfabricated reactors," Lab Chip, vol. 1, pp. 22–28, 2001.

[103] T. V. Nguyen and J. C. S. Wu, "Photoreduction of CO_2 to fuels under sunlight using optical-fiber reactor," Sol. Energy Mater. Sol. Cells, vol. 92, pp. 864–872, 2008.

[104] D. Li, L. Wang, and G. Zhang, "A photocatalytic reactor derived from microstructured polymer optical fiber preform," Opt. Commun., vol. 286, pp. 182–186, 2013.

[105] N. J. Peill, M. R. Hoffmann, and M. M. K. Laboratories, "Development and Optimization of a TiO_2-Coated Fiber-Optic Cable Reactor : Photocatalytic Degradation of 4-Chlorophenol Development and Optimization of a TiO_2-Coated FiberiOptic Cable Photocatalytic Degradation of 4-Chlorophenol," Environ. Sci. Technol., vol. 29, pp. 2974–2981, 1995.

[106] J. C. S. Wu, T. H. Wu, T. Chu, H. Huang, and D. Tsai, "Application of Optical-fiber Photoreactor for CO_2 Photocatalytic Reduction," Top. Catal., vol. 47, pp. 131–136, 2008.

[107] E. Bessa, J. Sant' Anna, and M. Dezotti, "Photocatalytic/H_2O_2 treatment of oil field produced waters," Appl. Catal. B Environ., vol. 29, pp. 125–134, 2001.

[108] H. Lindstrom, R. Wootton, and A. Iles, "High surface area titania photocatalytic microfluidic reactors," AIChE J., vol. 53, pp. 695–702, 2007.

[109] T. M. Squires and S. R. Quake, "Microfluidics: Fluid physics at the nanoliter scale," Rev. Mod. Phys., vol. 77, pp. 977–1026, 2005.

[110] G. M. Whitesides, "The origins and the future of microfluidics," Nature, vol. 442, pp. 368–373, 2006.

[111] N. T. Nguyen and S. T. Wereley, Fundamentals and applications of microfluidics, Artech House, pp. 471, 2002.

[112] M. Oelgemoeller, "Highlights of Photochemical Reactions in Microflow Reactors," Chem. Eng. Technol., vol. 35. pp. 1144–1152, 2012.

[113] K. Mori, "Photoautotrophic bioreactor using solar rays condensed by fresnel lenses," Biotechnol. Bioeng. Symp., vol. 15, pp. 331–345, 1985.

[114] K. Mori, H. Ohya, K. Matsumoto, H. Furuune, K. Isozaki, and P. Siekmeier, "Design for a bioreactor with sunlight supply and operations systems for use in the space environment.," Adv. Space Res., vol. 9, pp. 161–168, 1989.

[115] S. A. Angermayr, K. J. Hellingwerf, P. Lindblad, and M. J. Teixeira de, "Energy biotechnology with cyanobacteria," Curr. Opin. Biotechnol., vol. 20. pp. 257–263, 2009.

[116] T. V. Laurinavichene, A. S. Fedorov, M. L. Ghirardi, M. Seibert, and A. A. Tsygankov, "Demonstration of sustained hydrogen photoproduction by immobilized, sulfur-deprived Chlamydomonas reinhardtii cells," Int. J. Hydrogen Energy, vol. 31, pp. 659–667, 2006.

[117] D. J. Bayless, G. Kremer, M. Vis, B. Stuart, L. Shi, E. Ono, and J. L. Cuello, "Photosynthetic CO_2 mitigation using a novel membrane-based photobioreactor," J. Environ. Eng. Manag., vol. 16, pp. 209–215, 2006.

[118] S. Atsumi, W. Higashide, and J. C. Liao, "Direct photosynthetic recycling of carbon dioxide to isobutyraldehyde.," Nat. Biotechnol., vol. 27, pp. 1177–1180, 2009.

[119] C. Tan, S. J. Lo, P. R. LeDuc, and C. M. Cheng, "Frontiers of optofluidics in synthetic biology," Lab Chip, vol. 12. p. 3654, 2012.

[120] E. E. Coyle and M. Oelgemöller, "Micro-photochemistry: photochemistry in microstructured reactors. The new photochemistry of the future?," Photochem. Photobiol. Sci., vol. 7, pp. 1313–1322, 2008.

[121] S. S. Ahsan, A. Gumus, and D. Erickson, "Redox mediated photocatalytic water-splitting in optofluidic microreactors.," Lab Chip, vol. 13, pp. 409–14, 2013.

[122] J. R. Adleman, D. A. Boyd, D. G. Goodwin, and D. Psaltis, "Heterogenous catalysis mediated by plasmon heating," Nano Lett., vol. 9, pp. 4417–4423, 2009.

[123] J. S. Lee, S. H. Lee, J. H. Kim, and C. B. Park, "Artificial photosynthesis on a chip: microfluidic cofactor regeneration and photoenzymatic synthesis under visible light.," Lab Chip, vol. 11, pp. 2309–2311, 2011.

[124] Y. Matsushita, T. Ichimura, N. Ohba, S. Kumada, K. Sakeda, T. Suzuki, H. Tanibata, and T. Murata, "Recent progress on photoreactions in microreactors," Pure Appl. Chem., vol. 79. pp. 1959–1968, 2007.

[125] Y. Matsushita, N. Ohba, S. Kumada, T. Suzuki, and T. Ichimura, "Photocatalytic N-alkylation of benzylamine in microreactors," Catal. Commun., vol. 8, pp. 2194–2197, 2007.

[126] Y. Matsushita, N. Ohba, T. Suzuki, and T. Ichimura, "N-Alkylation of amines by photocatalytic reaction in a microreaction system," Catal. Today, vol. 132, pp. 153–158, 2008.

[127] Y. Matsushita, S. Kumada, K. Wakabayashi, K. Sakeda, and T. Ichimura, "Photocatalytic Reduction in Microreactors," Chem. Lett., vol. 35. pp. 410–411, 2006.

[128] N. B. Jackson, C. M. Wang, Z. Luo, J. Schwitzgebel, J. G. Ekerdt, J. R. Brock, and A. Heller, "Attachment of TiO_2 powders to hollow glass microbeads-activity of the TiO_2-coated beads in the photoassisted oxidation of ethanol to acetaldehyde," J. Electrochem. Soc., vol. 138, pp. 3660–3664, 1991.

[129] X. Li, H. Wang, K. Inoue, M. Uehara, H. Nakamura, M. Miyazaki, E. Abea, and H. Maeda, "Modified micro-space using self-organized nanoparticles for reduction of methylene blue.," Chem. Commun. (Camb)., pp. 964–965, 2003.

[130] K. Oda, Y. Ishizaka, T. Sato, T. Eitoku and K. Katayama, "Analysis of photocatalytic reactions using a TiO_2 immobilized microreactor," Anal. Sci., vol. 26, pp. 969–972, 2010.

[131] Z. Zhang, H. Wu, Y. Yuan, Y. Fang, and L. Jin, "Development of a novel capillary array photocatalytic reactor and application for degradation of azo dye," Chem. Eng. J., vol. 184, pp. 9–15, 2012.

[132] N. Tsuchiya, K. Kuwabara, A. Hidaka, K. Oda, and K. Katayama, "Reaction kinetics of dye decomposition processes monitored inside a photocatalytic microreactor," Physical Chemistry Chemical Physics, vol. 14. p. 4734, 2012.

[133] G. Charles, T. Roques-Carmes, N. Becheikh, L. Falk, J. M. Commenge, and S. Corbel, "Determination of kinetic constants of a photocatalytic reaction in micro-channel reactors in the presence of mass-transfer limitation and axial dispersion," J. Photochem. Photobiol. A Chem., vol. 223, pp. 202–211, 2011.

[134] D. Daniel and I. G. R. Gutz, "Microfluidic cell with a TiO_2-modified gold electrode irradiated by an UV-LED for in situ photocatalytic decomposition of organic matter and its potentiality for voltammetric analysis of metal ions," Electrochem. commun., vol. 9, pp. 522–528, 2007.

[135] T. H. Yoon, L. Y. Hong, and D. P. Kim, "Photocatalytic reaction using novel inorganic polymer derived packed bed microreactor with modified TiO_2 microbeads," Chem. Eng. J., vol. 167, pp. 666–670, 2011.

[136] Y. Matsushita, N. Ohba, S. Kumada, K. Sakeda, T. Suzuki, and T. Ichimura, “Photocatalytic reactions in microreactors,” Chem. Eng. J., vol. 135, pp. S303–S308, 2008.

[137] R. Gorges, S. Meyer, and G. Kreisel, “Photocatalysis in microreactors,” J. Photochem. Photobiol. A Chem., vol. 167, pp. 95–99, 2004.

[138] H. C. Aran, D. Salamon, T. Rijnaarts, G. Mul, M. Wessling, and R. G. H. Lammertink, “Porous Photocatalytic Membrane Microreactor (P2M2): A new reactor concept for photochemistry,” J. Photochem. Photobiol. A Chem., vol. 225, pp. 36–41, 2011.

[139] N. Wang, L. Lei , X. M. Zhang, D. P. Tsai, and H. L.W. Chan, "Solar-powered microfluidic photocatalysis", The 6th Annual IEEE International Conference on Nano/Micro Engineered and Molecular Systems (IEEE-NEMS 2011), 20-23 February 2011, Kaohsiung, Taiwan, R. O. China

[140] N. Wang, Z. K. Liu and X. M. Zhang, “Photocatalytic microfluidic reactor with a novel compound catalyst film using solar energy,” proceeding of conference (microtas 2012).

[141] N. Wang, X. M. Zhang, B. Chen, W. Z. Song, N. Y. Chan, and H. L. W. Chan, “Microfluidic photoelectrocatalytic reactors for water purification with an integrated visible-light source,” Lab Chip, vol. 12. pp. 3983-3990, 2012.

[142] G. Takei, T. Kitamori, and H. B. Kim, "Photocatalytic redox-combined synthesis of l-pipecolinic acid with a titania-modified microchannel chip," Catal. Commun., vol. 6, pp. 357–360, 2005.

[143] A. Q. Liu, H. J. Huang, L. K. Chin, Y. F. Yu, and X. C. Li, "Label-free detection with micro optical fluidic systems (MOFS): A review," Anal. Bioanalytical Chem., vol. 391. pp. 2443–2452, 2008.

[144] C. Monat, P. Domachuk, and B. J. Eggleton, "Integrated optofluidics: A new river of light," Nat. Photonics, vol. 1. pp. 106–114, 2007.

[145] D. Psaltis, S. R. Quake, and C. Yang, "Developing optofluidic technology through the fusion of microfluidics and optics.," Nature, vol. 442, pp. 381–386, 2006.

[146] J. Mo, Y. Zhang, Q. Xu, Y. Zhu, J. J. Lamson, and R. Zhao, "Determination and risk assessment of by-products resulting from photocatalytic oxidation of toluene," Appl. Catal. B Environ., vol. 89, pp. 570–576, 2009.

[147] C. Wei, W. Y. Lin, Z. Zainal, N. E. Williams, K. Zhu, A. P. Kruzic, R. L. Smith, and K. Rajeshwar, "Bactericidal Activity of TiO_2 Photocatalyst in Aqueous Media: Toward a Solar-Assisted Water Disinfection System.," Environ. Sci. Technol., vol. 28, pp. 934–938, 1994.

[148] Z. Zou, J. Ye, K. Sayama, and H. Arakawa, "Direct splitting of water under visible light irradiation with an oxide semiconductor photocatalyst.," Nature, vol. 414, pp. 625–627, 2001.

[149] T. Van Gerven, G. Mul, J. Moulijn, and A. Stankiewicz, "A review of intensification of photocatalytic processes," Chem. Eng. Process. Process Intensif., vol. 46, pp. 781–789, 2007.

[150] H. Lu, M. A. Schmidt, and K. F. Jensen, "Photochemical reactions and on-line UV detection in microfabricated reactors.," Lab Chip, vol. 1, pp. 22–28, 2001.

[151] G. Takei, T. Kitamori, and H. B. Kim, "Photocatalytic redox-combined synthesis of l-pipecolinic acid with a titania-modified microchannel chip," Catal. Commun., vol. 6, pp. 357–360, 2005.

[152] R. C. R. Wootton, R. Fortt, and A. J. De Mello, "A microfabricated nanoreactor for safe, continuous generation and use of singlet oxygen," Org. Process Res. Dev., vol. 6, pp. 187–189, 2002.

[153] D. Bahnemann, "Photocatalytic water treatment: solar energy applications," Sol. Energy, vol. 77, pp. 445–459, 2004.

[154] R. Goslich, R. Dillert, and D. Bahnemann, "Solar water treatment: Principles and reactors," Water Sci. Technol., vol. 35, pp. 137–148, 1997.

[155] M. Nazeeruddin, A. Kay, and I. Rodicio, "Conversion of light to electricity by cis-X2bis (2, 2'-bipyridyl-4, 4'-dicarboxylate) ruthenium (II) charge-transfer

sensitizers (X= Cl-, Br-, I-, CN-, and SCN-) on nanocrystalline titanium dioxide electrodes," J. Am. Chem. Soc., vol. 115, pp. 6382-6390, 1993.

[156] S. Ito, P. Chen, P. Comte, M. K. Nazeeruddin, P. Liska, P. Péchy, and M. Grätzel, "Fabrication of screen-printing pastes from TiO_2 powders for dye-sensitised solar cells," Prog. Photovoltaics Res. Appl., vol. 15, pp. 603–612, 2007.

[157] J. Yu, X. Zhao, and Q. Zhao, "Effect of surface structure on photocatalytic activity of TiO_2 thin films prepared by sol-gel method," Thin Solid Films, vol. 379, pp. 7–14, 2000.

[158] D. Bartolo, G. Degré, P. Nghe, and V. Studer, "Microfluidic stickers.," Lab Chip, vol. 8, pp. 274–279, 2008.

[159] L. Lei, N. Wang, X. M. Zhang, Q. Tai, D. P. Tsai, and H. L. W. Chan, "Optofluidic planar reactors for photocatalytic water treatment using solar energy.," Biomicrofluidics, vol. 4, pp. 43004, 2010.

[160] D. W. Chen, F. M. Li, and A. K. Ray, "Effect of mass transfer and catalyst layer thickness on photocatalytic reaction," Aiche J., vol. 46, pp. 1034–1045, 2000.

[161] H. Lin and K. T. Valsaraj, "Development of an optical fiber monolith reactor for photocatalytic wastewater treatment," J. Appl. Electrochem., vol. 35, pp. 699–708, 2005.

[162] P. Nalini Vijaya Laxmi, P. Saritha, N. Rambabu, V. Himabindu, and Y. Anjaneyulu, "Sonochemical degradation of 2chloro-5methyl phenol assisted by TiO_2 and H_2O_2," J. Hazard. Mater., vol. 174, pp. 151–155, 2010.

[163] R. E. Bird, R. L. Hulstrom, and L. J. Lewis, "Terrestrial solar spectral data sets," Sol. Energy, vol. 30, pp. 563–573, 1983.

[164] R. Asahi, T. Morikawa, T. Ohwaki, K. Aoki, and Y. Taga, "Visible-light photocatalysis in nitrogen-doped titanium oxides.," Science, vol. 293, pp. 269–271, 2001.

[165] E. Kowalska, O. O. P. Mahaney, R. Abe, and B. Ohtani, "Visible-light-induced photocatalysis through surface plasmon excitation of gold on titania surfaces.," Phys. Chem. Chem. Phys., vol. 12, pp. 2344–2355, 2010.

[166] J. Hegyi and O. Horváth, "Photocatalytic reduction of mercury(II) and simultaneous oxidative degradation of surfactants in titanium dioxide suspensions," Prog. Colloid Polym. Sci., vol. 125, no. 10–16, 2004.

[167] M. R. Hoffmann, S. T. Martin, W. Choi, and D. W. Bahnemannt, "Environmental Applications of Semiconductor Photocatalysis," Chem. Rev., vol. 95, pp. 69–96, 1995.

[168] G. Velve Casquillas, C. Fu, M. Le Berre, J. Cramer, S. Meance, A. Plecis, D. Baigl, J. J. Greffet, Y. Chen, M. Piel, and P. T. Tran, "Fast microfluidic

temperature control for high resolution live cell imaging," Lab Chip, vol. 11, pp. 484–489, 2011.

[169] X. Li, H. Wang, K. Inoue, M. Uehara, H. Nakamura, M. Miyazaki, E. Abea, and H. Maeda, "Modified micro-space using self-organized nanoparticles for reduction of methylene blue.," Chem. Commun. (Camb)., pp. 964–965, 2003.

[170] H. Zhang, J. J. Wang, J. Fan, and Q. Fang, "Microfluidic chip-based analytical system for rapid screening of photocatalysts," Talanta, vol. 116, pp. 946–950, 2013.

[171] W. Ehrfeld, V. Hessel and H. Löwe, Microreactors: New Technology for Modern Chemistry, Germany: Wiley, 2004.

[172] K. F. Jensen, "Microreaction engineering-is small better?" Chem. Eng. Sci., vol. 56. pp. 293–303, 2001.

[173] S. Walter, S. Malmberg, B. Schmidt, and M. A. Liauw, "Mass transfer limitations in microchannel reactors," Catal. Today, vol. 110, pp. 15–25, 2005.

[174] P. Watts and C. Wiles, "Micro reactors: a new tool for the synthetic chemist," Org. Biomol. Chem., vol. 5, pp. 727–732, 2007.

[175] L. Li , R. Chen, X. Zhu, H. Wang, Y. Z. Wang , Q. Liao and D. Wang., "Optofluidic Microreactors with TiO_2-Coated Fiberglass," ACS Appl. Mater. Interfaces, vol. 5, pp. 12548-12553, 2013.

[176] S. S. Ahsan, A. Gumus, and D. Erickson, “Redox mediated photocatalytic water-splitting in optofluidic microreactors.,” Lab Chip, vol. 13, pp. 409–14, 2013.

[177] N. Wang, X. Zhang, B. Chen, W. Song, N. Y. Chan, and H. L. W. Chan, “Microfluidic photoelectrocatalytic reactors for water purification with an integrated visible-light source,” Lab Chip, vol. 12. p. 3983, 2012.

[178] N. Wang, X. Zhang, Y. Wang, W. Yu, and H. L. W. Chan, “Microfluidic reactors for photocatalytic water purification.,” Lab Chip, vol. 14, pp. 1074–82, 2014.

[179] B. Liu, X. Zhao, C. Terashima, A. Fujishima, and K. Nakata, “Thermodynamic and kinetic analysis of heterogeneous photocatalysis for semiconductor systems.,” Phys. Chem. Chem. Phys., vol. 16, pp. 8751–60, 2014.

[180] N. A. Oladoja, C. O. Aboluwoye, and Y. B. Oladimeji, “Kinetics and isotherm studies on Methylene Blue adsorption onto ground palm kernel coat,” Turkish J. Eng. Environ. Sci., vol. 32, pp. 303–312, 2008.

[181] T. Oyama, A. Aoshima, S. Horikoshi, H. Hidaka, J. Zhao, and N. Serpone, “Solar photocatalysis, photodegradation of a commercial detergent in aqueous TiO2 dispersions under sunlight irradiation,” Sol. Energy, vol. 77, pp. 525–532, 2004.

[182] D. Robert and S. Malato, “Solar photocatalysis: A clean process for water detoxification,” Sci. Total Environ., vol. 291, pp. 85–97, 2002.

[183] M. Shang, W. Wang, L. Zhou, S. Sun, and W. Yin, "Nanosized $BiVO_4$ with high visible-light-induced photocatalytic activity: Ultrasonic-assisted synthesis and protective effect of surfactant," J. Hazard. Mater., vol. 172, pp. 338–344, 2009.

[184] J. Tang, Z. Zou, and J. Ye, "Efficient photocatalytic decomposition of organic contaminants over CaBi2O4 under visible-light irradiation," Angew. Chem. Int. Ed., vol. 43, pp. 4463–4466, 2004.

[185] J. M. Herrmann, "Fundamentals and misconceptions in photocatalysis," J. Photochem. Photobiol. A Chem., vol. 216, pp. 85–93, 2010.

[186] R. E. Bird, R. L. Hulstrom, and L. J. Lewis, "Terrestrial solar spectral data sets," Sol. Energy, vol. 30, pp. 563–573, 1983.

[187] T. Van Gerven, G. Mul, J. Moulijn, and A. Stankiewicz, "A review of intensification of photocatalytic processes," Chem. Eng. Process. Process Intensif., vol. 46, pp. 781–789, 2007.

[188] S. Malato, J. Blanco, A. Vidal, D. Alarcón, M. I. Maldonado, J. Cáceres, and W. Gernjak, "Applied studies in solar photocatalytic detoxification: An overview," Sol. Energy, vol. 75, pp. 329–336, 2003.

[189] O. M. Alfano, D. Bahnemann, A. E. Cassano, R. Dillert, and R. Goslich, "Photocatalysis in water environments using artificial and solar light," Catal. Today, vol. 58, pp. 199–230, 2000.

[190] T. J. Johnson, D. Ross, and L. E. Locascio, "Rapid microfluidic mixing," Anal. Chem., vol. 74, pp. 45–51, 2002.

[191] M. A. Shannon, P. W. Bohn, M. Elimelech, J. G. Georgiadis, B. J. Mariñas, and A. M. Mayes, "Science and technology for water purification in the coming decades.," Nature, vol. 452, pp. 301–310, 2008.

[192] P. R. Gogate and A. B. Pandit, "A review of imperative technologies for wastewater treatment I: Oxidation technologies at ambient conditions," Advances in Environmental Research, vol. 8. pp. 501–551, 2004.

[193] N. Wang, L. Lei, X. M. Zhang, Y. H. Tsang, Y. Chen and H. L. W. Chan, "A comparative study of preparation methods of nanoporous TiO_2 films for microfluidic photocatalysis," Microelectron. Eng., vol. 88, pp. 2797–2799, 2011.

[194] Z. N. Wang, Y. P. Zhang, H. L. W. Chan and X. M. Zhang, "Photocatalytic microreactor using monochromatic visible light," Adv. Mater. Res., vol. 254, pp. 219–222, 2011.

[195] K. Mehrotra, G. S. Yablonsky, and A. K. Ray, "Macro kinetic studies for photocatalytic degradation of benzoic acid in immobilized systems," Chemosphere, vol. 60, pp. 1427–1436, 2005.

[196] D. W. Chen, F. M. Li, and A. K. Ray, "Effect of mass transfer and catalyst layer thickness on photocatalytic reaction," Aiche J., vol. 46, pp. 1034–1045, 2000.

[197] H. Zhang, G. Chen, and D. W. Bahnemann, "Photoelectrocatalytic materials for environmental applications," J. Mater. Chem., vol. 19. p. 5089, 2009.

[198] D. Wei and G. Amaratunga, "Photoelectrochemical cell and its applications in optoelectronics," Int. J. Electrochem. Sci, vol. 2, pp. 897–912, 2007.

[199] H. S. Hilal and J. A. Turner, "Controlling charge-transfer processes at semiconductor/liquid junctions," Electrochim. Acta, vol. 51, pp. 6487–6497, 2006.

[200] N. Chandrasekharan and P. Kamat, "Improving the Photoelectrochemical Performance of Nanostructured TiO_2 Films by Adsorption of Gold Nanoparticles," J. Phys. Chem. B, vol. 104, pp. 10851–10857, 2000.

[201] J. C. Colmenares, R. Luque, J. M. Campelo, F. Colmenares, Z. Karpiński, and A. A. Romero, "Nanostructured photocatalysts and their applications in the photocatalytic transformation of lignocellulosic biomass: An overview," Materials, vol. 2. pp. 2228–2258, 2009.

[202] T. An, Y. Xiong, G. Li, C. Zha, and X. Zhu, "Synergetic effect in degradation of formic acid using a new photoelectrochemical reactor," J. Photochem. Photobiol. A Chem., vol. 152, pp. 155–165, 2002.

[203] T. C. An, X. H. Zhu, Y. Xiong and S. J. Jiang, "A novel photoelectrochemical reactor three dimension electrode-slurry photocatalytic reactor," Chem. J. Internet, vol. 3, pp. 42–46, 2001.

[204] B. Zhou, X. Zhao, H. Liu, J. Qu, and C. P. Huang, "Visible-light sensitive cobalt-doped BiVO4 (Co-$BiVO_4$) photocatalytic composites for the degradation of methylene blue dye in dilute aqueous solutions," Appl. Catal. B Environ., vol. 99, pp. 214–221, 2010.

[205] T. C. An, X. H. Zhu, and Y. Xiong, "Feasibility study of photoelectrochemical degradation of methylene blue with three-dimensional electrode-photocatalytic reactor," Chemosphere, vol. 46, pp. 897–903, 2002.

[206] A. J. Bard and L. R. Faulkner, ElectrochemicalMethods – Fundamentals and Applications. New York, USA: John Wiley & Sons, 1980.

[207] R. A. Burns, J. C. Crittenden, D. W. Hand, V. H. Selzer, L. L. Sutter, and S. R. Salman, "Effect of Inorganic Ions in Heterogeneous Photocatalysis of TCE," J. Environ. Eng., vol. 125. pp. 77–85, 1999.

[208] T. An, W. Zhang, X. Xiao, G. Sheng, J. Fu, and X. Zhu, "Photoelectrocatalytic degradation of quinoline with a novel three-dimensional electrode-packed bed photocatalytic reactor," J. Photochem. Photobiol. A Chem., vol. 161, pp. 233–242, 2004.

[209] R. J. Candal, W. A. Zeltner, and M. A. Anderson, "Effects of pH and applied potential on photocurrent and oxidation rate of saline solutions of formic acid in a photoelectrocatalytic reactor," Environ. Sci. Technol., vol. 34, pp. 3443–3451, 2000.

[210] R. Pelegrini, P. Peralta-Zamora, A. R. De Andrade, J. Reyes, and N. Durán, "Electrochemically assisted photocatalytic degradation of reactive dyes," Appl. Catal. B Environ., vol. 22, pp. 83–90, 1999.

[211] W. H. Leng, Z. Zhang, and J. Q. Zhang, "Photoelectrocatalytic degradation of aniline over rutile TiO_2/Ti electrode thermally formed at 600℃," J. Mol. Catal. A Chem., vol. 206, pp. 239–252, 2003.

[212] G. Qin, Q. Wu, Z. Sun, Y. Wang, J. Luo, and S. Xue, "Enhanced photoelectrocatalytic degradation of phenols with bifunctionalized dye-sensitized TiO_2 film," J. Hazard. Mater., vol. 199–200, pp. 226–232, 2012.

[213] T. Oyama, A. Aoshima, S. Horikoshi, H. Hidaka, J. Zhao, and N. Serpone, "Solar photocatalysis, photodegradation of a commercial detergent in aqueous TiO_2 dispersions under sunlight irradiation," Sol. Energy, vol. 77, pp. 525–532, 2004.

[214] D. Robert and S. Malato, "Solar photocatalysis: A clean process for water detoxification," Sci. Total Environ., vol. 291, pp. 85–97, 2002.